José Miguel Ferreira Preto Marques Luzio

Mestre em Engenharia Electrotécnica e de Computadores

High Efficiency Transmission Techniques for Broadband Wireless Systems

Dissertação para obtenção do Grau de
Doutor em Engenharia Electrotécnica e de Computadores

Orientador: Rui Miguel Henriques Dias Morgado Dinis,
Prof. Auxiliar com Agregação,
Universidade Nova de Lisboa

Co-orientador: Paulo Miguel de Araújo Borges Montezuma de Carvalho,
Prof. Auxiliar, Universidade Nova de Lisboa

Júri:

Presidente:	Doutor Luips M. Camarinha Matos
Vogais:	Doutor Adão Paulo Soares da Silva
	Doutor Marco Alexandre Cravo Gomes
	Doutor Luis Filipe Lourenço Bernardo
	Doutor João Carlos Marques Silva
	Doutor Rui Miguel Henriques Dias Morgado Dinis

FACULDADE DE CIÊNCIAS E TECNOLOGIA
UNIVERSIDADE NOVA DE LISBOA

November, 2014

High Efficiency Transmission Techniques for Broadband Wireless Systems

Para mim.

Para que nunca me esqueça de aprender
através daquilo que parece insignificante.

ACKNOWLEDGEMENTS

I would like to thank professor Rui Dinis and Paulo Montezuma the opportunity to make this PhD, all the support of UNINOVA and IT, as well as FCT for the four year PhD grant. The time spent throughout this PhD gave me the opportunity to grow as a scientific researcher and as a human being.

I would like tho thank my family for the unconditional support. For being the anchor that was always there to support me when life requested it.

Finally, a great many thanks to my personal friends, for being most present in this period of my life.

Miguel Luzio

Abstract

Future broadband wireless systems are expected to cope with severely time dispersive channels, due to multi-path signal propagation between the transmitter and the receiver while having high power and spectral efficiency. Thus, advanced Frequency Domain Equalization techniques are required. The implementation complexity in mobile terminals should be as low as possible to achieve highest possible efficiency. Therefore, most of the signal processing requirements will be shifted to the base station and we will employ signals compatible with an efficient, grossly nonlinear power amplification. For this reason, we will consider offset modulation signals with quasi-constant envelope and develop receivers that will obtain good BER performance. However, these signals require a bandwidth significantly above the Nyquist rate, which can be reduced by an overlap of different frequency channels.

Keywords: SC-FDE; Offset Modulations; IB-DFE; IQI; ACI; CCI

RESUMO

Os futuros sistemas de banda larga sem fios devem suportar canais com distorção temporal severa, devido aos múltiplos caminhos de propagação do sinal entre o transmissor e o receptor enquanto apresentam alta eficiência espectral e de potência. Portanto, são necessárias técnicas avançadas de igualização no domínio da frequência. Uma vez que a complexidade de implementação dos terminais móveis deve ser tão baixa quanto possível, vamos transferir a maioria das exigências de processamento de sinal para a estação base e vamos usar sinais compatíveis com uma amplificação não linear eficiente. Por este motivo, vamos considerar modulações com desfasamento temportal que tenham uma envolvente constante ou praticamente constante e desenvolver receptores que consigam obter bons desempenhos. No entanto, estes sinais requerem uma largura de banda significativamente superior à de Nyquist, pelo que vamos também considerar a sobreposição de canais no domínio da frequência para reduzir a largura de banda necessária.

Palavras-chave: SC-FDE; Modulações com Offset; IB-DFE; IQI; ACI; CCI

CONTENTS

List of Figures

List of Tables

List of Acronyms

3GPP-LTE Third Generation Partnership Project - Long Term Evolution

ACI Adjacent-Channel Interference

BER Bit Error Rate

BiHDFE Bidirectional Hybrid Decision Feedback Equalizer

BPSK Binary Phase Shift Keying

BS Base Station

CCI Co-Channel Interference

CDMA Code Division Multiple Access

CI Conducted Interference

CP Cyclic Prefix

CPM Continuous Phase Modulation

DFE Decision feedback equalization

DFT Discrete Fourier Transform

ELHDFE ExtensionLess Hybrid Decision Feedback Equalizer

EMI Electromagnetic Interference

FDE Frequency Domain Equalization

FDMA Frequency Division Multiple Access

FFT Fast Fourier Transform

FSK Frequency Shift Keying

FT Fourier Transform

GMSK Gaussian Minimum Shift Keying

GSM Global System for Mobile Communications

HDFE Hybrid Decision Feedback Equalizer

HDFE-NP Hybrid Decision Feedback Equalizer with Noise Predictor

HPB High Protected Bit

I In-phase

IB-DFE Iterative Block Decision Feedback Equalizer

IB-DFE Iterative Block Decision Feedback Equalizer

IBI Inter Block Interference

IDFT Inverse Discrete Fourier Transform

ICI Inter-Carrier Interference

IFFT Inverse Fast Fourier Transform

IQI In-phase Quadrature Interference

ISI InterSymbol Interference

LPB Low Protected Bits

MFB Matched Filter Bound

MMSE Minimum Mean Square Error

MPB Medium Protected Bit

MSK Minimum Shift Keying

MT Mobile Terminal

MF-TDMA Multi-Frequency-Time Division Multiple Access

M-PSK M-ary Phase Shift Keying

M^2-OQAM M-ary Offset Quadrature Amplitude Modulation

M^2-QAM M-ary Quadrature Amplitude Modulation

OFDM Orthogonal Frequency Division Multiplexing

OQAM Offset Quadrature Amplitude Modulation

OQPSK Offset Quaternary Phase Shift Keying

PAM Pulse Amplitude Modulation

PAPR Peak-to-Average Power Ratio

PIC Parallel Interference Cancellation

PMEPR Peak-to-Mean Envelope Power Ratio

PN Pseudo Noise

PSK Phase Shift Keying

Q Quadrature

QAM Quadrature Amplitude Modulation

QPSK Quaternary Phase Shift Keying

SC Single Carrier

SCM Single Carrier Modulation

SC-FDE Single Carrier with Frequency Domain Equalization

SC-FDMA Single Carrier with Frequency Division Multiple Access

SIC Serial Iterative Cancellation

SIR Signal to Interference Ratio

SISO Soft Input Soft Output

SNIR Signal to Noise plus Interference Ratio

SNR Signal to Noise Ratio

TDDFE Time Domain Decision Feedback Equalizer

TCM Trellis Coded Modulation

UWB Ultra Wideband

WINNER Wireless INitiative NEw Radio

ZF Zero Forcing

LIST OF SYMBOLS

General Symbols

- a_n — n^{th} time-domain data symbol
  - a_n^I — real part of a_n ("in-phase bit")
  - a_n^Q — imaginary part of a_n ("quadrature bit")
  - $a_n^{(J)}$ — oversampled version of a_n
    - $a_n^{I(J)}$ — real part of $a_n^{(J)}$ (oversampled "in-phase bit")
    - $a_n^{Q(J)}$ — imaginary part of $a_n^{(J)}$ (oversampled "quadrature bit")
- $\widetilde{a}_n$ — estimate of a_n at the equalizer output
  - $\widetilde{a}_n^{(i)}$ — the i^{th} iteration of $\widetilde{a}_n$
  - $\widetilde{a}_n^I$ — real part of $\widetilde{a}_n$
  - $\widetilde{a}_n^Q$ — imaginary part of $\widetilde{a}_n$
  - $\widetilde{a}_n^{(J)}$ — oversampled version of $\widetilde{a}_n$
    - $\widetilde{a}_n^{I(J)}$ — real part of $\widetilde{a}_n^{(J)}$
    - $\widetilde{a}_n^{Q(J)}$ — imaginary part of $\widetilde{a}_n^{(J)}$
- $\widehat{a}_n$ — hard decision of $\widetilde{a}_n$
  - $\widehat{a}_n^{(i)}$ — the i^{th} iteration of $\widehat{a}_n$
  - $\widehat{a}_n^I$ — real part of $\widehat{a}_n$
  - $\widehat{a}_n^Q$ — imaginary part of $\widehat{a}_n$
  - $\widehat{a}_n^{(J)}$ — oversampled version of $\widehat{a}_n$
    - $\widehat{a}_n^{I(J)}$ — real part of $\widehat{a}_n^{(J)}$
    - $\widehat{a}_n^{Q(J)}$ — imaginary part of $\widehat{a}_n^{(J)}$
- $\overline{a}_n$ — soft decision of $\widetilde{a}_n$
  - $\overline{a}_n^{(i)}$ — the i^{th} iteration of $\overline{a}_n$
    - $\overline{a}_n^{I(i)}$ — real part of $\overline{a}_n^{(i)}$
    - $\overline{a}_n^{Q(i)}$ — imaginary part of $\overline{a}_n^{(i)}$
  - $\overline{a}_n^I$ — real part of $\overline{a}_n$
  - $\overline{a}_n^Q$ — imaginary part of $\overline{a}_n$
  - $\overline{a}_n^{(J)}$ — oversampled version of $\overline{a}_n$
    - $\overline{a}_n^{I(J)}$ — real part of $\overline{a}_n^{(J)}$
    - $\overline{a}_n^{Q(J)}$ — imaginary part of $\overline{a}_n^{(J)}$

$a_{n,u}$ n^{th} time-domain data symbol of the u^{th} user
- $a^{I}_{n,u}$ real part of $a_{n,u}$ ("in-phase bit")
- $a^{Q}_{n,u}$ imaginary part of $a_{n,u}$ ("quadrature bit")
- $a^{(J)}_{n,u}$ oversampled version of $a_{n,u}$
  - $a^{I(J)}_{n,u}$ real part of $a^{(J)}_{n,u}$
  - $a^{Q(J)}_{n,u}$ imaginary part of $a^{Q}_{n,u}$

$\widetilde{a}_{n,u}$ estimate of $a_{n,u}$ at the equalizer output
- $\widetilde{a}^{(i)}_{n,u}$ the i^{th} iteration of $\widetilde{a}_{n,u}$

$\widehat{a}_{n,u}$ hard decision of $\widetilde{a}_{n,u}$
- $\widehat{a}^{(i)}_{n,u}$ the i^{th} iteration of $\widehat{a}_{n,u}$
- $\widehat{a}^{I}_{n,u}$ real part of $\widetilde{a}_{n,u}$
- $\widehat{a}^{Q}_{n,u}$ imaginary part of $\widetilde{a}_{n,u}$

$\overline{a}_{n,u}$ soft decision of $\widetilde{a}_{n,u}$
- $\overline{a}^{(i)}_{n,u}$ the i^{th} iteration of $\overline{a}_{n,u}$
  - $\overline{a}^{I(i)}_{n,u}$ real part of $\overline{a}^{(i)}_{n,u}$
  - $\overline{a}^{Q(i)}_{n,u}$ imaginary part of $\overline{a}^{(i)}_{n,u}$
- $\overline{a}^{I}_{n,u}$ real part of $\overline{a}_{n,u}$
- $\overline{a}^{Q}_{n,u}$ imaginary part of $\overline{a}_{n,u}$

A_k k^{th} data symbol in the frequency domain
- A^{I}_{k} real part of A_k
- A^{Q}_{k} imaginary part of A_k
- $A^{(J)}_{k}$ oversampled version of A_k
  - $A^{I(J)}_{k}$ real part of $A^{(J)}_{k}$
  - $A^{Q(J)}_{k}$ imaginary part of $A^{(J)}_{k}$

$\widetilde{A}_k$ estimate of A_k at the equalizer output
- $\widetilde{A}^{(i)}_{k}$ the i^{th} iteration of $\widetilde{A}_k$
- $\widetilde{A}^{I}_{k}$ real part of $\widetilde{A}_k$
- $\widetilde{A}^{Q}_{k}$ imaginary part of $\widetilde{A}_k$
- $\widetilde{A}^{(J)}_{k}$ oversampled version of $\widetilde{A}_k$
  - $\widetilde{A}^{I(J)}_{k}$ real part of $\widetilde{A}^{(J)}_{k}$
  - $\widetilde{A}^{Q(J)}_{k}$ imaginary part of $\widetilde{A}^{(J)}_{k}$

$\widehat{A}_k$ hard decision of $\widetilde{A}_k$
- $\widehat{A}^{(i)}_{k}$ the i^{th} iteration of $\widetilde{A}_k$
- $\widehat{A}^{I}_{k}$ real part of $\widehat{A}_k$
- $\widehat{A}^{Q}_{k}$ imaginary part of $\widehat{A}_k$
- $\widehat{A}^{(J)}_{k}$ oversampled version of $\widehat{A}_k$
  - $\widehat{A}^{I(J)}_{k}$ real part of $\widehat{A}^{(J)}_{k}$
  - $\widehat{A}^{Q(J)}_{k}$ imaginary part of $\widehat{A}^{(J)}_{k}$

$\overline{A}_k$ soft decision of $\widetilde{A}_k$
- $\overline{A}^{(i)}_{k}$ the i^{th} iteration of $\overline{A}_k$

$\overline{A}_k^I$ real part of $\overline{A}_k$

$\overline{A}_k^Q$ real part of $\overline{A}_k$

$\overline{A}_k^{(J)}$ oversampled version of $\overline{A}_k$

$\overline{A}_k^{I(J)}$ real part of $\overline{A}_k^{(J)}$

$\overline{A}_k^{Q(J)}$ imaginary part of $\overline{A}_k^{(J)}$

$A_{k,u}$ k^{th} frequency-domain data symbol of the u^{th} user

$A_{k,u}^{(i)}$ the i^{th} iteration of $A_{k,u}$

$A_{k,u}^I$ real part of $A_{k,u}$ ("in-phase bit")

$A_{k,u}^Q$ imaginary part of $A_{k,u}$ ("quadrature bit")

$A_{k,u}^{(J)}$ oversampled version of $A_{k,u}$

$A_{k,u}^{I(J)}$ real part of $A_{k,u}^{(J)}$

$A_{k,u}^{Q(J)}$ imaginary part of $A_{k,u}^{(J)}$

$\widetilde{A}_{k,u}$ estimate of $A_{k,u}$ at the equalizer output

$\widetilde{A}_{k,u}^{(i)}$ the i^{th} iteration of $\widetilde{A}_{k,u}$

$\widehat{A}_{k,u}$ hard decision of $\widetilde{A}_{k,u}$

$\widehat{A}_{k,u}^{(i)}$ the i^{th} iteration of $\widehat{A}_{k,u}$

$\overline{A}_{k,u}$ soft decision of $\widetilde{A}_{k,u}$

$\overline{A}_{k,u}^{(i)}$ the i^{th} iteration of $\overline{A}_{k,u}$

$\overline{A}_{k,u}^{I(i)}$ real part of $\overline{A}_{k,u}^{(i)}$

$\overline{A}_{k,u}^{Q(i)}$ imaginary part of $\overline{A}_{k,u}^{(i)}$

$\overline{A}_{k,u}^I$ real part of $\overline{A}_{k,u}$

$\overline{A}_{k,u}^Q$ imaginary part of $\overline{A}_{k,u}$

$\overline{A}_{k,u}^{(J)}$ oversampled verseion of $\overline{A}_{k,u}$

A_c carrier wave amplitude

$b_n^{(m)}$ m^{th} bit of the n^{th} data symbol

$b_n^{I(m)}$ m^{th} in-phase bit of the n^{th} data symbol

$b_n^{Q(m)}$ m^{th} quadrature bit of the n^{th} data symbol

$\overline{b}_n^{(m)}$ soft decision of the m^{th} bit of the n^{th} data symbol

$\overline{b}_n^{I(m)}$ soft decision of the m^{th} in-phase bit of the n^{th} data symbol

$\overline{b}_n^{Q(m)}$ soft decision of the m^{th} quadrature bit of the n^{th} data symbol

$\widehat{b}_n^{(m)}$ hard decision of the m^{th} bit of the n^{th} data symbol

B bandwidth

B_k feedback equalizer coefficient for the k^{th} frequency-domain symbol

$B_k^{(i)}$ the i^{th} iteration of B_k

$B_k^{(J)}$ oversampled version of B_k

$B_{k,u}$ feedback equalizer coefficient for the k^{th} frequency and u^{th} user

$B_{k,u}^{(i)}$ the i^{th} iteration of $B_{k,u}$

$B_{k,u,p}$ feedback equalizer coefficient for the k^{th} frequency and u^{th} user relative to the p^{th} user

$B_{k,u,p}^{(i)}$ the i^{th} iteration of $B_{k,u,p}$
$B_{k,u,p}^{(J)}$ oversampled version of $B_{k,u,p}$
E_b average bit energy
$E_k^{(J)}$ sub-part of feedforward equalization
F_k feedforward equalizer coefficient for the k^{th} frequency
$F_k^{(i)}$ the i^{th} iteration of F_k
$F_k^{(J)}$ oversampled version of F_k
$F_{k,u}$ feedforward equalizer coefficient for the k^{th} frequency and u^{th} user
$F_{k,u}^{(i)}$ the i^{th} iteration of $F_{k,u}$
$F_{k,u}^{(J)}$ the oversampled version of $F_{k,u}$
f frequency
$f(t)$ feedforward equalizer
f_c sub-carrier frequency
f_u sub-carrier frequency for the u^{th} user
G value regarding constellation size: $G = log_2(M)$
$h(t)$ time domain overall channel response
H_k overall channel frequency response for the k^{th} frequency
$H_k^{(J)}$ oversampled version of H_k
$H_k^{(MB)(J)}$ minimum band of the channel impulse response with the highest power of the transmitter
$\breve{H}_k^{(J)}$ channel impulse response for the k^{th} frequency
$H_{k,u}$ channel frequency response for the k^{th} frequency and u^{th} user
$H_{k,u}^{(J)}$ oversampled version of $H_{k,u}$
$\breve{H}_{k,u}^{(J)}$ channel impulse response for the k^{th} frequency and u^{th} user
i iteration number
I in-phase
I_k frequency domain residual ISI for the k^{th} frequency
J oversampling factor
k frequency index
L Lagrangian function
M value regarding constellation size (ex. M^2-QAM)
n discrete time index
N number of samples/subcarriers
N_0 noise power espectral density
N_{cp} number of cyclic prefix samples
N_{FF} number of feedforward taps
N_{FB} number of feedback taps
N_I number of iterations
N_k channel frequency noise for the k^{th} frequency
$N_k^{(J)}$ oversampled version of N_k

$p(t)$ impulsive response after the reconstruction filter

$p_n^{(J)}$ n^{th} oversampled impulse response after the reconstruction filter

P (I)FFT size

$P(f)$ frequency domain impulse response after the reconstruction filter

P_k k^{th} frequency response after the reconstruction filter

$P_k^{(J)}$ oversampled version of P_k

P_k^{eq} equivalent equalized channel for a signal with N samples

$P_k^{Q,eq}$ quadrature version of P_k^{eq}

$P_k^{Q,even}$ even part of $P_k^{Q,eq}$

$P_k^{Q,odd}$ odd part of $P_k^{Q,eq}$

q oversampling index

Q quadrature

$r(t)$ shaping pulse

$r_n^{(J)}$ oversampled shaping pulse for the transmitted signal

$R(f)$ Fourier transform of $r(t)$

$R_k^{(J)}$ oversampled version of R_k

$R_k^{(MB)(J)}$ minimum band of the shaping pulse with the highest power

R_s symbol rate

$s(t)$ transmitted signal

$s_u(t)$ transmitted signal for the u^{th} user

t time variable

T_s symbol duration

T_o quadrature time offset

u user index

U number of users

$x(t)$ time-domain signal's complex envelope

$x_g(t)$ g^{th} OQPSK component obtained from the decomposition of M^2-QAM constellation

$x_u(t)$ time-domain signal's complex envelope for the u^{th} user

$X(f)$ Fourier transform of $x(t)$

X_k discrete Fourier transform of x_n

$X_k^{(J)}$ oversampled version of X_k

y_n n^{th} received sample

$y(t)$ received signal

Y_k received sample for the k^{th} frequency

$Y_k^{(J)}$ oversampled version of Y_k

$\overline{Y}_k^{I(J)}$ overall received oversampled frequency values for in-phase signal component

$\overline{Y}_k^{Q(J)}$ overall received oversampled frequency values for quadrature signal component

Greek Letters Symbols

$\Delta\theta$ phase deviation
ΔG gain deviation
$\Delta_k^{(i)}$ error term for the k^{th} frequency
$\Delta_{k,u}$ error term for the k^{th} frequency and u^{th} user
$\Delta_{k,u}^{(i)}$ the i^{th} iteration of $\Delta_{k,u}$
Θ_k result from T_o time shift in the k^{th} frequency
α inverse of the signal-to-noise ratio
β raised cosine roll-off factor
Δf sub-carrier separation
$\delta_n^{eq(i)}$ error term for the n^{th} data estimate of the IB-DFE equalizer at the i^{th} iteration
$\gamma^{(i)}$ average channel frequency response at the i^{th} iteration
γ_u average channel frequency response for the u^{th} user
$\gamma_u^{(i)}$ the i^{th} iteration of γ_u
$\varepsilon_k^{eq(i)}$ overall error for the k^{th} frequency-domain symbol
κ normalization factor
$\kappa^{(i)}$ the i^{th} iteration of κ
κ_u normalization factor for the u^{th} user
$\kappa_u^{(i)}$ the i^{th} iteration of κ_u
$\lambda^{(i)}$ Lagrangian multiplier at the i^{th} iteration
λ_u Lagrangian multiplier for the u^{th} user
$\lambda_u^{(i)}$ the i^{th} iteration of λ_u
λ_k Lagrangian multiplier for the k^{th} frequency I-Q interference cancellation
λ^{clip} limiting factor of λ_k
λ_k^{clip} limited version of λ_k
$\Lambda_n^{(m)}$ log-likelihood ratio for the m^{th} bit of the n^{th} symbol
$\Lambda_n^{I(m)}$ real part of $\Lambda_n^{(m)}$
$\Lambda_n^{Q(m)}$imaginary part of $\Lambda_n^{(m)}$
Λ_n^I in-phase log-likelihood ratio for the n^{th} symbol
$\Lambda_n^{I(i)}$ the i^{th} iteration of Λ_n^I
Λ_n^Q quadrature log-likelihood ratio for the n^{th} symbol
$\Lambda_n^{Q(i)}$ the i^{th} iteration of Λ_n^Q
$\Lambda_{n,u}^I$ in-phase log-likelihood ratio for the n^{th} symbol for the u^{th} user

$\Lambda_{n,u}^{I(i)}$ the i^{th} iteration of $\Lambda_{n,u}^{I}$

$\Lambda_{n,u}^{Q}$ quadrature log-likelihood ratio for the n^{th} symbol for the u^{th} user

$\Lambda_{n,u}^{Q(i)}$ the i^{th} iteration of $\Lambda_{n,u}^{Q}$

$\varphi^{(g)}$ resolution of the g^{th} bit for hierarchic constellations

ϕ quadrature phase deviation ratio

ϕ_n phase deviation for the n^{th} symbol

Φ interval of N samples with the highest power at the transmitter

$\Phi_{1/-1}^{(m)}$ constellations' subset associated with the symbols' m^{th} bit at 1 or -1

$\Psi_k^{(a)}$ set of the (a) frequencies group for OQAM and OQPSK equalization

ρ correlation coefficient regarding block wise reliability

$\rho^{(i)}$ the i^{th} iteration of ρ

$\rho_n^{(m)}$ correlation coefficient of the m^{th} bit of the n^{th} symbol

$\rho_n^{I(m)}$ correlation coefficient regarding the real part of $\rho_n^{(m)}$

$\rho_n^{Q(m)}$ correlation coefficient regarding the imaginary part of $\rho_n^{(m)}$

ρ_u correlation coefficient of the u^{th} user

$\rho_u^{(i)}$ the i^{th} iteration of ρ_u

σ_N^2 channel noise variance

σ_S^2 symbol variance

$\sigma_{S,u}^2$ symbol variance of the u^{th} user

$\sigma_{N,u}^2$ noise variance of the u^{th} user

$\sigma_{N,u}^{(i)\ 2}$ the i^{th} iteration of $\sigma_{N,u}^2$

Matrix Symbols

$\widetilde{\boldsymbol{a}}_n$ estimation matrix regarding the sent data symbols

$\widehat{\boldsymbol{a}}_n$ hard decision matrix of $\widetilde{\boldsymbol{a}}_n$

$\overline{\boldsymbol{a}}_n$ hard decision matrix of $\widetilde{\boldsymbol{a}}_n$

$\boldsymbol{A}_k$ k^{th} data symbol vector in the frequency domain

$\boldsymbol{A}_k^{(J)}$ oversampled version of $\boldsymbol{A}_k$

$\widetilde{\boldsymbol{A}}_k$ estimate of $\boldsymbol{A}_k$ at the equalizer output

$\widetilde{\boldsymbol{A}}_k^{(i)}$ the i^{th} iteration of $\widetilde{\boldsymbol{A}}_k$

$\widetilde{\boldsymbol{A}}_k^{I(i)}$ real part of $\widetilde{\boldsymbol{A}}_k^{(i)}$

$\widetilde{\boldsymbol{A}}_k^{Q(i)}$ imaginary part of $\widetilde{\boldsymbol{A}}_k^{(i)}$

$\widetilde{\boldsymbol{A}}_k^{(J)}$ oversampled version of $\widetilde{\boldsymbol{A}}_k$

$\widehat{\boldsymbol{A}}_k$ soft decisions of $\widetilde{\boldsymbol{A}}_k$

$\widehat{\boldsymbol{A}}_k^{(i)}$ the i^{th} iteration of $\widehat{\boldsymbol{A}}_k$

$\widehat{\boldsymbol{A}}_k^{I(i)}$ real part of $\widehat{\boldsymbol{A}}_k^{(i)}$

$\widehat{\boldsymbol{A}}_k^{Q(i)}$ imaginary part of $\widehat{\boldsymbol{A}}_k^{(i)}$
$\widehat{\boldsymbol{A}}_k^{(J)}$ oversampled version of $\widehat{\boldsymbol{A}}_k$
$\overline{\boldsymbol{A}}_k$ soft decisions of $\widetilde{\boldsymbol{A}}_k$
$\overline{\boldsymbol{A}}_k^{(i)}$ the i^{th} iteration of $\overline{\boldsymbol{A}}_k$
$\overline{\boldsymbol{A}}_k^{I(i)}$ real part of $\overline{\boldsymbol{A}}_k^{(i)}$
$\overline{\boldsymbol{A}}_k^{Q(i)}$ imaginary part of $\overline{\boldsymbol{A}}_k^{(i)}$
$\overline{\boldsymbol{A}}_k^{(J)}$ oversampled version of $\overline{\boldsymbol{A}}_k$
$\boldsymbol{B}_k$ feedback equalizer coefficient matrix for the k^{th} user
$\boldsymbol{B}_k^{(J)}$ oversampled version of $\boldsymbol{B}_k$
$\boldsymbol{B}_k^{(i)}$ the i^{th} iteration of $\boldsymbol{B}_k$
$\boldsymbol{B}_{k,u}$ feedback equalizer coefficient matrix for the u^{th} user
$\boldsymbol{B}_{k,u}^{(i)}$ the i^{th} iteration of $\boldsymbol{B}_{k,u}$
$\boldsymbol{e}$ error matrix associated with the data symbols' estimation for every user
$\boldsymbol{F}_k$ feedforward equalizer coefficient matrix for the k^{th} frequency
$\boldsymbol{F}_k^{(J)}$ oversampled version of $\boldsymbol{F}_k$
$\boldsymbol{F}_k^{(i)}$ the i^{th} iteration of$\boldsymbol{F}_k$
$\boldsymbol{F}_{k,u}$ feedforward equalizer coefficient matrix for the u^{th} user
$\boldsymbol{F}_{k,u}^{(i)}$ the i^{th} iteration of $\boldsymbol{F}_{k,u}$
$\boldsymbol{K}$ normalization factor matrix
$\boldsymbol{K}^{(i)}$ the i^{th} iteration of $\boldsymbol{K}$
$\boldsymbol{K}_u$ normalization factor matrix for the u^{th} user
$\boldsymbol{K}_u^{(i)}$ the i^{th} iteration of $\boldsymbol{K}_u$
$\boldsymbol{H}_k$ channel frequency response matrix
$\boldsymbol{H}_k^{(J)}$ oversampled version of $\boldsymbol{H}_k$
$\breve{\boldsymbol{H}}_k^{(J)}$ channel impulse response matrix for the k^{th} frequency
$\boldsymbol{H}_{k,u}$ channel frequency response matrix for the u^{th} user
$\breve{\boldsymbol{H}}_{k,u}^{(J)}$ channel impulse response matrix for the k^{th} frequency and u^{th} user
$\boldsymbol{I}_x$ identity x by x matrix
$\boldsymbol{N}_k$ channel frequency noise vector
$\boldsymbol{R}_N$ expected value of the correlation between the noise symbols
$\boldsymbol{R}_S$ expected value of the correlation between the data symbols
$\boldsymbol{R}_\Delta$ expected value of the correlation between the data symbols' estimation
$\boldsymbol{R}_\Delta^{(i)}$ the i^{th} iteration of $\boldsymbol{R}_\Delta$
$\boldsymbol{Y}_k$ received samples vector
$\overline{\boldsymbol{Y}}_k^{I(i)}$ soft decision of $\boldsymbol{Y}_k^I$ at the i^{th} iteration
$\overline{\boldsymbol{Y}}_k^{Q(i)}$ soft decision of $\boldsymbol{Y}_k^Q$ at the i^{th} iteration
$\boldsymbol{\alpha}$ matrix with the inverse of the signal to noise ratio
$\boldsymbol{\Delta}_k$ error terms matrix

$\boldsymbol{\Delta}_k^{(i)}$ the i^{th} iteration of $\boldsymbol{\Delta}_k$

$\boldsymbol{\Gamma}$ average channel frequency response matrix

$\boldsymbol{\Gamma}^{(i)}$ the i^{th} iteration of $\boldsymbol{\Gamma}$

$\boldsymbol{\Gamma}_u$ average channel frequency response vector for the u^{th} user

$\boldsymbol{\Gamma}_u^{(i)}$ the i^{th} iteration of $\boldsymbol{\Gamma}_u$

$\boldsymbol{\lambda}^{(i)}$ Lagrangian coefficients matrix at the i^{th} iteration

$\boldsymbol{\lambda}_u^{(i)}$ Lagrangian coefficients vector for the u^{th} user at the i^{th} iteration

$\boldsymbol{\Theta}_k$ result from T_Q time shift in the k^{th} frequency matrix

$\boldsymbol{\Omega}^{(i)}$ correlation coefficient matrix at the i^{th} iteration

$\boldsymbol{\Omega}_u$ correlation coefficient matrix for the u^{th} user

$\boldsymbol{\rho}$ correlation coefficient matrix for block wise reliability

$\boldsymbol{\rho}^{(i)}$ the i^{th} iteration of $\boldsymbol{\rho}$

Common Operators

$x \bmod y$	reminder of the division of x by y
$\mathrm{Re}\{x\}$	real part of x
$\mathrm{Im}\{x\}$	imaginary part of x
x^*	conjucate of x
$\partial x/\partial y$	partial derivative of x regarding y
$E[x]$	expected value of x
$O(x)$	complexity order regarding x complex multiplications
∇	nabla operator
$\boldsymbol{A}^T$	transpose of matrix $\boldsymbol{A}$
$\boldsymbol{A}^*$	conjugate of matrix $\boldsymbol{A}$
$\boldsymbol{A}^H$	hermitian of matrix $\boldsymbol{A}$
$\mathrm{FT}\{x\}$	Fourier transform of x
$\mathrm{DFT}\{x\}$	Discrete Fourier transform of x
$\mathrm{IDFT}\{x\}$	Inverse discrete Fourier transform of x
$\mathrm{FFT}\{x\}$	Fast Fourier transform of x
$\mathrm{IFFT}\{x\}$	Inverse fast Fourier transform of x
$\mathrm{rect}(x)$	rect funcion of x
$\mathrm{sinc}(x)$	sinc funcion of x
$\tanh(x)$	hyperbolic tangent of x

CHAPTER 1

INTRODUCTION

Broadband wireless systems are expected to have high power and spectral efficiency and can be subjected to severely time-dispersive channels, due to multi-path signal propagation between the transmitter and the receiver. Future systems must be able to surpass these challenges using advanced equalization techniques to compensate the high level of signal distortion and obtain high bit rates. DFE is a good alternative to linear equalization, with better performance and slight increased complexity due to high channel impulse response lengths that make time-domain equalization inadequate, since their complexity grow linearly with the length of the channel impulse response [Ben+10]. This justifies the use of block transmission techniques with FDE [Fal+02; Ga+00] where the complexity per data symbol is lower and somewhat independent from the length of the channel impulse response.

Single Carrier (SC) transmission schemes employing FDE and OFDM [Cim85; Sar+94a] have become popular and are advisable to be used in future wireless communication systems to deal with severely time-dispersive channels, since their complexity grows only logarithmically with the block length.

At the uplink transmission, these challenges increase with the limited power consumption of the Mobile Terminal (MT) as to preserve battery power. Consequently, the MT shall resort to low cost and high efficient power amplification, focusing the signal processing load and power amplification complexity at the Base Station (BS). Grossly nonlinear amplification is only advisable when quasi-constant envelope modulations are employed. To achieve constant envelope, we need to consider Continuous Phase Modulation (CPM) like MSK, and Gaussian Minimum Shift Keying (GMSK). OQPSK is a special version of QPSK modulation where the envelope fluctuation is also quasi-constant [GM76]. The same principle can be apply to OQAM and QAM signals [Mon+11], specially for the case of 4-OQAM and 4-QAM, where the envelope fluctuations are comparable to those of QPSK signals. For higher constellation sizes, the signals will no longer have quasi-constant

envelop and will need to be dealt with accordingly .

By using SC-FDE schemes, it is possible to achieve a complexity transfer from the MT to the BS in terms of signal processing, reducing the transmitter block complexity. Therefore, it is advisable to use this scheme in the uplink of the MT to preserve battery power as well as to keep the hardware's complexity low. Combined with efficient nonlinear equalization techniques: a linear filter to remove part of the intersymbol interference followed by a feedback interference cancellation using previously detected data, these techniques provide similar capacity than OFDM in highly time-dispersive channels. [BT02b]

1.1 Research Question, Hypothesis and Approach

The objective of this thesis is to design transmission schemes that have very low BER and good spectral efficiency, using signals compatible with an efficient and low-cost power amplification subjected to severely time dispersive channels. Therefore, the research question of this thesis is: "Is it possible to have low complexity transmission schemes with high power and spectral efficiency?".

The main concerns of this thesis are the maximization of power and spectral efficiency. The first problem, power efficiency, will be tackled by combining the design of pulse shape and OQPSK-type signals with different number of constellation points, decomposing them into sub OQPSK constellations with constant envelope able to sustain nonlinear amplification and designing receivers employing iterative equalization based on Iterative Block Decision Feedback Equalizers (IB-DFEs) integrated with Soft Input Soft Output (SISO) decoders, to achieve very low BER. The former, spectral efficiency, will be approached by combining those special pulse shape designs, capable of going through a low cost nonlinear amplifier without suffering major bandwidth regrowth, with the overlap of frequency channels to overcome the fact that quasi-constant envelop modulations require bandwidths higher than the Nyquist rate. The design of this receiver should allow an efficient equalization, capable of overcoming highly distorted channels, overlapped channel spectrum and offset modulations. Therefore, the hypothesis of this thesis is: "By combining offset schemes with frequency domain processing and overlapping several frequency channel users, it is possible to improve spectral efficiency while preserving transmission performance.".

1.2 Outline

The thesis is organized as follows: after this brief introduction, chapter 2 presents the state of the art, some transmission techniques principles and interference types. Chapter 3 deals with the frequency domain equalization of OQPSK signals and presents several methods to reduce and eliminate interference between the in-phase and quadrature signals. In chapter 4, pragmatic receivers are designed to achieve good performances for higher order OQAM constellations and in chapter 5, equalization techniques from the previous

chapters will be extended to cope with frequency division multiple access subjected to both strong ACI and Co-Channel Interference (CCI). Final conclusions and remarks are made in chapter 6, as well as some outlines about future work.

1.3 Major Contributions

The major contributions from this work are the creation of a seamless receiver capable of successfully equalizing SC-FDE signals using offset modulations for any given M^2-OQAM constellation and several linear and nonlinear equalization methods were developed for OQPSK, OQAM and M^2-OQAM, with very good BER results, even for very high-order constellations. Furthermore, the pursuit of increased spectral efficiency lead to systems with severe ACI and CCI. Our receivers are also capable of mitigating the interference produced by these interfering channels. Part of the work presented in this thesis was published in two journal publications:

1. Luzio, M. ; Dinis, R. ; Montezuma, P. *Pragmatic Frequency Domain Equalization for Single Carrier with Offset Modulations*, IEEE Transactions on Wireless Communications, Volume: 12, Issue: 9 , 2013;

2. Luzio, M. ; Dinis, R. ; Montezuma, P. *SC-FDE for Offset Modulations: An Efficient Transmission Technique for Broadband Wireless Systems*, IEEE Transactions on Communications, Volume: 60, Issue: 7 , 2012;

and in ten conferences:

1. Luzio, M. ; Dinis, R. ; Montezuma, P. *Low Complexity Multiple User Detection for SC-FDE with OQPSK Signals*, IEEE International Conference on Telecommunications & Multimedia, 2014.

2. Luzio, M. ; Dinis, R. ; Montezuma, P. *A Pragmatic Design of Frequency-Domain Equalizers for Offset Modulations*, IEEE Vehicular Technology Conference (VTC Fall), 2012;

3. Luzio, M. ; Dinis, R. ; Montezuma, P. ; Astucia, V. ; Beko, M. *Efficient receivers for SC-FDE with offset modulations*, Military Communications Conference, 2012;

4. Luzio, M. ; Dinis, R. ; Montezuma, P. *On the Use of Multiple Grossly Nonlinear Amplifiers for an Efficient Amplification of OQAM Signals with FDE Receivers*, IEEE Vehicular Technology Conference (VTC Fall), 2011;

5. Montezuma, P. ; Dinis, R. ; Luzio, M. *Power efficient coded 16-OQAM schemes over nonlinear transmitters*, IEEE Sarnoff Symposium, 2011;

6. Dinis, R. ; Luzio, M. ; Montezuma, P. *On the design of frequency-domain equalizers for OQPSK modulations*, IEEE Sarnoff Symposium, 2010;

7. Luzio, M. ; Dinis, R. ; Montezuma, P. *On the Design of Linear Receivers for SC-FDE Schemes Employing OQPSK Modulation*, IEEE Vehicular Technology Conference Fall (VTC 2010-Fall), 2010;

8. Luzio, M. ; Dinis, R. ; Montezuma, P. *On the design of iterative FDE receivers for OQAM modulations*, IEEE GLOBECOM Workshops (GC Wkshps), 2010;

9. Montezuma, P. ; Dinis, R. ; Luzio, M. *Analytical characterization of nonlinearly distorted TC-OQAM signals*, 3rd International Conference on Signal Processing and Communication Systems, 2009;

10. Luzio, M. ; Dinis, R. ; Montezuma, P. *Frequency-domain parallel multiuser detection for quasi-constant envelope OQPSK schemes with high spectral efficiency*, 3rd International Conference on Signal Processing and Communication Systems, 2009.

CHAPTER 2

LITERATURE REVIEW

2.1 Introduction

The most important aspects for Broadband wireless systems are high power and spectral efficiency. Nevertheless, the high transmission rates associated to these systems cause multi-path propagation and often lead to severe time-dispersion effects. One consequence of channel effects can be the introduction of interference. To cope with interference two solutions are possible: to increase the transmitted power or to maximize the power and spectral efficiency of the system. From [IEE09], the first solution falls short, since the transmitted power is already constricted to prohibitive levels. Moreover, increasing the transmitted power only solve external interference (from other systems), all the internal interference (generated within our system) due to other signal components will remain unaffected. In the second one, internal and external interference can be reduced without increments on the transmitted power, but will require very efficient transmission techniques [Kim+03]: Not only conventional spatial diversity techniques [Din+04; FG98; RC98], but also unconventional multiple access schemes [Din+05; Luz+09], effective equalization methods [Sar+94b; WE71], novel modulations [Mon+09], error correction models [CF07] and even distributed antenna techniques [Ada+09].

2.2 Interference Types

There are several kinds of interference: InterSymbol Interference (ISI), In-phase Quadrature Interference (IQI), Adjacent-Channel Interference (ACI), Co-Channel Interference (CCI), Inter-Carrier Interference (ICI), Conducted Interference (CI), and Electromagnetic Interference (EMI). Every single one, despite their different origins, alters, modifies or disrupts the signal and should be either avoided, by planning the communication system in a specific

way, or compensated using efficient equalization. The compensation of ISI, IQI, ACI, and CCI will be one of the main focus of this work.

2.2.0.1 InterSymbol Interference

As the name implies, ISI refers to the interference that each symbol causes on the subsequent ones. This effect occurs when multi-path propagation is present, where symbols will arrive at different times and with amplitude and phase variations due to reflection and refraction. Another common cause of ISI are band limited channels, channels that have a cut-off frequency. This is easily understood since any signal that has a limited frequency spectrum will be infinite in time [Tra+07]. Equalization is the best technique to compensate ISI effects, since increasing the transmitted power will also increases the power level of the interfering symbols.

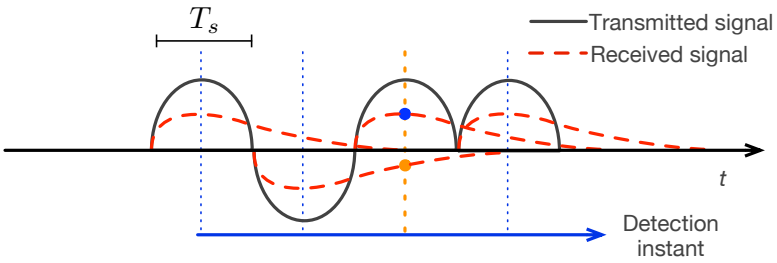

Figure 2.1: InterSymbol Interference.

2.2.0.2 In-phase Quadrature Interference

This effect appears mostly when the In-phase (I) and Quadrature (Q) components of a signal are not aligned in time, for example, in an offset modulation. If the I and Q components have an inherent time delay, they will be sampled at different instants at the receiver. As a consequence of multi-path propagation, the support pulse at the equalizer's output can become complex and the I component will interfere with the Q component. Therefore, this kind of interference, IQI, will appear, lowering the overall performance of the system [Luz+10b].

2.2.0.3 Adjacent-Channel Interference

Adjacent-Channel Interference can be caused either by an external signal that still has transmitting power on an adjacent channel or due the interference from adjacent channels in a multi-carrier signal (such as the Multi-Frequency-Time Division Multiple Access (MF-TDMA) scheme). There are several reasons that drive this type of interference. The most common ones are nonlinear distortion introduced by a high power amplifier, poor filtering and poor frequency planning [Tra+07]. The last one can be avoided through proper frequency planning (this is the case of Global System for Mobile Communications (GSM)

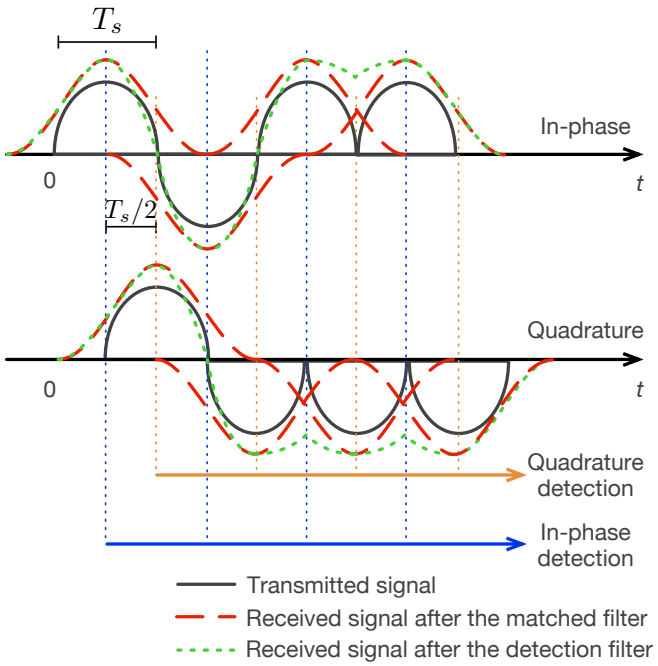

Figure 2.2: In-phase Quadrature Interference.

where the frequency planning is done to avoid ACI[1]). For the other causes, when a system suffers ACI it is possible to mitigate its effect by using equalization techniques if the receiver has some knowledge about the interfering signals [Din+05; Luz+09].

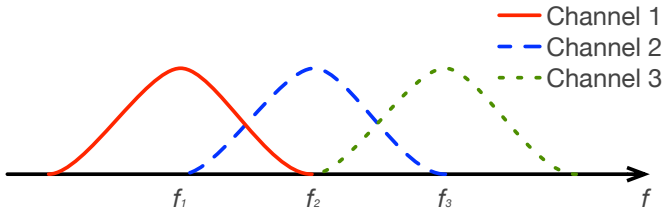

Figure 2.3: Adjacent-Channel Interference.

2.2.0.4 Co-Channel Interference

Co-Channel Interference, also known by crosstalk, is the interference produced by two different signals that coexist in the same frequency channel. This kind of interference can materialize with poor frequency planning and in an over crowded open spectrum, also known as unlicensed radio frequency spectrum. Technologies that use Ultra Wide-band (UWB) or spread spectrum techniques often suffer from this interference. In spread

[1]Frequency planing imposes restrictions to carrier allocation in each serving area. This compromises the efficient spectrum usage.

spectrum systems as UWB and Code Division Multiple Access (CDMA) this kind of interference can be avoided through the right selection of the spreading codes used by the different users. Even so, due to impairments on the codes, there is always some residual interference that limits the maximum number of users allowed in a specific region.

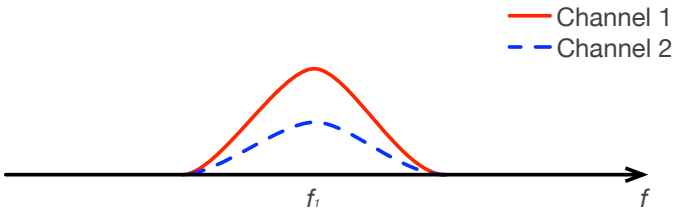

Figure 2.4: Co-Channel Interference.

2.2.0.5 Inter-Carrier Interference

This type of interference is inherent to OFDM systems and is cause by the existence of frequency offset caused by the Doppler shift [Mol11]. Several techniques exist that can effectively mitigate the ICI [LH09; Nik+09].

2.2.0.6 Other types of interference

Other types of interference are the CI and EMI. The Conducted Interference is an undesired voltage or current generated within, or conducted into, a receiver, transmitter, or associated equipment, and appearing at the antenna terminals. The Electromagnetic Interference is a disturbance that affects an electrical circuit due to either electromagnetic induction or electromagnetic radiation emitted from an external source [PS02]. The source of this interference can be any object that carries rapid changes of electric current. This type of interference is often used to produce radio jamming.

2.3 Bit Modulation

A sinusoidal wave can be modulated by a digital signal on its amplitude, frequency or phase. In this section some phase and amplitude modulation are considered, more specifically Phase Shift Keying (PSK) and QAM, due to their lower envelope fluctuations and the absence of spectral lines inherent to Frequency Shift Keying (FSK), which allows these schemes to have better power efficiency.

2.3.1 Binary Phase Shift Keying

The Binary Phase Shift Keying (BPSK) contains phase shifts of $\pm\pi$ radians. The waveform of a BPSK signal is shown in Figure 2.5. This modulation can be expressed as

$$s(t) = x(t)\cos\left(2\pi f_c t\right), \tag{2.1}$$

where $x(t)$ is the baseband component described by

$$x(t) = \sum_n a_n \, r\left(t - nT_s\right), \tag{2.2}$$

and $r(t)$ denotes the transmitted pulse shape[1] and $a_n = \pm 1$ as the phase shifting factor[2]. T_s denotes the symbol duration and f_c the carrier frequency.

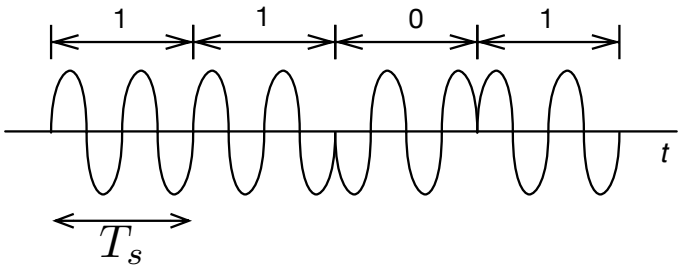

Figure 2.5: BPSK waveform.

2.3.2 Quaternary Phase Shift Keying

A Quaternary Phase Shift Keying (QPSK) can be regarded as the sum of two BPSK signals in quadrature. This modulation, shown in the left side of Figure 2.6, can be described as

$$s(t) = \mathrm{Re}\left\{x(t)e^{2\pi f_c t}\right\} \tag{2.3}$$

$$x(t) = \textstyle\sum_n a_n^I \, r\left(t - nT_s\right) + j\sum_n a_n^Q \, r\left(t - nT_s\right), \tag{2.4}$$

with $a_n^I = \pm 1$ as the in-phase bit and $a_n^Q = \pm 1$ as the quadrature bit.

2.3.3 Offset Quaternary Phase Shift Keying

Staggered or Offset Quaternary Phase Shift Keying (OQPSK) were defined to reduce envelope variations [GM76]. A typical nonlinear amplifier will flatten out these envelope fluctuations, and will increase the bandwidth due to spectral regrowth [CC09]. The OQPSK signal can be characterized in the same way as (2.3), where

$$x(t) = \sum_n a_n^I \, r\left(t - nT_s\right) + j\sum_n a_n^Q \, r\left(t - nT_s - T_o\right), \tag{2.5}$$

where T_o is the time offset between components and is usually $T_s/2$ seconds, $a_n^I = \pm 1$ and $a_n^Q = \pm 1$.

With the time delay between components, the phase of the OQPSK can never shift more than $\pm\pi/2$ radians. This means that the zero-crossing existent in the envelope of a QPSK signal will never happens in an OQPSK signal, resulting in smaller envelope fluctuation

[1] Support pulses will be detailed in section 2.4.
[2] Note that $cos(t + \pi) = -cos(t)$.

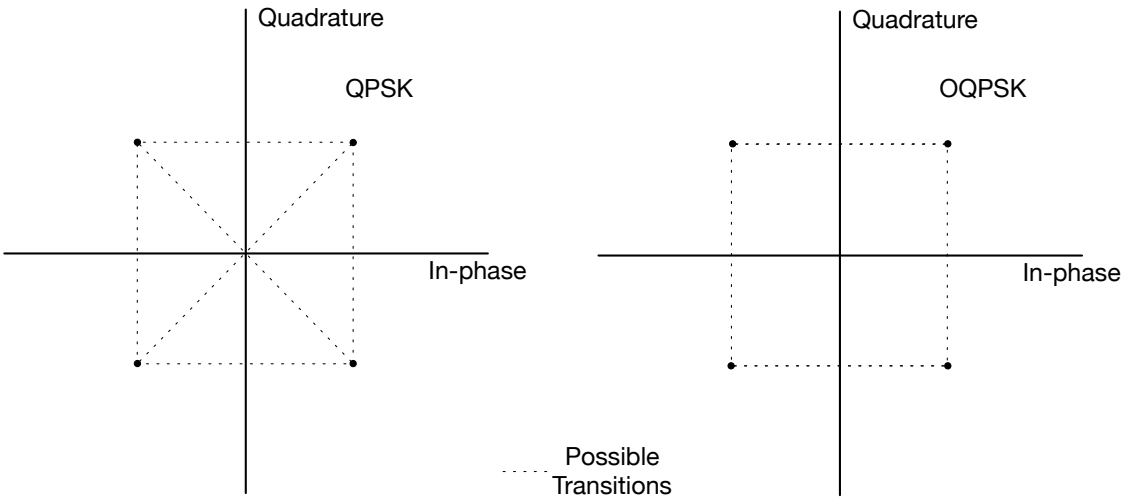

Figure 2.6: QPSK signal constellation (left) and OQPSK signal constellation (right).

(Figure 2.6). These signals are able to go through a grossly nonlinear amplification without suffering neither strong nonlinear distortion nor spectral regrowth, and therefore, are a good choice when power-efficient and low cost amplification is intended [GM76].

2.3.4 M-ary Phase Shift Keying

In an M-ary Phase Shift Keying (M-PSK) the phase of the signal can have M different values. In this modulation, the different symbols are equispaced by $2\pi/M$ radians, as illustrated in its I-Q diagram (Figure 2.7). This system can be characterized in the following

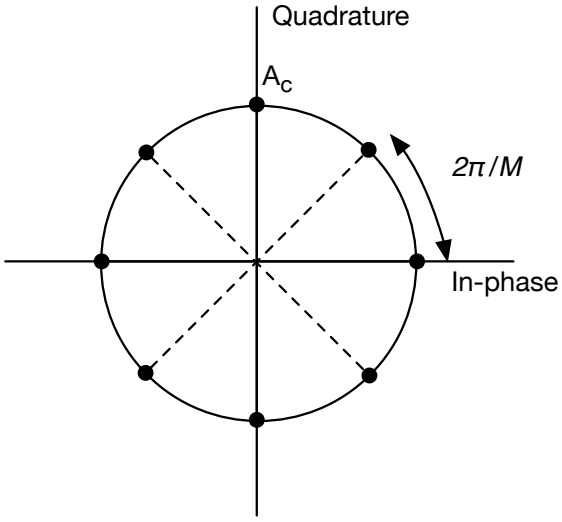

Figure 2.7: M-ary PSK signal constellation.

way

$$s(t) = A_c \sum_n \cos\left(2\pi f_c t + \phi_n\right) r\left(t - nT_s\right), \tag{2.6}$$

where A_c is the amplitude of the carrier wave and the phase deviation ϕ_n relates to the sent bit a_n as

$$\phi_n = \frac{2\pi a_n}{M}, a_n = 0, 1, \ldots, M-1. \tag{2.7}$$

2.3.5 Multi-level Constellations

A different approach can be made to phase modulations. Since the in-phase and quadrature signals are orthogonal, it is possible to use amplitude modulation together with phase modulations, to obtain higher order constellations. One example is the QAM and OQAM that is formally equivalent to QPSK and OQPSK. Nevertheless, these modulations can increase the number of points in the amplitude, becoming M-ary Quadrature Amplitude Modulation (M^2-QAM) or M^2-OQAM for any given number of M (Figure 2.8).

The data bits of either an M^2-QAM or an M^2-OQAM constellation with a general grey mapping can be described as

$$a_n^I = \sum_{g=1}^{G} 2^{G-g} \prod_{m=1}^{g} b_n^{I(m)}, \tag{2.8}$$

for the in-phase component and

$$a_n^Q = \sum_{g=1}^{G} 2^{G-g} \prod_{m=1}^{g} b_n^{Q(m)}, \tag{2.9}$$

for the quadrature component, where $b_n^{I(m)} = \pm 1$ and $b_n^{Q(m)} = \pm 1$ are the m's in-phase and quadrature sent data bits [Din+10a],

$$G = \log_2(M), \tag{2.10}$$

with $g = 1, ..., G$. This implies that the values associated to a_n^I and a_n^Q for an 4-OQAM constellation are ± 1, for 16-OQAM ± 1 and ± 3, for 64-OQAM ± 1, ± 3, ± 5, and ± 7 and so forth. Therefore, $s(t)$ is sill the same as in (2.3), and the complex envelope of the transmitted signal is

$$x(t) = \sum_{n=-N_{cp}}^{N-1} a_n^I\, r(t - nT_s) \; + \; j a_n^Q\, r(t - nT_s - T_o), \tag{2.11}$$

with $T_o = 0$ for the non-offset modulation and usually $T_o = T_s/2$ for the offset modulation.

2.3.6 Hierarchic Constellations

Furthermore, we might also want to make several bits have a higher noise protection than others [Din+10c]. Therefore, we can add hierarchic levels to the bits of the previous

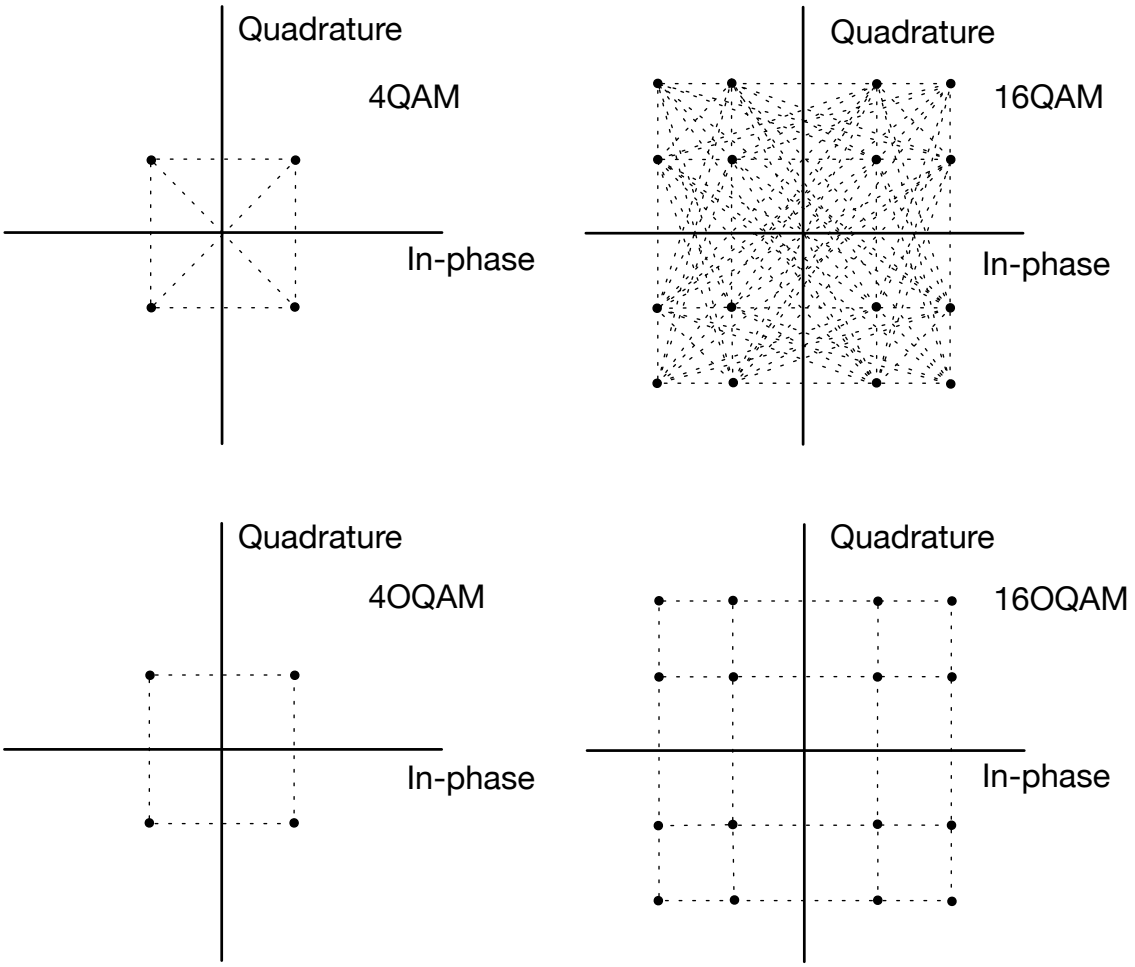

Figure 2.8: QAM and OQAM signal constellations.

modulation changing only the data bits from (2.8) and (2.9) to

$$a_n^I = \sum_{g=1}^{G} \varphi^{(g)} \prod_{m=1}^{g} b_n^{I(m)}, \tag{2.12}$$

and

$$a_n^Q = \sum_{g=1}^{G} \varphi^{(g)} \prod_{m=1}^{g} b_n^{Q(m)}. \tag{2.13}$$

This will ensure that the resolution block $\{\varphi^{(g)}; g = 1, ..., G\}$, with $\varphi^{(1)}$ as the highest order resolution bit and $\varphi^{(G)}$ the lowest, will grant higher or lower bit protection, depending on the $\varphi^{(g)}$ value.

2.3.7 Decomposition of M^2-OQAM into several OQPSK components

To apply highly nonlinear power amplification directly to these schemes, it is necessary to ensure that the complex envelope, $x(t)$, has the minimum amount of envelope fluctuations possible. Clearly, all multi-level constellations from subsection 2.3.5 and 2.9 have high

envelope fluctuations due to the different values of a_n^I and a_n^Q. Nevertheless, it is possible to decompose $x(t)$ into $G = log_2(M)$ different components with constant or quasi-constant envelope, depending on the adopted pulse shape.

To decompose $x(t)$, lets consider the constellation symbols for hierarchic constellations, since they include all the previous modulations explained. Merging (2.11), (2.12) and (2.13) it is possible to re-write $x(t)$ as

$$x(t) = \sum_{g=1}^{G} x_g(t), \tag{2.14}$$

where

$$x_g(t) = \varphi^{(g)} \sum_{n=-N_{cp}}^{N-1} \left(\prod_{m=1}^{g} b_n^{I(m)} r(t - nT_s) + \prod_{m=1}^{g} b_n^{Q(m)} r(t - nT_s - T_o) \right). \tag{2.15}$$

Now, every $x_g(t)$ component can be regarded as an OQPSK signal, which in fact has constant or quasi-constant envelope, allowing highly nonlinear amplification.

The main problem with this scheme is that G balanced power amplifiers are needed (Fig. 2.9) to produce the initially desired modulation.

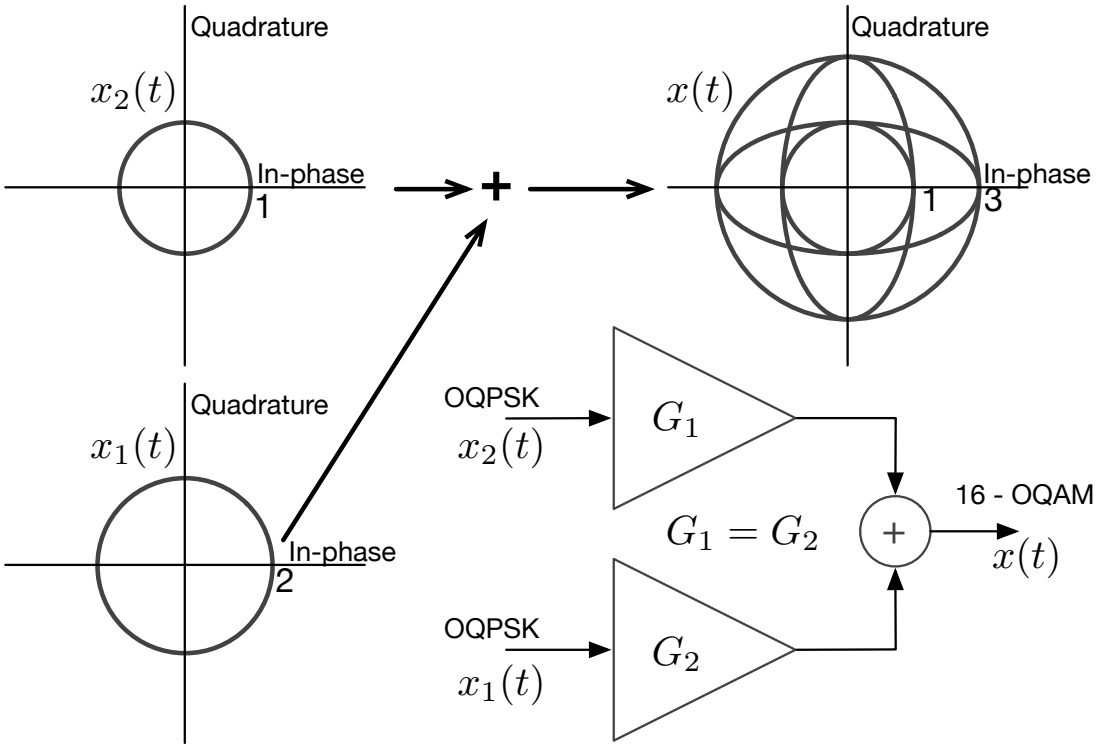

Figure 2.9: Decomposition of M^2-OQAM for highly nonlinear amplification.

2.4 Support Pulses

In every digital modulation, the choice of the pulse shape implies bandwidth and envelope fluctuation restrictions. By choosing a proper pulse shape, it is possible to control the

ISI that results from the communication channel, while simultaneously optimizing the spectrum of the transmitted signal.

Nyquist defined a strategy to limit the spectrum of a signal avoiding at the same time ISI [CC09]. Let us consider

$$y(t) = \sum_n a_n p\left(t - nT_s\right) \tag{2.16}$$

as the received waveform. To guarantee zero ISI, $p(t)$ needs to have the following property

$$p(t) = \begin{cases} 1 & t = 0 \\ 0 & t = \pm nT_s \end{cases}, \quad n \neq 0. \tag{2.17}$$

Under this condition, the only symbol different than zero at the decision time $t = nT_s$, will be a_n, which means null inter symbol interference.

2.4.1 Raised Cosine Pulses

One common pulse shape in digital modulation is the raised cosine pulse. This class of pulse shapes is characterized by a roll-off factor, usually denoted by β. In the frequency domain its mathematical description is

$$P(f) = \begin{cases} T_s & , \quad f \leq \frac{1-\beta}{2T_s} \\ \frac{T_s}{2}\left\{1 + \cos\left[\frac{\pi T_s}{\beta}\left(|f| - \frac{1-\beta}{2T_s}\right)\right]\right\} & , \quad \frac{1-\beta}{2T_s} \leq f \leq \frac{1+\beta}{2T_s} \\ 0 & , \quad f \geq \frac{1+\beta}{2T_s} \end{cases}. \tag{2.18}$$

In time domain we may write

$$p(t) = \text{sinc}\left(\frac{t}{T_s}\right) \frac{\cos\left(\frac{\pi\beta t}{T_s}\right)}{1 - \frac{4\beta^2 t^2}{T_s^2}}. \tag{2.19}$$

Figure 2.10 illustrates these kind of pulses, for different roll-of factors. When a raised cosine pulse with $\beta = 1$ is applied, it is possible to reach a quasi-constant envelope fluctuation [GM76]. However, even in this case, there are still slight envelope fluctuations.

2.4.2 Minimum Shift Keying Pulses (half sinusoid)

The minimum shift keying modulation is a continuous phase modulation that can be regarded as a subtype of OQPSK modulation. In MSK signals, the adopted pulse shape is a half sinusoid, resulting in a constant envelope signal. This support pulse[1] is defined as

$$r(t) = \cos\left(\frac{\pi t}{2T_s}\right) \text{rect}\left(\frac{t}{2T_s}\right), \tag{2.20}$$

and has the following frequency spectrum

$$R(f) = T_s\text{sinc}\left[2T_s\left(f - \frac{1}{4T_s}\right)\right] + T_s\text{sinc}\left[2T_s\left(f + \frac{1}{4T_s}\right)\right]. \tag{2.21}$$

[1] $r(t)$ is the pulse shape before the matched filter and $p(t)$ is the pulse shape after the matched filter.

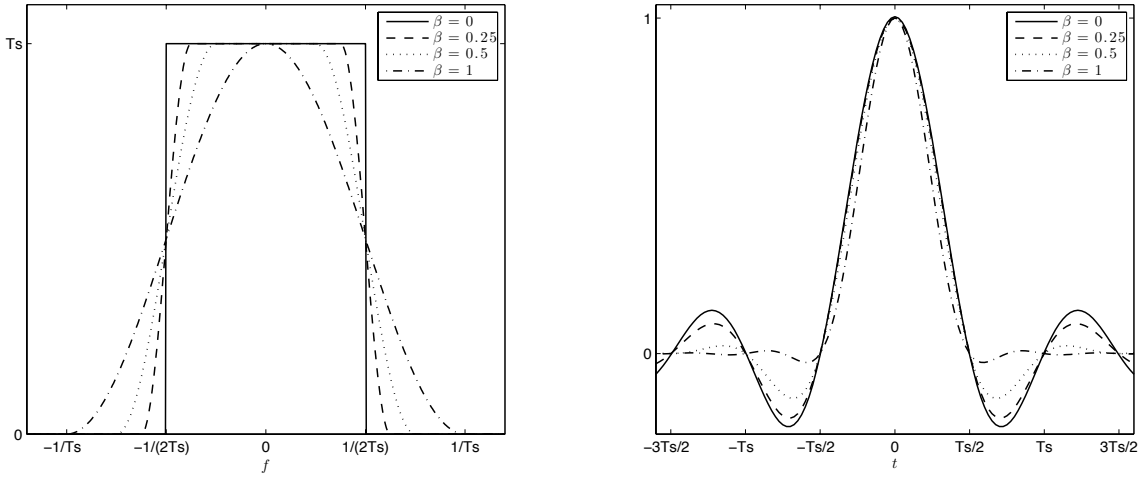

Figure 2.10: Raised cosine with different roll-off factors. Frequency spectrum (left) and time domain pulse (right).

As mentioned before, a constant envelope signal has great robustness to nonlinear amplification distortion. In fact, it can be shown that bandpass memoryless nonlinear devices do not distort constant envelope signals [GM76]. In Figure 2.11 it is possible to see the time and frequency behavior of this modulation. Compared to raised cosines pulses, this modulation has much higher bandwidth occupation, but its envelope is constant.

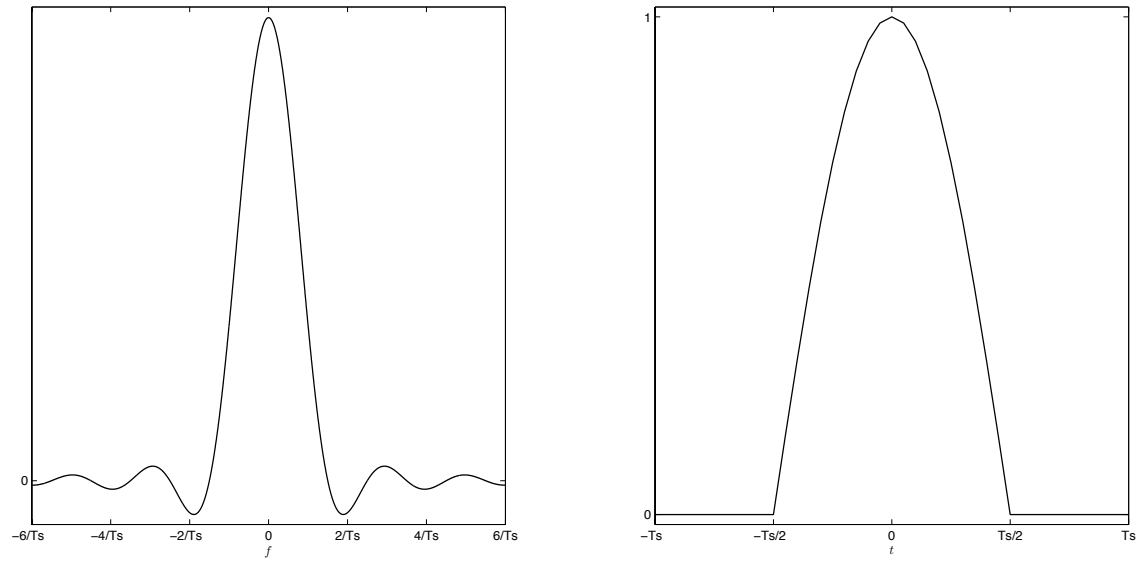

Figure 2.11: Half sinusoid support pulse. Frequency spectrum (left) and time domain pulse (right).

2.5 Envelope Fluctuations and Dynamic Range

For very-low-cost MT it is desirable to have grossly nonlinear power amplifiers, which are simpler to implement, have higher amplification efficiency and output power. However, these amplifiers are only recommendable if the signal at its input has an almost constant envelope, otherwise it will distort the transmitted signal.

CPM schemes [Aul+81] are constant-envelope modulations that include MSK and GMSK, among others. These modulations can be denoted as OQPSK-type modulations since they can be decomposed as the sum of OQPSK components [Ga+97; Lau86]. OQPSK-type modulations also include other "non-CPM" schemes with constant or almost constant envelope and good trade-offs between spectral and power efficiencies [Mon06]. The OQPSK format can even be employed to define Trellis Coded Modulation (TCM) schemes with good code gains [MG99]. OQPSK-type schemes are particularly important in the context of a nonlinear amplification since an OQPSK-type signal retains its OQPSK-type structure when submitted to bandpass memoryless nonlinear devices (that agree with the usual model for power amplifiers [Sal81]) which simplifies the performance evaluation and receiver design [DGa95]. The major problem with OQPSK signals with very low envelope fluctuations is that their bandwidth is much higher than the symbol rate.

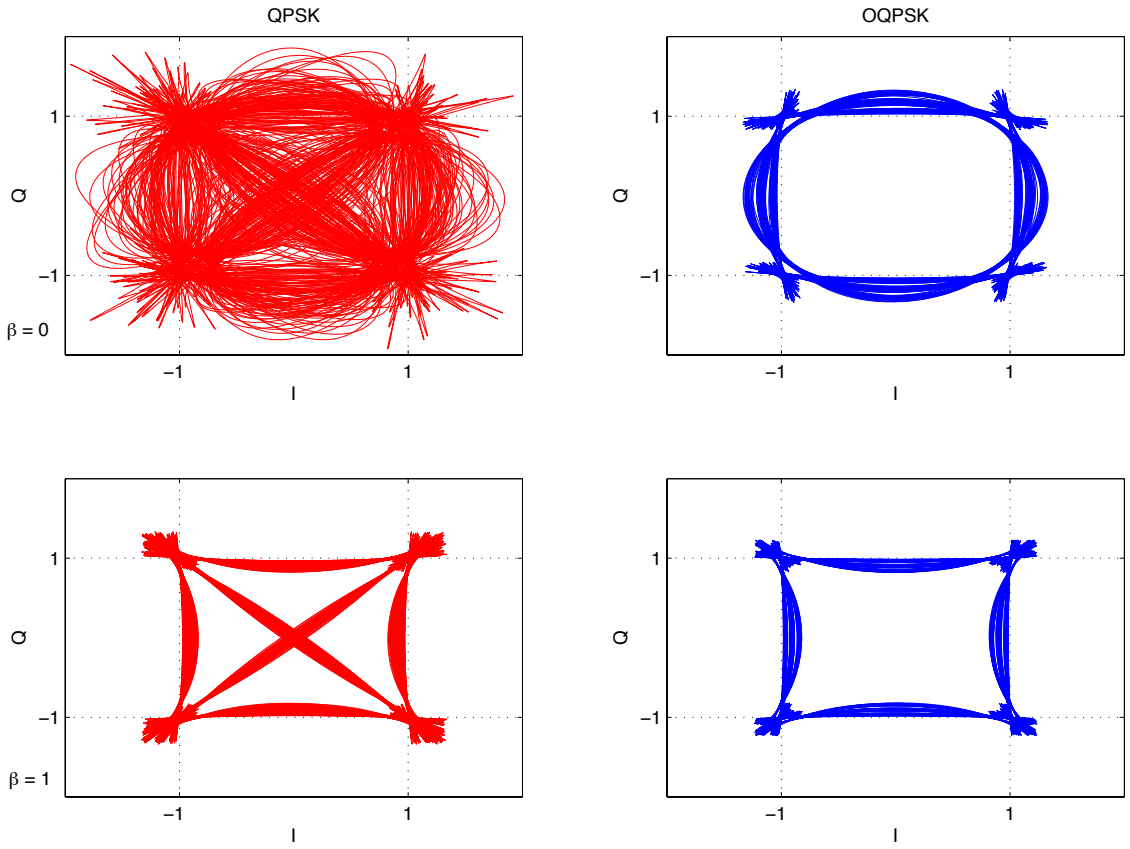

Figure 2.12: IQ Diagrams for QPSK and OQPSK signals with raised cosine support pulses with different roll off factors.

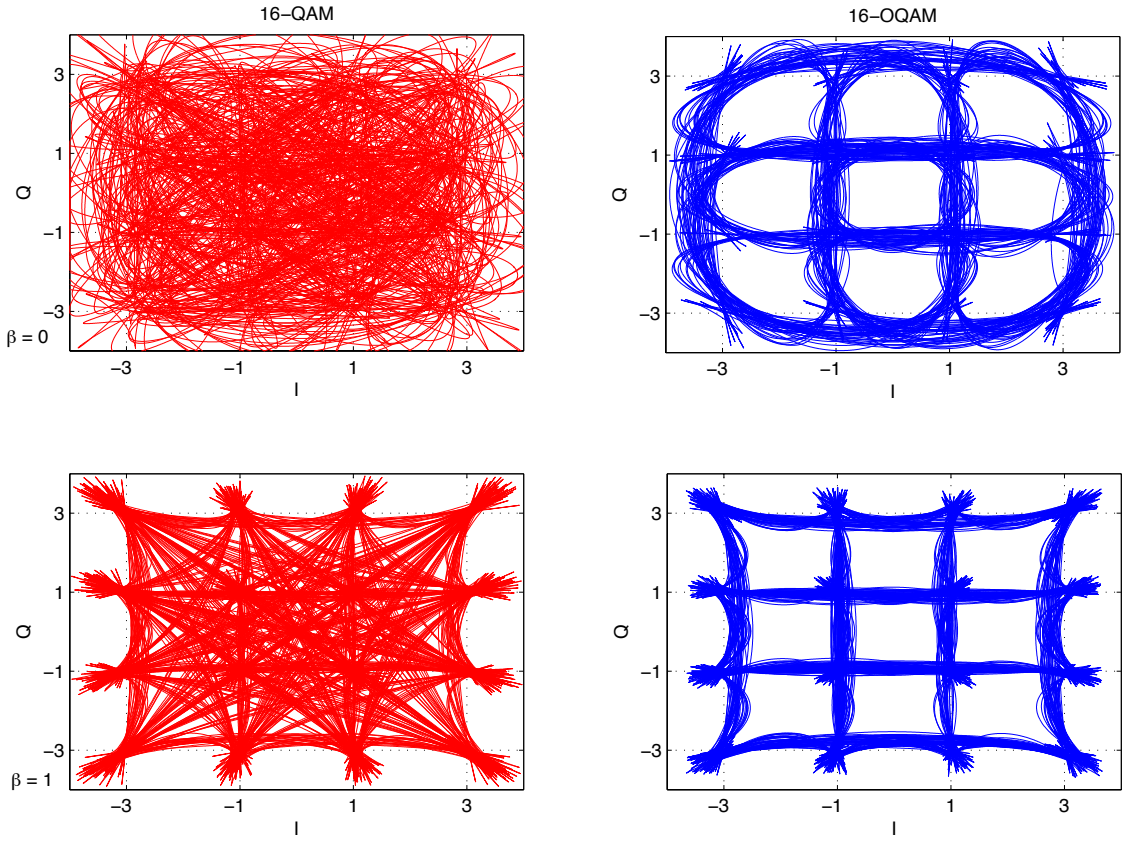

Figure 2.13: IQ Diagrams for 16-QAM and 16-OQAM signals with raised cosine support pulses with different roll off factors.

On the other hand, to avoid ACI, a high separation between frequency channels is required, which reduces the overall spectral efficiency. A promising technique was proposed in [Din+05] for QPSK signals where the separation between frequency channels is equal to the symbol rate, regardless of the transmission bandwidth associated to each channel. To cope with the high interference levels associated to the overlap between adjacent channels, an iterative frequency-domain receiver with joint equalization and ACI suppression was proposed in [Din+05]. That receiver can be regarded as a frequency-domain iterative equalizer [BT02a; Ga+07] that takes advantage of spectral correlations for the separation of cyclostationary signals in overlapping bands. Unfortunately, the receiver of [Din+05] has poor performance for OQPSK schemes due to the inherent IQI of offset modulations [Luz+09]. Moreover, conventional synchronization and channel estimation techniques [Din+08; SS00] are not appropriate in scenarios with strong ACI.

2.6 Block Transmission Techniques

In recent years, Single Carrier Modulation (SCM) has become a complementary alternative to multicarrier modulations such as OFDM [Cim85; Ga+00], largely due to the use of nonlinear equalizer structures implemented in the frequency domain [Sar+94a]. The

performance and complexity of SCM combined with FDE is similar to OFDM. However, since the Peak-to-Average Power Ratio (PAPR) is much lower than that of the OFDM schemes, it allows less peak power backoff on power amplification and is less susceptible to frequency offsets [Fal+02]. Therefore, SC-FDE schemes are particularly interesting for the uplink transmission (from the MT to the BS). Moreover, to reduce costs, increase coverage and autonomy, the MT should only have moderate complexity, achieve efficient low-cost power amplification and all the complex signal processing operations should be kept at the BS.

The transmitter and receiver structures in both approaches are very similar. The main difference is that the Inverse Fast Fourier Transform (IFFT) block on OFDM is present on the transmitter, whether in SC-FDE, it appears on the receiver (Figure 2.14). This makes a crucial difference between both methods: in OFDM there are several narrow subcarriers in parallel, with each one of them carrying one data stream. In SCM data streams are carried over one single carrier, in a serial fashion. Therefore the equalization and channel estimation techniques in OFDM are less complex, since the channel response over each single subcarrier is assumed to be flat, making possible to equalize every subcarrier by a simple gain and phase factor. Nevertheless, the robustness to radio frequency hardware impairments, specially for low cost and power consumption wireless MT turns SC-FDE an attractive alternative to OFDM [Ben+10].

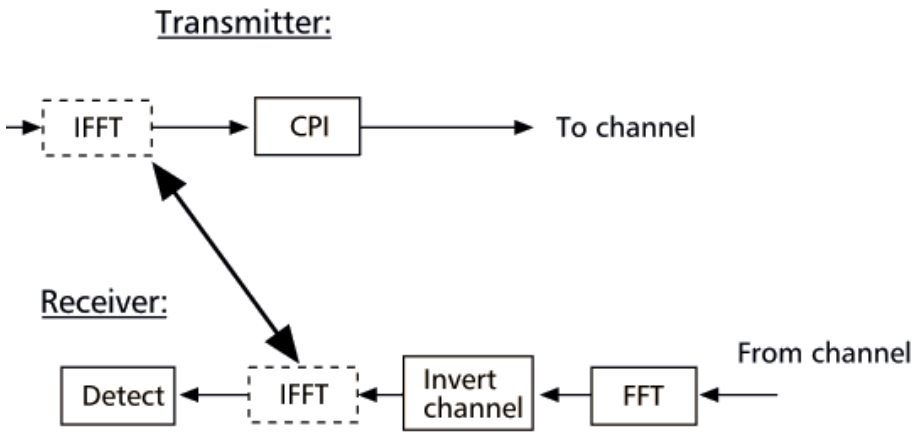

Figure 2.14: SC-FDE and OFDM interoperability [Fal+02].

Nowadays, SC-FDE is not trying to replace OFDM, but rather complement it. In fact, SC-FDE can morph to a special form of multicarrier transmission that can be called Discrete Fourier Transform (DFT)-precoded OFDM. In the European 6th framework program, the Wireless INitiative NEw Radio (WINNER) project proposed DFT-precoded OFDM for its uplink transmission and OFDM for the downlink [IST06]. The Third Generation Partnership Project - Long Term Evolution (3GPP-LTE) and now LTE-Advanced standards group also propose Single Carrier with Frequency Division Multiple Access (SC-FDMA) for the uplink of next-generation wide area cellular broadband wireless systems, which

is formally equivalent to DFT-precoded OFDM, with OFDM for the downlink channel [Myu+06]. Furthermore, the WiMAX metropolitan area concept, that followed the early 802.16a standard has two transmission modes based on OFDM and one based on SCM. In fact, when coded and iterative or turbo equalization is employed, the performance of SCM improves even further, exceeding that of OFDM for both ideal channel knowledge and for iterative channel estimation [Lam+07]. Nevertheless, the differences are not large and always depend on the employed system's equalization, coding, multiuser detection, channel estimation and coding techniques [Ben+10].

This thesis will focus on uplink transmission and, therefore, its main focus will be on SC-FDE schemes. Nevertheless the work in this thesis is easily extended to DFT-precoded OFDM or SC-FDMA systems.

2.6.1 Single Carrier with Frequency Domain Equalization

A linear single carrier modulation is a modulation where the energy associated to each symbol spreads along the total transmission band. The complex envelope of a N symbol burst can be described as

$$x(t) = \sum_{n=0}^{N-1} a_n r\left(t - nT_s\right), \tag{2.22}$$

where $r(t)$ represents the transmitted pulse, T_s is the symbol duration and a_n is a complex coefficient representing the n^{th} data symbol mapped in the selected signal constellation (e.g., PSK or QAM constellation). Applying the DFT to (2.22) we obtain the frequency domain description of the complex envelope given by

$$X(f) = \text{DFT}\left\{x\left(t\right)\right\} = \sum_{k=0}^{N-1} A_k R\left(f\right) e^{-j2\pi f k T_s}, \tag{2.23}$$

where $R(f)$ represents the Fourier Transform (FT) of $r(t)$ and A_k the FT of a_n. Therefore, the transmission band, associated with each data symbol, is the same as the band occupied by $R(f)$.

For ISI-free transmission at the receiver's matched filter bound, the pulse $r(t)$ shall verify the orthogonality condition

$$\int_{-\infty}^{\infty} r\left(t - nT_s\right) r^*\left(t - n'T_s\right) dt = 0, n \neq n'. \tag{2.24}$$

In conventional SC modulations, offering bit rates of Mbits/s over severely time-dispersive channels is hard to achieve, since the transmission bandwidth becomes much greater than the transmission channel's coherence bandwidth. This leads to high distortion levels which require complex receiver equalization.

The use of block-wise transmission using FDE at the receiver's side is based on the DFT [Fal+02; Ga+00], which can be efficiently implemented through the Fast Fourier Transform (FFT) algorithm. This approach reduces significantly the complexity of the receiver, and can achieve low Peak-to-Mean Envelope Power Ratio (PMEPR), when associated

to modulations with low envelope fluctuations, which relaxes power amplification requirements. This kind of block-wise transmission has been called single carrier frequency domain equalization.

SC-FDE schemes require a Cyclic Prefix (CP) before every transmitted block. This prefix, shown in Figure 2.15, is a repetition of the last N_{cp} data symbols in a block and is needed to prevent block contamination by ISI from the previous block. Another purpose is to make the received block appear to be cyclic with a period of NT_s.

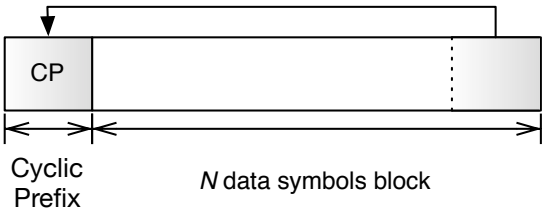

Figure 2.15: Cyclic Prefix.

To ensure that the Inter Block Interference (IBI), from the previous block, is non-existent, the length of the CP shall be greater than the channel impulse response. This means that the first data symbol only has ISI from the CP symbols, and since these can be estimated, it is possible to remove its interference from the following symbols. The complex envelope of a N symbol burst, including the CP, is similar to one of a normal SC (2.22),

$$x(t) = \sum_{n=-N_{cp}}^{N-1} a_n r\left(t - nT_s\right), \tag{2.25}$$

but has N_{cp} more symbols to remove the IBI. The negatively indexed a_n values are given by $a_{-n} = a_{N-n}$. Therefore, at the transmitter node (Figure 2.16 and 2.17) will be necessary to do the following simple procedures:

- add the CP,
- modulate the data symbols in the desired modulation,
- and multiply the remaining block with the transmitted impulse $r(t)$.

On the other hand, the signal processing at the receiver, forces SC-FDE to have the same order of complexity of an OFDM scheme, and its set of actions depends on the type of equalization employed [Cim85].

2.7 Equalization Methods

Equalization techniques try to minimize the channel effects inflicted on the transmitted signal. This process depends on the modulation used in the transmission technique. Therefore, only the relevant modulation scenarios will be discussed.

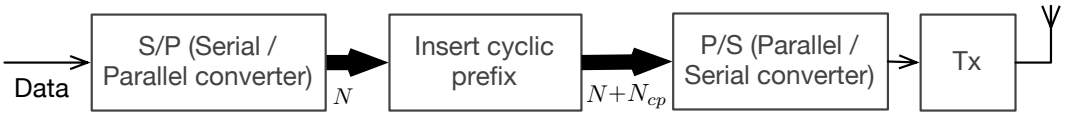

Figure 2.16: SC-FDE Transmitter (Tx block is detailed in Figure 2.17).

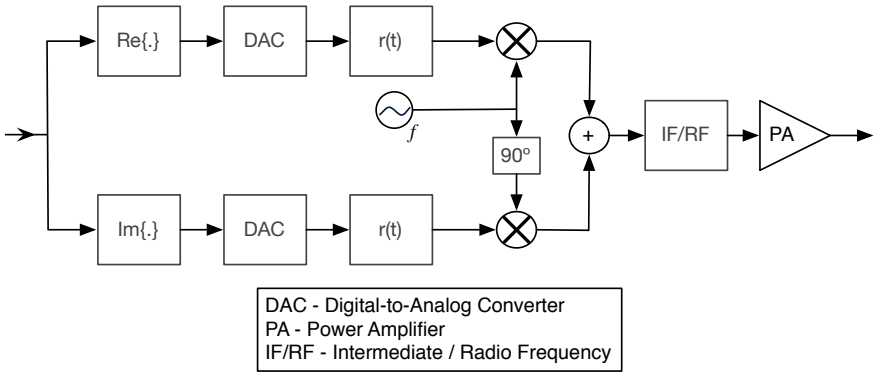

Figure 2.17: Tx Block.

After applying a channel estimation technique, the channel is defined for a given period of time, and the equalization process takes place considering that estimation. From this point, the equalization process has to mitigate the channel effects and all interference in the best possible way to obtain the highest Signal to Noise plus Interference Ratio (SNIR). Due to the tradeoff between the channel equalization and noise enhancement at the decision point, linear equalization has always less than ideal performance in terms of BER over dispersive channels [Ben+10]. Nonlinear equalizers that remove interference by cancellation, such as DFE, have higher performance than linear equalizers and can come close to the optimum sequence detector, the Viterbi algorithm, with a much lower complexity [For72].

The signal processing complexity in time domain equalization increases linearly with the number of data symbol intervals spanned by the channel impulse response, whether in the frequency domain, its complexity is much lower per data symbol [Ben+10]. Therefore, SC-FDE and OFDM have become increasingly interesting due to the existence of cheap FFT blocks that implement DFT [WE71], yielding a signal complexity that grows only logarithmically with the channel impulse response length [Ben+10]. There are several approaches on the equalization of SCM. They can be categorized in linear or nonlinear and time or frequency domain equalization.

In the early times, when the computationally complexity of the DFT was prohibitive, the only option was time domain equalization. The approach was to implement a Time Domain Decision Feedback Equalizer (TDDFE). Its complexity, in terms of complex multiplications, is equivalent to the sum of the number of feedforward (N_{FF}) and feedback taps

(N_{FB}), which relates to the length of the channel impulse response.

After FDE became practical, by the implementation of the FFT and IFFT, the first obvious choice was to develop a linear frequency domain equalization.

2.7.1 Linear Frequency Domain Equalization

The option of a linear frequency domain equalization requires an efficient implementation of the DFT to shift the processing domain of the equalization. The FFT and IFFT are used because of its robustness and speed. The signal processing of a linear FDE (2.18 and 2.19), after receiving $N + N_{cp}$ data symbols, implements the following steps:

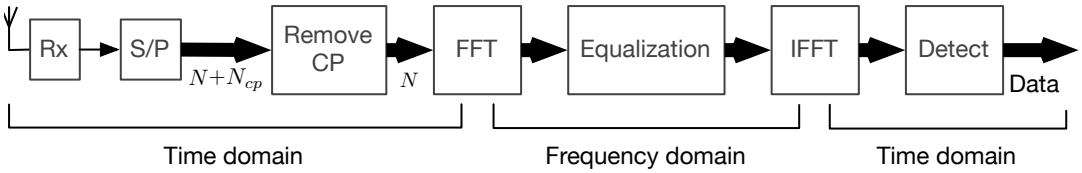

Figure 2.18: SC-FDE Receiver with linear equalization (Rx block is detailed in Figure 2.19).

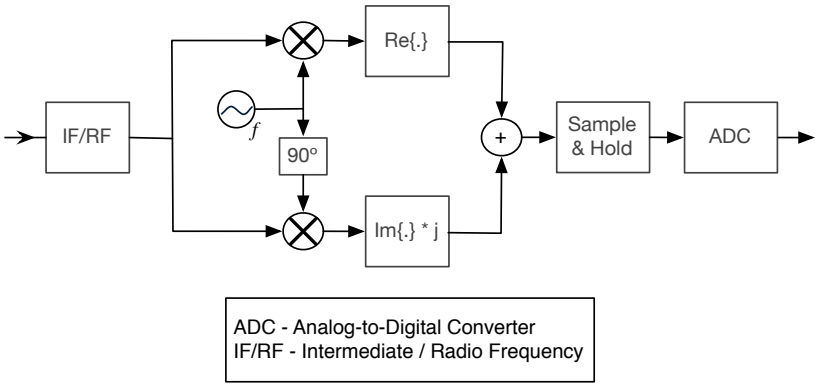

Figure 2.19: Rx Block.

- converts the received bits to parallel,
- removes the CP,
- changes the domain of the time block to frequency using FFT function,
- applies a different coefficient value to each discrete frequency (F_k),
- changes the system back to time domain
- and detects the received symbols.

The coefficient F_k can be optimized under the Zero Forcing (ZF) criteria or the Minimum Mean Square Error (MMSE) criteria.

When the CP is longer than the overall channel impulse response, the samples $\{Y_k; k = 0, 1, \ldots, N-1\}$ which are the DFT from the time domain received block $\{y_n; n = 0, 1, \ldots, N-1\}$ can be written as

$$Y_k = H_k A_k + N_k, \tag{2.26}$$

where H_k and N_k denote the channel frequency response and the noise term for the kth frequency, respectively. $\{A_k; k = 0, 1, \ldots, N-1\}$ = DFT $\{a_n; n = 0, 1, \ldots, N-1\}$ denotes the DFT of the transmitted time domain data block. For a linear FDE, the estimated frequency data block, after equalization, is given by

$$\widetilde{A}_k = F_k Y_k, \tag{2.27}$$

where $\{F_k; k = 0, 1, \ldots, N-1\}$ are the equalizer coefficients for the kth frequencies. Using ZF, we can completely invert the channel effects, reaching

$$F_k = \frac{H_k^*}{|H_k|^2}. \tag{2.28}$$

Since this criteria offers complete channel inversion, when the channel has several deep faded frequencies, the Signal to Noise Ratio (SNR) will greatly decrease due to a reinforcement of the noise in the faded frequencies. Alternatively, the use of the MMSE avoids this problem. The equalizer coefficients obtained with this method are given by

$$F_k = \frac{H_k^*}{|H_k|^2 + \alpha}, \tag{2.29}$$

with α as the inverted SNR. Depending on α, this method can bring non-ideal channel inversion for some deeply faded frequencies.

2.7.2 Hybrid Time-Frequency Decision Feedback Equalization

After FDE became practical, the second logical option was Hybrid Decision Feedback Equalizers (HDFEs), to take advantage of the fact that nonlinear equalization such as DFE increase overall performance with only a small complexity increase. Therefore, employing DFE in FDE is desirable.

The initial approach in [Fal+02] merged both linear FDE and time-domain DFE. The feedforward equalization was done in the frequency domain and the feedback equalization, in the time domain. According to [Fal+02], the decision feedback equalization suffers from the same problems described in time domain equalization: a growing complexity with the length of channel response, due to the time domain feedback equalization. In Figure 2.20 we can see an example of hybrid time-frequency DFE. This type of equalization uses the detected symbols to remove its interference effect in sub-sequential detected symbols. There is a performance enhancement compared to linear FDE, but has a complexity

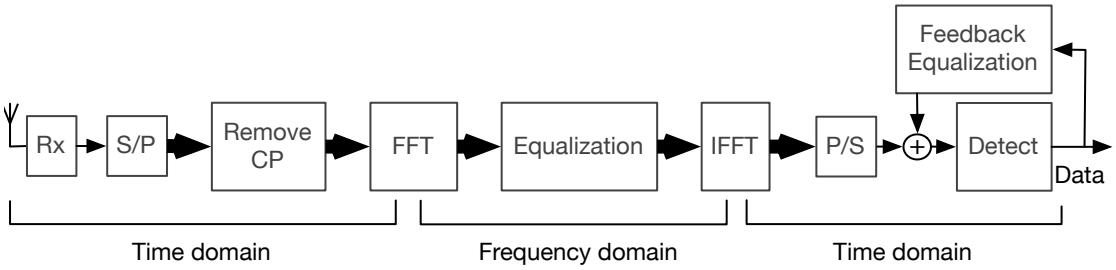

Figure 2.20: Hybrid time-frequency DFE.

drawback, due to the time-domain feedback equalization and can also suffer from error propagation effects.

One of the limitations of this approach is that a Pseudo Noise (PN) extension should be used instead of the more conventional CP. Its complexity is the sum of the two P sized (I)FFTs, one multiplication per each block of M symbols in the frequency domain and N_{FB} in the time domain.

Several variations of this receiver were developed. The Hybrid Decision Feedback Equalizer with Noise Predictor (HDFE-NP) has few advantages over HDFE when adaptive methods are used to update filter coefficients. In this method, the feedforward filter design does not depend on the feedback filter design, and the complexity is the same as that of HDFE.

The previous FDE implementations rely on the use of either CP or PN which reduce the bandwidth efficiency and cannot be applied on transmissions complying with standards that do not include the transmission format. The ExtensionLess Hybrid Decision Feedback Equalizer (ELHDFE) [Tom05] exploits the principle of overlap and save, to allow extensionless transmission. Therefore, the interblock interference must be continuously removed, but its computational complexity remains the same as the initial HDFE.

Bidirectional Hybrid Decision Feedback Equalizer (BiHDFE), another version of the HDFE, processes the received samples in two ways: a direct HDFE and a backward HDFE that processes the samples backwards. The computational complexity of this method is roughly the double of the HDFE.

2.7.3 Iterative Block Decision Feedback Equalizer

Decision feedback equalizers can significantly outperform linear equalizers and have a good trade-off between performance and complexity. However, when the time length of the channel response increases, conventional time-domain DFE becomes too complex and can suffer from error propagation, specially when the feedback filters have large number of taps. Ideally, the feedforward and feedback equalization should be kept completely in the frequency domain.

Recently, a new iterative equalization method, the IB-DFE, has been proposed [BT02a].

This method has the feedback filter in the frequency domain which reduces computational complexity for both filter design and signal processing, and allows performance results close to the Matched Filter Bound (MFB). The ability of using error correction codes in the feedback data signal further improves its performance [SF08]. Many parameters of this method can be further improved by the use of soft decisions, instead of hard decisions [TB04], better reliability coefficients, among others. This method was later extended to multiple antennas [Din+04] and to offset modulations [Luz+10a; Luz+10b].

These IB-DFE schemes implement both feedforward and feedback equalization in the frequency domain in an iterative way. On the first iteration, there is only feedforward equalization, or linear FDE. Whereas in the next iterations, the decisions from the previous iteration is fed to the system in the frequency domain. The performance of this method increases together with the number of iterations (N_I). Figure 2.21 shows the receiver structure of IB-DFE.

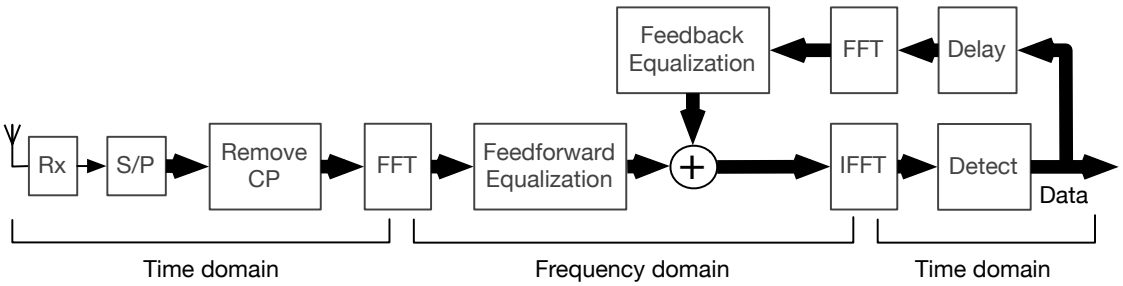

Figure 2.21: IB-DFE receiver

Since the feedback loop takes into account not only the decisions for each block, but also the overall block reliability, the error propagation problem is significantly reduced.

2.7.4 Comparison between methods

From [Ben+10], we can say that IB-DFE, after four iterations, provides the lowest BER, outperforming all the other methods. The computational complexity in the frequency domain equalization is also reduced when compared with the time domain equalization (Table 2.1 and Table 2.2).

2.8 The Iterative Block Decision Feedback Equalizer

2.8.1 Definition

Let us consider an IB-DFE for SC scheme. For a given iteration i, the frequency output samples are defined as

$$\widetilde{A}_k^{(i)} = F_k^{(i)} Y_k - B_k^{(i)} \widehat{A}_k^{(i-1)}, \tag{2.30}$$

Structure	Complexity of Equalizer Structures
TDDFE	$N_{FF} + N_{FB}$
HDFE ELHDFE HDFE-NP	$\frac{P}{N}\log_2 P - \frac{P}{N} + N_{FB}$
BiDFE	$\frac{3P}{2N}\log_2 P - \frac{3P}{2N} + 2N_{FB} + \frac{P}{N}$
IBDFE	$\frac{N_I P}{N}\log_2 P$

Table 2.1: Computational complexity of equalizer structures [Ben+10].

Structure	Complexity of Parameter Design
TDDFE	N_{FF}^3
HDFE ELHDFE HDFE-NP	$N_{FB}^2 + P\log_2 P + \frac{P}{2}\log_2 P$
BiDFE	P^3
IBDFE	$3P$

Table 2.2: Computational complexity of parameter design [Ben+10].

where $\{F_k^{(i)}; k = 0, 1, ..., N-1\}$ and $\{B_k^{(i)}; k = 0, 1, ..., N-1\}$ denote the feedforward and feedback equalizer coefficients, respectively. $\{Y_k; k = 0, 1, ..., N-1\}$ is the DFT of the time-domain received block $\{y_n; n = 0, 1, ..., N-1\}$, $\{\widehat{A}_k^{(i)}; k = 0, 1, ..., N-1\}$ is the DFT of the time-domain hard decision data symbols' block $\{\widehat{a}_n^{(i)}; n = 0, 1, ..., N-1\}$ and $\{\widetilde{A}_k^{(i)}; k = 0, 1, ..., N-1\}$ is the DFT of the data symbols' $\{a_n; n = 0, 1, ..., N-1\}$ estimation. $F_k^{(i)}$ and $B_k^{(i)}$, the forward and backward IB-DFE coefficients, are chosen as to maximize the SNIR.

2.8.2 Computation of the Receiver Parameters for IB-DFE

According to [Din+07], the estimated data symbols can be written as

$$\widehat{a}_n^{(i)} = \rho^{(i)} a_n + \delta_n^{eq(i)}, \tag{2.31}$$

where $\rho^{(i)}$ represents the correlation coefficient that provides a block wise reliability measure of the estimates used in the feedback loop and is given by

$$\rho^{(i)} = \frac{E\left[\widehat{a}_n^{(i-1)} a_n^*\right]}{E\left[|a_n|^2\right]} = \frac{E\left[\widehat{A}_k^{(i-1)} A_k^*\right]}{E\left[|A_k|^2\right]}.^{1} \tag{2.32}$$

[1] According to Parseval's discrete power theorem.

Using the DFT it is possible to rewrite (2.31), in the frequency domain, as

$$\widehat{A}_k^{(i)} = \rho^{(i)} A_k + \Delta_k^{(i)}, \tag{2.33}$$

where $\Delta_k^{(i)}$ denotes a zero-mean error term with the expected value

$$E\left[\left|\Delta_k^{(i)}\right|^2\right] \approx \left(1 - {\rho^{(i)}}^2\right) E\left[|A_k|^2\right]. \tag{2.34}$$

Using (2.26) and (2.33), it is possible to rewrite (2.30) as

$$\widetilde{A}_k^{(i)} = F_k^{(i)} \left(A_k H_k + N_k\right) - B_k^{(i)} \left(\rho^{(i-1)} A_k + \Delta_k^{(i-1)}\right). \tag{2.35}$$

The ISI component, in the frequency domain, associated to the difference between the average channel frequency response after the feedforward filter, is defined as

$$\gamma^{(i)} = \frac{1}{N} \sum_{k=0}^{N-1} F_k^{(i)} H_k, \tag{2.36}$$

which would have a constant value for null ISI. If the estimates of the transmitted block are reliable, the feedback filter can be used to remove this residual interference. Therefore, the equalized frequency domain samples associated to each iteration can be written as

$$\widetilde{A}_k^{(i)} = \gamma^{(i)} A_k + \varepsilon_k^{eq(i)}, \tag{2.37}$$

where

$$\varepsilon_k^{eq(i)} = \left(F_k^{(i)} H_k - \gamma^{(i)} - \rho^{(i-1)} B_k^{(i)}\right) A_k - B_k^{(i)} \Delta_k^{(i-1)} + F_k^{(i)} N_k. \tag{2.38}$$

Clearly, $\varepsilon_k^{eq(i)}$ have three noise components: inter symbol interference $(F_k^{(i)} H_k - \gamma^{(i)} - \rho^{(i-1)} B_k^{(i)})$, interference from the inaccuracy of the data estimation that is fed back to the system $(B_k^{(i)} \Delta_k^{(i-1)})$ and the usual noise component $(F_k^{(i)} N_k)$.

The next objective is to maximize the SNIR, which can be obtained by the following equation:

$$\text{SNIR}_k = \frac{E\left[\left|\gamma^{(i)} A_k\right|^2\right]}{E\left[\left|\varepsilon_k^{eq(i)}\right|^2\right]} = \frac{\left|\gamma^{(i)}\right|^2 E\left[|A_k|^2\right]}{E\left[\left|\varepsilon_k^{eq(i)}\right|^2\right]}. \tag{2.39}$$

The maximization of $SNIR_k$ can be achieved by the minimization of

$$\begin{aligned} E\left[\left|\varepsilon_k^{eq(i)}\right|^2\right] = E\left[\left|F_k^{(i)} H_k - \gamma^{(i)} - \rho^{(i-1)} B_k^{(i)}\right|^2\right] 2\sigma_S^2 + \\ + \left|B_k^{(i)}\right|^2 \left(1 - \left(\rho^{(i-1)}\right)^2\right) 2\sigma_S^2 + \left|F_k^{(i)}\right|^2 2\sigma_N^2, \end{aligned} \tag{2.40}$$

conditioned to a given $\gamma^{(i)}$, with σ_N^2 denoting the variance of the noise terms and σ_S^2, the variance of the data symbols. This leads to an optimization problem that can be solved using the Lagrange multipliers' method. Lets define the Lagrangian function as

$$L = E\left[\left|\varepsilon_k^{eq(i)}\right|^2\right] + \lambda^{(i)} \left(\frac{1}{N} \sum_{k=0}^{N-1} F_k^{(i)} H_k - 1\right) \tag{2.41}$$

Solving the following equations leads to the optimum receiver coefficients.

$$\begin{aligned}\frac{\partial L}{\partial F_k^{(i)}} &= 4\sigma_S^2 H_k^* \left(F_k^{(i)} H_k - 1 - \rho^{(i-1)} B_k^{(i)} + \frac{\gamma^{(i)}}{2\sigma_S^2 N} \right) + \\ &\quad + 4\sigma_N^2 F_k^{(i)} = 0, \end{aligned} \tag{2.42}$$

$$\begin{aligned}\frac{\partial L}{\partial B_k^{(i)}} &= -4\sigma_S^2 \rho^{(i-1)} \left(F_k^{(i)} H_k - 1 - \rho^{(i-1)} B_k^{(i)} \right) + \\ &\quad + 4\sigma_S^2 \left(1 - \rho^{(i-1)^2} \right) B_k^{(i)} = 0 \end{aligned} \tag{2.43}$$

and

$$\frac{\partial L}{\partial \lambda^{(i)}} = \frac{1}{N} \sum_{k=0}^{N-1} F_k H_k - 1 = 0. \tag{2.44}$$

As expected, (2.44) is equivalent to have $\gamma^{(i)} = 1$. After some algebraic manipulation we may write for the feedforward coefficients

$$F_k^{(i)} = \frac{\kappa^{(i)} H_k^*}{\alpha + \left(1 - \rho^{(i-1)^2} \right) |H_k|^2}, \tag{2.45}$$

and for the feedback coefficients

$$B_k^{(i)} = \rho^{(i-1)} \left(F_k^{(i)} H_k - 1 \right), \tag{2.46}$$

where α as the inverse of the SNR defined as

$$\alpha = \frac{\sigma_N^2}{\sigma_S^2}. \tag{2.47}$$

The normalization factor $\kappa^{(i)}$ of (2.45) is defined as

$$\kappa^{(i)} = 1 - \rho^{(i-1)^2} - \frac{\lambda^{(i)}}{2\sigma_N^2 N}. \tag{2.48}$$

From (2.44) and (2.45) we can obtain $\lambda^{(i)}$ solving

$$N = \sum_{k=0}^{N-1} \frac{\left(1 - \rho^{(i-1)^2} - \frac{\lambda^{(i)}}{2\sigma_N^2 N} \right) |H_k|^2}{\left(1 - \rho^{(i-1)^2} \right) |H_k|^2 + \alpha}. \tag{2.49}$$

For the first iteration, the information about a_n is unavailable, which means $\rho^{(-1)} = 0$ and $B_k^{(0)} = 0$. Under these conditions, the values of $F_k^{(0)}$ are easily obtained by a simple substitution of $\rho^{(-1)} = 0$, resulting in

$$F_k^{(0)} = \frac{\kappa^{(0)} H_k^*}{|H_k|^2 + \alpha}. \tag{2.50}$$

Therefore, the IB-DFE is equivalent to a linear FDE on the first iteration.

2.8.3 IB-DFE with soft decisions

To increase the immunity against error propagation, it is possible to use soft decisions, $\overline{a}_n^{(i)}$, instead of using hard decisions, $\widehat{a}_n^{(i)}$. For a normalized QPSK constellation, i.e. $a_n^I = \text{Re}\{a_n\} = \pm 1$ and $a_n^Q = \text{Im}\{a_n\} = \pm 1$, following [BT05] and [Ga+07] we may write

$$\overline{a}_n^{I(i)} = \tanh\left(\frac{\Lambda_n^{I(i)}}{2}\right) \tag{2.51}$$

and

$$\overline{a}_n^{Q(i)} = \tanh\left(\frac{\Lambda_n^{Q(i)}}{2}\right), \tag{2.52}$$

where $\Lambda_n^{I(i)}$ and $\Lambda_n^{Q(i)}$ are the Log-likelihood Ratios of the in-phase, a_n^I, and quadrature, a_n^Q, data bit estimation described as

$$\Lambda_n^{I(i)} = \frac{2\,\text{Re}\left\{\widetilde{a}_n^{(i)}\right\}}{\sigma_N^2} \tag{2.53}$$

and

$$\Lambda_n^{Q(i)} = \frac{2\,\text{Im}\left\{\widetilde{a}_n^{(i)}\right\}}{\sigma_N^2}, \tag{2.54}$$

respectively. The total variance of the channel and interference noise, σ_N^2, is given by

$$\sigma_N^2 = \frac{1}{2}\text{E}[|a_n - \widetilde{a}_n^{(i)}|^2] \approx \frac{1}{2N}\sum_{n=0}^{N-1} |\widehat{a}_n^{(i)} - \widetilde{a}_n^{(i)}|^2. \tag{2.55}$$

The feedforward coefficients, $F_k^{(i)}$ are still given by (2.45) and, since $\overline{A}_k^{(i)}$ is equivalent to $\rho^{(i)}\widehat{A}_k^{(i)}$, the feedback coefficients are given by

$$B_k^{(i)} = F_k^{(i)} H_k - 1. \tag{2.56}$$

Finally, the estimated data symbols are obtained by

$$\widetilde{A}_k^{(i)} = F_k^{(i)}\, Y_k - B_k^{(i)}\, \overline{A}_k^{(i-1)}. \tag{2.57}$$

From this point forward in this thesis the $^{(i)}$ superscript will be dropped to lower the complexity of mathematic expressions.

CHAPTER 3

FDE RECEIVER DESIGNS FOR OFFSET MODULATIONS

3.1 Introduction

Future broadband wireless systems are expected to have high transmission rates while requiring good power and spectral efficiency. To reduce the cost of mobile terminals, its complexity should be minimal. Moreover, an efficient, low-cost power amplification is also required, to increase the coverage and/or battery autonomy.

Due to high transmission rates, the multi-path propagation can lead to severe time-dispersion effects. For this reason, block transmission techniques combined with FDE techniques such as OFDM [Cim85] and SC-FDE [Sar+94a] should be employed. SC-FDE schemes are particularly suitable for the uplink transmission (i.e., the transmission from the mobile terminal to the base station), since the envelope fluctuations of the transmitted signals are much lower than those of OFDM schemes [Fal+02; Ga+00]. Although, SC-FDE schemes have acceptable performance with a simple linear FDE, the performance is substantially increased with more powerful iterative FDE schemes [TH00; TH01; Tüc+02]. One of the most promising iterative FDE is the IB-DFE [BT02a; Ben+10], which can be regarded as a DFE where the feedforward and feedback filters are implemented in the frequency domain. The main problem with QPSK schemes is that we still need a linear amplifier for SC modulations, since the transmitted signal still has envelope fluctuations[1].

It is widely accepted that SC-FDE is an excellent candidate for broadband wireless systems, especially when an efficient power amplification is intended. If grossly nonlinear power amplifiers are employed, conventional QPSK or QAM modulations should be replaced by their offset modulations counterparts, OQPSK and OQAM. In fact, offset signals have much lower dynamic range than non-offset signals, with OQPSK signals being able to have an almost constant envelope. For very-low-cost mobile terminals, it is

[1] The exception is the case where rectangular pulses are employed, which is usually not employed due to their poor spectral characteristics.

desirable to have grossly nonlinear power amplifiers, which are simpler to implement and have higher amplification efficiency and output power. However, these amplifiers are only recommendable when the signal at its input has an almost constant envelope. In this case, OQPSK modulations, also denoted by staggered modulations [Tu93], are strongly recommendable since the transmitted signals can have very low envelope fluctuations or even quasi-constant envelope. It should be pointed out that for QPSK/OQPSK constellations the main degradation due to a nonlinear amplifier is associated to the spectral widening effects (i.e., increased out-of-band radiation levels); due to the reduced dynamic range of OQPSK signals (without zeros crossings) the spectral widening effects are much smaller than with corresponding QPSK signals, even when we employ signals without constant envelope.

The most famous OQPSK modulation is MSK [GM76], but GMSK signals [MH81] and other CPM signals [Aul+81] can also be written as the sum of OQPSK components [Lau86]. Moreover, this description in terms of OQPSK components can be employed to define TCM-OQAM schemes with good code gains [Mon06; MG99]. Naturally, OQAM signals have significant envelope fluctuations, making them prone to nonlinear distortion effects. However, they can be decomposed as the sum of several OQPSK signals that can be separately amplified almost without distortion [Mon+11]. Nevertheless, we should be cautious when extending to offset modulation receivers that were designed for non-offset modulations [LV02; Tu93].

Combining OQPSK modulations with SC-FDE schemes seems a natural choice for the uplink of highly power efficient broadband wireless systems. Since OQPSK signals with constant or quasi-constant envelope have bandwidth much higher than the minimum Nyquist band, the FDE should be designed with several samples per symbol to take full advantage of diversity effects, inherent to the larger transmission bandwidth and/or to be able to cope with synchronization errors [Oba+09].

This chapter considers frequency-domain receiver's design for OQPSK and OQAM schemes. It is shown that the FDE designed for non-offset modulations are not suitable for offset modulations due to the residual IQI, i.e. the interference between In-phase (I) and Quadrature (Q) components at the sampling instants. Although the time-domain receivers especially designed for offset modulations such as those of [LV02; Tu93] can address this problem, their complexity is too high for severely time-dispersive channels. Therefore, we propose several FDE designs where there is no IQI at the sampling instants and iterative FDE receivers with IQI cancellation.

This chapter is organized as follows: section 3.2, characterizes linear and iterative FDE designs for non-offset and offset modulations, as well as the multiplicity concept. Several methods to mitigate IQI in linear FDE are proposed in section 3.3. In section 3.4 is presented an alternative approach to minimize the overall interference. The characterization, relevant properties and performance results of iterative FDE with IQI cancellation, are presented in section 3.5. Finally, the chapter is summarized in section 3.8.

3.2 Linear and Iterative FDE Designs with Oversampling

3.2.1 FDE for QPSK Schemes

The length-N data block to be transmitted is $\{a_n; n = 0, 1, ..., N-1\}$, where $a_n = a_n^I + j a_n^Q$ is the nth data symbol with $a_n^I = \pm 1$ and $a_n^Q = \pm 1$ associated to the "in-phase" and "quadrature" bits, respectively. For a QPSK scheme the transmitted signal is

$$s(t) = \text{Re}\left\{x(t)e^{j2\pi f_c t}\right\}, \tag{3.1}$$

where f_c is the carrier frequency and $s(t)$ is its the complex envelope, given by

$$x(t) \quad = \quad \sum_{n=-N_{cp}}^{N-1} a_n r(t - nT_s), \tag{3.2}$$

with $r(t)$ denoting the adopted pulse shape and N_{cp} the length of the cyclic prefix [Fal+02] (it is assumed that the block $\{a_n; n = 0, 1, ..., N-1\}$ is periodic with period N, i.e., $a_n = a_{n+N}$).

Let us first assume that $x(t)$ is the complex envelope of a QPSK scheme with pulse shape $r(t)$ and data symbols $a_n, n = 0, 1, \ldots, N-1$. If a given block is sampled with rate J/T_s, i.e., with J samples per symbol, then the samples associated to the useful part of the block (i.e., without cyclic prefix) are $\{x_n^{(J)}; n = 0, 1, \ldots, JN-1\}$, with $x_n^{(J)} \triangleq x(nT_s/J)$ (it is assumed that the rate J/T_s is large enough to avoid aliasing effects). Since $x(t)$ is cyclostationary[2] [Gar91], the frequency domain block associated to $\{x_n^{(J)}; n = 0, 1, \ldots, JN-1\}$ is $\{X_k^{(J)}; k = 0, 1, \ldots, JN-1\}$ = DFT $\{\check{x}_n; n = 0, 1, \ldots, JN-1\}$, with

$$X_k^{(J)} = A_k^{(J)} R_k^{(J)}, \tag{3.3}$$

where $\{R_k^{(J)}; k = 0, 1, \ldots, JN-1\}$ is the DFT of $\{r_n^{(J)} \triangleq r((n - JN/2)T_s/J); n = 0, 1, \ldots, JN-1\}$ (without loss of generality, we assume that $r(t)$ is centered in 0 and $\{A_k^{(J)}; k = 0, 1, \ldots, JN-1\}$ is the DFT of $\{a_n^{(J)}; n = 0, 1, \ldots, JN-1\}$, with

$$a_n^{(J)} = \begin{cases} a_{n'}, & n = Jn' \\ 0, & \text{otherwise} \end{cases} \tag{3.4}$$

It can easily be shown that

$$A_k^{(J)} = \frac{1}{J} A_k, \tag{3.5}$$

where $\{A_k; k = 0, 1, \ldots, N-1\}$ denotes the DFT of $\{a_n; n = 0, 1, \ldots, N-1\}$ (once again the time-domain and frequency-domain blocks associated to the the data are periodic with period N). This means that there is an implicit multiplicity in the frequency-domain block when the adopted pulse shape has bandwidth above the Nyquist band (i.e., when $R_k^{(J)}$ is not restricted to N non-zero samples), since the frequency-domain sample A_k is repeated in several $X_k^{(J)}$ samples (which are separated by multiples of N) as shown in Figure 3.1.

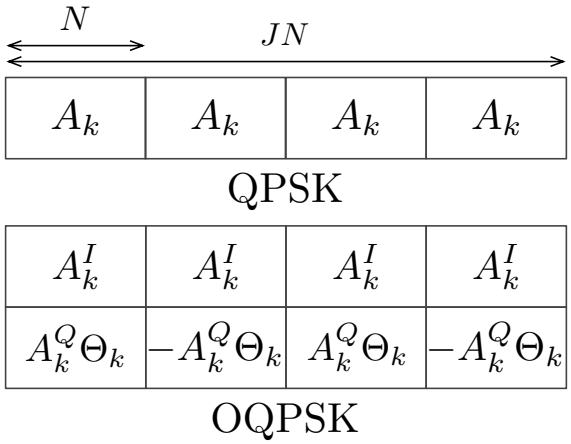

Figure 3.1: Frequency-domain multiplicity in QPSK (up) and OQPSK (down) signals.

This multiplicity can be regarded as a frequency diversity effect that can be used by the FDE.

The received block is sampled with the rate J/T_s, the cyclic prefix is removed and the resulting blocks, $\{y_n^{(J)}; n = 0, 1, \ldots, JN-1\}$, are passed to the frequency domain, leading to the blocks $\{Y_k^{(J)}; k = 0, 1, \ldots, JN-1\}$. If the cyclic prefix is longer than the overall channel impulse response length then

$$Y_k^{(J)} = A_k^{(J)} H_k^{(J)} + N_k^{(J)}, \tag{3.6}$$

where $H_k^{(J)}$ is the overall channel impulse response for the kth subcarrier (which includes the adopted pulse shape, the channel and the $1/J$ factor inherent to (3.5)) and $N_k^{(J)}$ is the corresponding noise component.

For a linear FDE the output is

$$\widetilde{A}_k = \sum_{q=0}^{J-1} F_{k+qN}^{(J)} Y_{k+qN}^{(J)}, \quad k = 0, 1, \ldots, N-1, \tag{3.7}$$

where the FDE coefficients, optimized under the MMSE criterion (Minimum Mean Squared Error), are given by

$$F_k^{(J)} = \frac{H_k^{(J)*}}{\alpha + \sum_{q=0}^{J-1} \left| H_{(k \bmod N)+qN}^{(J)} \right|^2}, k = 0, 1, \ldots, JN-1, \tag{3.8}$$

with $(\cdot)^*$ denoting complex conjugate, x mod y denoting the modulo operator, i.e. the integer remainder of x/y, and

$$\alpha = E[|N_k^{(J)}|^2] / E[|A_k^{(J)}|^2] \tag{3.9}$$

denoting the inverse of the SNR.

[2] $E[x(t)x(t-\tau)]$ is periodic in t, with period T_s.

For a given iteration of the IB-DFE, the FDE output is

$$\widetilde{A}_k = \sum_{q=0}^{J-1} F_{k+qN}^{(J)} Y_{k+qN}^{(J)} - B_k \overline{A}_k, \quad k = 0, 1, \ldots, N-1, \tag{3.10}$$

where $\{\overline{A}_k; k = 0, 1, \ldots, N-1\}$ is the DFT of $\{\overline{a}_n; n = 0, 1, \ldots, N-1\}$, with $\overline{a}_n$ denoting the average values of $\widetilde{a}_n$ associated to the previous iteration, conditioned to the FDE output. For QPSK constellations with Grey mapping these average values can be obtained as described in [Ga+07] and for 16-QAM constellations with Grey mapping they can be obtained as described in [SF09]. For general M^2-QAM constellations we can employ the approach of [Din+10a] where the constellation symbols are expressed as a function of the corresponding bits as follows:

$$a_n = \sum_{g=1}^{G} 2^{G-g} \prod_{m=1}^{g} b_n^{I(m)} + j \sum_{g=1}^{G} 2^{G-g} \prod_{m=1}^{g} b_n^{Q(m)}, \tag{3.11}$$

with $G = log_2(M)$, $b_n^{I(m)} = \pm 1$ and $b_n^{Q(m)} = \pm 1$. The log-likelihood ratio of the mth bit of the nth transmitted symbol is given by

$$\Lambda_n^{(m)} = log \left(\frac{\sum_{a \in \Phi_1^{(m)}} \exp\left(-\frac{|\widetilde{a}_n - a|^2}{2\sigma_N^2} \right)}{\sum_{a \in \Phi_{-1}^{(m)}} \exp\left(-\frac{|\widetilde{a}_n - a|^2}{2\sigma_N^2} \right)} \right), \tag{3.12}$$

where $\Phi_1^{(m)}$ and $\Phi_{-1}^{(m)}$ are the constellation's subsets associated to the symbols with the mth bit at 1 or -1, respectively and

$$\sigma_N^2 = \frac{1}{2N} \sum_{n=0}^{N-1} E[|\widetilde{a}_n - a_n|^2]. \tag{3.13}$$

To obtain the average symbol values conditioned to the FDE output, $\overline{a}_n$, we need the average bit values conditioned to the FDE output, $\overline{b}_n^{(m)}$. They can be related as

$$\overline{b}_n^{(m)} = \tanh\left(\frac{\Lambda_n^{(m)}}{2} \right) = \rho_n^{(m)} \hat{b}_n^{(m)}, \tag{3.14}$$

with $\hat{b}_n^{(m)}$ denoting the hard decisions' estimate of $b_n^{(m)}$ and $\rho_n^{(m)}$ its reliability. From (3.11), (3.14) and assuming uncorrelated bits due to the usage of a suitable interleaver, we have

$$\overline{a}_n = \sum_{g=1}^{G} 2^{G-g} \prod_{m=1}^{g} \overline{b}_n^{I(m)} + j \sum_{g=1}^{G} 2^{G-g} \prod_{m=1}^{g} \overline{b}_n^{Q(m)}. \tag{3.15}$$

Having in mind the results of [Din+03] it can be shown that the IB-DFE coefficients are given by

$$F_k^{(J)} = \frac{\kappa H_k^{(J)*}}{\alpha + (1-\rho^2) \sum_{q=0}^{J-1} \left| H_{(k \bmod N)+qN}^{(J)} \right|^2}, k = 0, 1, \ldots, JN-1, \tag{3.16}$$

and

$$B_k = \sum_{q=0}^{J-1} F_{k+qN}^{(J)} H_{k+qN}^{(J)} - 1, \quad k = 0, 1, \ldots, N-1, \tag{3.17}$$

respectively, where κ is selected to ensure that

$$\frac{1}{N} \sum_{k=0}^{JN-1} F_k^{(J)} H_k^{(J)} = 1, \tag{3.18}$$

α is defined by (3.9), and the correlation coefficient ρ that regards block-wise reliability of the decisions used in the feedback loop is given by

$$\rho = \frac{E\left[\bar{a}_n a_n^*\right]}{E\left[|a_n|^2\right]} \approx \frac{E\left[\bar{a}_n \widehat{a}_n^*\right]}{E\left[|\widehat{a}_n|^2\right]}. \tag{3.19}$$

For general M^2-QAM constellations we have

$$\rho = \frac{1}{2N} \sum_{n=0}^{N-1} \sum_{g=1}^{G} \frac{\left|4^{G-g} \prod_{m=1}^{g} \rho_n^{(m)}\right|}{4^{G-g}}, \tag{3.20}$$

where

$$\rho_n^{(m)} = \tanh\left(\frac{|\Lambda_n^{(m)}|}{2}\right). \tag{3.21}$$

3.2.2 Multiplicity in OQPSK Signals

For an OQPSK scheme we still have

$$s(t) = \mathrm{Re}\left\{x(t) e^{j2\pi f_c t}\right\}, \tag{3.22}$$

but with the complex envelope given by

$$x(t) = \sum_{n=-N_{cp}}^{N-1} a_n^I r(t - nT_s) + j \sum_{n=-N_{cp}}^{N-1} a_n^Q r(t - nT_s - T_o), \tag{3.23}$$

Clearly, the OQPSK signal can be regarded as the sum of two binary Pulse Amplitude Modulation (PAM) signals each with symbols (bits) separated by T_s (the average bit rate is $1/2T_s$), and with an offset T_o between them (which usually is $T_s/2$).

Although, the in-phase and quadrature components of OQPSK signals are cyclostationary with period T_s, the OQPSK signal is cyclostationary with period $T_s/2$. Therefore, as in subsection 3.2.1, when we sample the received signal with the rate J/T_s we obtain the time-domain block $\{x_n^{(J)}; n = 0, 1, \ldots, JN-1\}$ = IFFT $\{X_k^{(J)} = A_k^{(J)} R_k^{(J)}; k = 0, 1, \ldots, JN-1\}$, where $R_k^{(J)}$ is previously defined and $\{A_k^{(J)}; k = 0, 1, \ldots, JN-1\}$ = DFT $\{a_n^{(J)}; n = 0, 1, \ldots, JN-1\}$. However, contrary to (3.4), we have

$$a_n^{(J)} = \begin{cases} a_{n'}^I, & n = n'J \\ a_{n'}^Q, & n = n'J + J/2 \\ 0, & \text{otherwise} \end{cases} \tag{3.24}$$

Therefore, $a_n^{(J)} = a_n^{I(J)} + a_{n-J/2}^{Q(J)}$ where $a_n^{I(J)}$ and $a_n^{Q(J)}$ are related with a_n^I and a_n^Q, respectively, as in (3.4). This means that $A_k^{(J)} = A_k^{I(J)} + A_k^{Q(J)}\Theta_k$, with $\Theta_k = j\exp(-j\pi k/N)$. Since $A_k^{I(J)}$ and $A_k^{Q(J)}$ are related to $\{A_k^I; k = 0,1,\ldots,N-1\}$ = DFT $\{a_n^I; n = 0,1,\ldots,N-1\}$ and $\{A_k^Q; k = 0,1,\ldots,N-1\}$ = DFT $\{a_n^Q; n = 0,1,\ldots,N-1\}$, respectively, there is an implicit multiplicity in the frequency-domain block when the adopted pulse shape has bandwidth above the Nyquist band (see Fig. 3.1). The simplest way to take advantage of this multiplicity is to design separate FDEs for the in-phase and quadrature components (naturally, the quadrature FDE manipulates the samples shifted by $J/2$ relatively to the in-phase FDE). If we consider IB-DFE receivers, the F_k and B_k coefficients could still be given by (3.16) and (3.17). Nevertheless, the major problem with this approach consists on the interference between the I and Q components at the sampling points, i.e., for the sample associated to the I component there is a residual interference due to the Q component (the same effect applies to the Q component). This residual interference can significantly compromise the performance. Moreover, the performance does not change significantly when we employ a conventional IB-DFE receiver.

3.3 Linear FDE without IQI

In this section we propose an FDE design for OQPSK without IQI at the sampling instants. A simple way to achieve this is forcing the overall impulse response after the feedforward part (the time-domain block associated to the frequency-domain samples $F_k H_k$) to be real. For this purpose, it is necessary to ensure that $F_k H_k$ is symmetrical with respect to the central frequency of the spectrum[3] (this is usually true for the transmitted signals but it is not necessarily true at the channel output). On the other hand, the FDE should take full advantage of the diversity effects inherent to the frequency multiplicity (see Fig. 3.1).

In the particular case of offset modulations, the I and Q components have an inherent delay (T_o) and they must be sampled at different instants at the receiver. If the received support pulses are real, there will be no interference between the I and Q components, even when a contribution from the quadrature component is present at the in-phase component detection. Due to the channel effects, the pulse at the equalizer's output can become complex and we will have interference between both in-phase and quadrature components, lowering the overall performance of the system.

Defining $P_k^{(J)}$ as $P_k^{(J)} = F_k^{(J)} H_k^{(J)}, k = 0,1,\ldots,JN-1$, which can be regarded as the equivalent frequency response at the FDE output, and the corresponding time-domain block as $\{p_n^{(J)}; n = 0,1,\ldots,JN-1\}$ = IFFT $\{P_k^{(J)}; k = 0,1,\ldots,JN-1\}$, which can be regarded as the equivalent impulse response at the FDE output. Under zero ISI conditions, $p_{nJ}^{(J)} = 0, n \neq 0$, which is formally equivalent to impose the condition

$$\sum_{q=0}^{J-1} P_{k+qN}^{(J)} = \text{constant}. \tag{3.25}$$

[3]Since $F_k \propto H_k$, it is clear the overall frequency response is real.

The objective of the FDE is to achieve this condition, at least approximately.[4] For OQPSK schemes, there is an additional constraint to mitigate the IQI:

$$\mathrm{Im}\left\{p^{(J)}_{J/2+nJ}\right\} = 0, \forall_n. \tag{3.26}$$

A possible way to achieve (3.25) and (3.26) is to have $p^{(J)}_{nJ/2} = 0$ for $n \neq 0$, which corresponds to employ Nyquist pulses with half symbol duration (this implies twice the bandwidth which it is not desirable). Instead, we will design the FDE in the MMSE sense (implicitly achieving (3.25)), but constrained to avoid IQI. An important idea is that if we have $\mathrm{Im}\{p^{(J)}_n\} = 0$, the condition (3.26) is met and there will be no IQI. In the following subsections, we will present three different methods to avoid IQI.

3.3.1 Method I

The objective of Method I is to ensure that $p^{(J)}_n$ is real. Since $F^{(J)}_k \propto H^{(J)^*}_k$, $P^{(J)}_k$ is real and non-negative. Therefore, this means that $P^{(J)}_k$ should have even symmetry (see Fig. 3.2), i.e.,

$$P^{(J)}_k = P^{(J)}_{JN-k}, \tag{3.27}$$

for $k = 1, \ldots, JN/2 - 1$. In this case $k = 0$ will have no constraints, and assuming

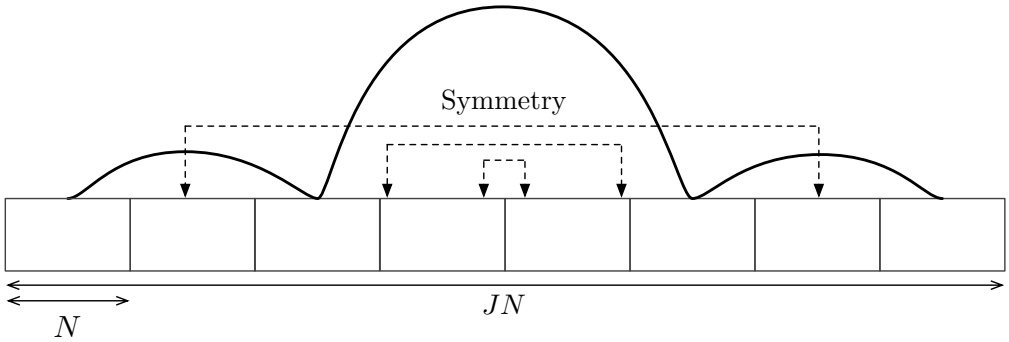

Figure 3.2: Symmetry groups for method I.

an oversampling factor J high enough to ensure $H^{(J)}_{JN/2} = 0$, neither will $k = JN/2$. Consequently, the FDE design corresponds to the minimization of

$$E\left[\left|F^{(J)}_k Y^{(J)}_k - A^{(J)}_k\right|^2\right] + E\left[\left|F^{(J)}_{JN-k} Y^{(J)}_{JN-k} - A^{(J)}_{JN-k}\right|^2\right], \tag{3.28}$$

conditioned to (3.27), which is equivalent to

$$F^{(J)}_k H^{(J)}_k = F^{(J)}_{JN-k} H^{(J)}_{JN-k}, \tag{3.29}$$

for $k = 1, \ldots, JN/2 - 1$.

[4] For a ZF FDE, the equation (3.25) holds true, but for a MMSE FDE, considered here, (3.25) is only true for very high SNR.

Using Lagrangian multipliers' method it can easily be shown that the optimum values of $F_k^{(J)}$ are

$$F_k^{(J)} = \frac{(1-\lambda_k)\, H_k^{(J)^*}}{\alpha + \left|H_k^{(J)}\right|^2}, \tag{3.30}$$

and

$$F_{JN-k}^{(J)} = \frac{(1+\lambda_k)\, H_{JN-k}^{(J)^*}}{\alpha + \left|H_{JN-k}^{(J)}\right|^2}, \tag{3.31}$$

with $k = 1, 2, \ldots, JN/2$ and

$$\lambda_k = \frac{\left|H_k^{(J)}\right|^2 \left(\alpha + \left|H_{JN-k}^{(J)}\right|^2\right) - \left|H_{JN-k}^{(J)}\right|^2 \left(\alpha + \left|H_k^{(J)}\right|^2\right)}{\left|H_k^{(J)}\right|^2 \left(\alpha + \left|H_{JN-k}^{(J)}\right|^2\right) + \left|H_{JN-k}^{(J)}\right|^2 \left(\alpha + \left|H_k^{(J)}\right|^2\right)}. \tag{3.32}$$

Due to the absence of constraints for $k = 0$ and $k = JN/2$, $F_0^{(J)}$ and $F_{JN/2}^{(J)}$ are defined by (3.16).

3.3.2 Method II

The main problem with Method I is the imposition of too many unnecessary symmetry constrains on $P_k^{(J)}$, because it forces $p_n^{(J)}$ to be real for any value of n, compromising the performance. Instead, Method II only forces $p_{nJ/2}^{(J)}$ to be real ($n = 0, 1, \ldots, 2N-1$), which is enough to ensure that there will be no IQI at the sampling instants (naturally, we are assuming that $J \geq 2$). It should be pointed out that the frequency samples can be organized in symmetry groups and multiplicity groups, as shown in Fig. 3.3. In symmetry groups, both frequency samples must have the same value, to guarantee no IQI. On the other hand, the multiplicity groups have information concerning the same kth frequency sample. Let us define four different groups:

$$\begin{aligned}
\Psi_k^{(1)} &= \{k + 2qN; q = 0, 1, ..., J/2-1\}, \\
\Psi_k^{(2)} &= \{N - k + 2qN; q = 0, 1, ..., J/2-1\}, \\
\Psi_k^{(3)} &= \{N + k + 2qN; q = 0, 1, ..., J/2-1\}, \text{and} \\
\Psi_k^{(4)} &= \{2N - k + 2qN; q = 0, 1, ..., J/2-1\},
\end{aligned}$$

where $k = 1, \ldots, N/2$. The symmetry groups are $\Psi_k^{(1)} \cup \Psi_k^{(4)}$ and $\Psi_k^{(2)} \cup \Psi_k^{(3)}$, and the multiplicity groups are $\Psi_k^{(1)} \cup \Psi_k^{(3)}$ and $\Psi_k^{(2)} \cup \Psi_k^{(4)}$.

Therefore, the relations needed to mitigate the IQI are

$$\sum_{k' \in \Psi_k^{(i)}} F_{k'}^{(J)} H_{k'}^{(J)} = \sum_{k' \in \Psi_k^{(5-i)}} F_{k'}^{(J)} H_{k'}^{(J)}, \tag{3.33}$$

with $i = 1$ or 2 and $k' = 1, \ldots, N/2$. This problem leads to the minimization of

$$E\left[\left|\sum_{k' \in \Psi_k^{(1)} \cup \Psi_k^{(3)}} F_{k'}^{(J)} Y_{k'}^{(J)} - A_k\right|^2\right] + E\left[\left|\sum_{k' \in \Psi_k^{(2)} \cup \Psi_k^{(4)}} F_{k'}^{(J)} Y_{k'}^{(J)} - A_{N-k}\right|^2\right] \tag{3.34}$$

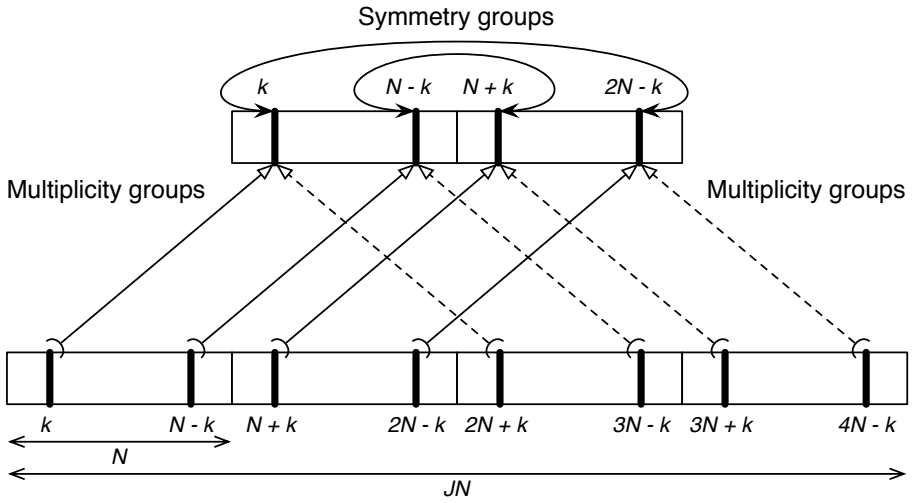

Figure 3.3: Symmetry and multiplicity groups for method II.

conditioned to (3.33). By employing the Lagrange multipliers' method, and after some straightforward but lengthy manipulations, it can be shown that the optimum values of $F_k^{(J)}$ are

$$F_{k'}^{(J)} = \begin{cases} \dfrac{\left(1-\lambda_k^{(a)}\right) H_{k'}^{(J)*}}{\alpha+\sum_{k'\in\Psi_k^{(1)}\cup\Psi_k^{(3)}}\left|H_{k'}^{(J)}\right|^2}, & k' \in \Psi_k^{(1)} \\ \dfrac{\left(1-\lambda_k^{(b)}\right) H_{k'}^{(J)*}}{\alpha+\sum_{k'\in\Psi_k^{(2)}\cup\Psi_k^{(4)}}\left|H_{k'}^{(J)}\right|^2}, & k' \in \Psi_k^{(2)} \\ \dfrac{\left(1+\lambda_k^{(b)}\right) H_{k'}^{(J)*}}{\alpha+\sum_{k'\in\Psi_k^{(1)}\cup\Psi_k^{(3)}}\left|H_{k'}^{(J)}\right|^2}, & k' \in \Psi_k^{(3)} \\ \dfrac{\left(1+\lambda_k^{(a)}\right) H_{k'}^{(J)*}}{\alpha+\sum_{k'\in\Psi_k^{(2)}\cup\Psi_k^{(4)}}\left|H_{k'}^{(J)}\right|^2}, & k' \in \Psi_k^{(4)}, \end{cases} \tag{3.35}$$

with $\lambda_k^{(a)}$ and $\lambda_k^{(b)}$ given by

$$\lambda_k^{(a)} = \frac{\beta_k^{(124)} - \beta_k^{(413)}}{\beta_k^{(124)} + \beta_k^{(413)}} \tag{3.36}$$

and

$$\lambda_k^{(b)} = \frac{\beta_k^{(213)} - \beta_k^{(324)}}{\beta_k^{(213)} + \beta_k^{(324)}}, \tag{3.37}$$

respectively, where $\beta_k^{(xyz)} = G_k^{(x)}\left(\alpha + G_k^{(y)} + G_k^{(z)}\right)$, and $G_k^{(a)} = \sum_{k\in\Psi_k^{(a)}}\left|H_k^{(J)}\right|^2$. Since this leads to a solution where $p(t - nT_s/2)$ is real for every $n = 0, 1, \ldots, N-1$, this method mitigates all IQI, while still taking into account the multiplicity groups.

3.3.3 Method III

Let us take the previous equalization method one step further. It is known that a matched filter will guarantee $p(t - nT_s) = 0$, for $n \neq 0$. Assuming that the FDE mitigates the ISI, it thus becomes clear that is unnecessary to force $\mathrm{Im}\{p_{nJ}^{(J)}\} = 0$ where the FDE guarantees zero ISI (see also [LV02; Tu93]). Consequently, the only condition needed to assure an IQI free system will be

$$\mathrm{Im}\left\{p_{J/2+nJ}^{(J)}\right\} = 0, \forall_n \tag{3.38}$$

which corresponds to the exact time where the IQI interferes with the symbol detection. Note that the block $\left\{p_{Jn}^{(J)}; n = 0, \ldots, N-1\right\}$ is the IFFT of the block $\left\{\sum_{q=0}^{J-1} P_{k+qN}^{(J)}; k = 0, \ldots, N-1\right\}$, and the block $\left\{p_{Jn+J/2}^{(J)}; n = 0, \ldots, N-1\right\}$ is the IFFT of the block $\left\{\Theta_k \sum_{q=0}^{J-1} (-1)^q P_{k+qN}^{(J)}; k = 0, \ldots, N-1\right.$

Under these conditions, the desired equalizer output, $\widetilde{A}_k$ can be written as

$$\widetilde{A}_k = \sum_{q=0}^{J-1} P_{k+qN}^{(J)} A_{k+qN}^{I(J)} + jP_{k+qN}^{(J)} A_{k+qN}^{Q(J)} \Theta_{k+qN}. \tag{3.39}$$

Clearly, we have $\Theta_{k'+N} = -\Theta_{k'}$ and $\Theta_{k'-N} = -\Theta_{k'}^*$. Therefore we may write

$$\widetilde{A}_k = A_k^I \sum_{q=0}^{J-1} P_{k+qN}^{(J)} + jA_k^Q \Theta_k \sum_{q=0}^{J-1} (-1)^q P_{k+qN}^{(J)}. \tag{3.40}$$

To ensure that $p_{Jn+J/2}^{(J)}$ is real (and, consequently, to guarantee an IQI free system), $P_k^{(J)}$ has to verify

$$\sum_{q=0}^{J-1} (-1)^q P_{k+qN}^{(J)} = -\sum_{q=0}^{J-1} (-1)^q P_{N-k+qN}^{(J)}. \tag{3.41}$$

Such as in Method II, we still have symmetry groups and the multiplicity groups. Obviously, considering (3.41) and the symmetry groups it is possible to write the following condition

$$\sum_{k' \in \Psi_k^{(1)}} F_{k'}^{(J)} H_{k'}^{(J)} - \sum_{k' \in \Psi_k^{(3)}} F_{k'}^{(J)} H_{k'}^{(J)} = -\sum_{k' \in \Psi_k^{(2)}} F_{k'}^{(J)} H_{k'}^{(J)} + \sum_{k' \in \Psi_k^{(4)}} F_{k'}^{(J)} H_{k'}^{(J)}, \tag{3.42}$$

which is equivalent to

$$\sum_{k' \in \left(\Psi_k^{(1)} \cup \Psi_k^{(2)}\right)} F_{k'}^{(J)} H_{k'}^{(J)} = \sum_{k' \in \left(\Psi_k^{(3)} \cup \Psi_k^{(4)}\right)} F_{k'}^{(J)} H_{k'}^{(J)} \tag{3.43}$$

with the groups $\Psi_k^{(1)}$, $\Psi_k^{(2)}$, $\Psi_k^{(3)}$ and $\Psi_k^{(4)}$ defined in a similar way as in method II (see Fig. 3.4).

To optimize the values of $F_{k'}^{(J)}$ it is needed to minimize

$$E\left[\left|\sum_{k' \in \left(\Psi_k^{(1)} \cup \Psi_k^{(3)}\right)} F_{k'}^{(J)} Y_{k'}^{(J)} - A_k\right|^2\right] + E\left[\left|\sum_{k' \in \left(\Psi_k^{(2)} \cup \Psi_k^{(4)}\right)} F_{k'}^{(J)} Y_{k'}^{(J)} - A_{N-k}\right|^2\right], \tag{3.44}$$

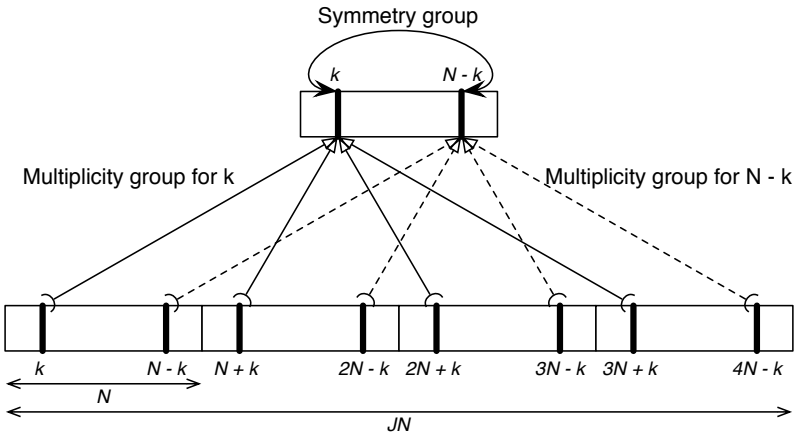

Figure 3.4: Symmetry and multiplicity groups for method III.

with $k = 1, 2, ..., N/2 - 1$, conditioned to (3.43). Once again, using the Lagrangian multipliers' method and after some straightforward but lengthy algebraic manipulations, we obtain the optimum coefficients

$$F_{k'}^{(J)} = \begin{cases} \dfrac{(1-\lambda_k) H_{k'}^{(J)*}}{\alpha + \sum_{k' \in \left(\Psi_k^{(1)} \cup \Psi_k^{(3)}\right)} \left|H_{k'}^{(J)}\right|^2} & , \quad k' \in \Psi_k^{(1)} \\ \dfrac{(1-\lambda_k) H_{k'}^{(J)*}}{\alpha + \sum_{k' \in \left(\Psi_k^{(2)} \cup \Psi_k^{(4)}\right)} \left|H_{k'}^{(J)}\right|^2} & , \quad k' \in \Psi_k^{(2)} \\ \dfrac{(1+\lambda_k) H_{k'}^{(J)*}}{\alpha + \sum_{k' \in \left(\Psi_k^{(1)} \cup \Psi_k^{(3)}\right)} \left|H_{k'}^{(J)}\right|^2} & , \quad k' \in \Psi_k^{(3)} \\ \dfrac{(1+\lambda_k) H_{k'}^{(J)*}}{\alpha + \sum_{k' \in \left(\Psi_k^{(2)} \cup \Psi_k^{(4)}\right)} \left|H_{k'}^{(J)}\right|^2} & , \quad k' \in \Psi_k^{(4)} \end{cases}. \tag{3.45}$$

To obtain λ_k we need to solve the following equation:

$$\frac{(1-\lambda_k) \sum_{k' \in \Psi_k^{(1)}} \left|H_{k'}^{(J)}\right|^2 - (1+\lambda_k) \sum_{k' \in \Psi_k^{(3)}} \left|H_{k'}^{(J)}\right|^2}{\alpha + \sum_{k' \in \left(\Psi_k^{(1)} \cup \Psi_k^{(3)}\right)} \left|H_{k'}^{(J)}\right|^2} = - \frac{(1-\lambda_k) \sum_{k' \in \Psi_k^{(2)}} \left|H_{k'}^{(J)}\right|^2 - (1+\lambda_k) \sum_{k' \in \Psi_k^{(4)}} \left|H_{k'}^{(J)}\right|^2}{\alpha + \sum_{k' \in \left(\Psi_k^{(2)} \cup \Psi_k^{(4)}\right)} \left|H_{k'}^{(J)}\right|^2}, \tag{3.46}$$

where the solution is

$$\lambda_k = \frac{\left(Z_k^{(1)} - Z_k^{(2)}\right)\left(\alpha + Z_k^{(3)} + Z_k^{(4)}\right) + \left(Z_k^{(3)} - Z_k^{(4)}\right)\left(\alpha + Z_k^{(1)} + Z_k^{(2)}\right)}{\left(Z_k^{(1)} + Z_k^{(2)}\right)\left(\alpha + Z_k^{(3)} + Z_k^{(4)}\right) + \left(Z_k^{(3)} + Z_k^{(4)}\right)\left(\alpha + Z_k^{(1)} + Z_k^{(2)}\right)}, \tag{3.47}$$

with $Z_k^{(a)} = \sum_{k' \in \Psi_k^{(a)}} \left|H_{k'}^{(J)}\right|^2$.

For $k = 0$ we have

$$F_0^{(J)} = \frac{H_0^{(J)*}}{\alpha + \sum_{k' \in \Psi_0} \left| H_0^{(J)} \right|^2}, \tag{3.48}$$

leading to $\lambda_0 = 0$. For $k = N/2$, it is necessary to guarantee

$$\mathrm{Im}\left\{ \Theta_{N/2} \sum_{q=0}^{J-1} (-1)^q P_{N/2+qN}^{(J)} \right\} = 0. \tag{3.49}$$

Since $\Theta_{N/2} = \Theta_{N-N/2} = -j$, the previous condition can be simplified to

$$\sum_{q=0}^{J-1} (-1)^q P_{N/2+qN}^{(J)} = 0. \tag{3.50}$$

Therefore, the groups $\Psi_{N/2}^{(1)}$ and $\Psi_{N/2}^{(2)}$ will be the same as $\Psi_{N/2}^{(3)}$ and $\Psi_{N/2}^{(4)}$, respectively.

This leads to a simplified optimization problem, for $k = N/2$, equivalent to the minimization of

$$E\left[\left| \sum_{k' \in \left(\Psi_{N/2}^{(1)} \cup \Psi_{N/2}^{(3)} \right)} F_{k'}^{(J)} Y_{k'}^{(J)} - A_{N/2} \right|^2 \right], \tag{3.51}$$

conditioned to

$$\sum_{k' \in \Psi_{N/2}^{(1)}} F_{k'}^{(J)} H_{k'}^{(J)} = \sum_{k' \in \Psi_{N/2}^{(3)}} F_{k'}^{(J)} H_{k'}^{(J)}. \tag{3.52}$$

Applying the Lagrange multiplier's method will result

$$F_{k'}^{(J)} = \begin{cases} \dfrac{(1-\lambda_{N/2}) H_{k'}^{(J)*}}{\alpha + \sum_{k' \in \left(\Psi_{N/2}^{(1)} \cup \Psi_{N/2}^{(3)} \right)} \left| H_{k'}^{(J)} \right|^2}, & k' \in \Psi_{N/2}^{(1)} \\ \dfrac{(1+\lambda_{N/2}) H_{k'}^{(J)*}}{\alpha + \sum_{k' \in \left(\Psi_{N/2}^{(1)} \cup \Psi_{N/2}^{(3)} \right)} \left| H_{k'}^{(J)} \right|^2}, & k' \in \Psi_{N/2}^{(3)} \end{cases}, \tag{3.53}$$

with $\lambda_{N/2}$ as the solution of

$$\frac{(1-\lambda_{N/2}) \sum_{k' \in \Psi_{N/2}^{(1)}} \left| H_{k'}^{(J)} \right|^2}{\alpha + \sum_{k' \in \left(\Psi_{N/2}^{(1)} \cup \Psi_{N/2}^{(3)} \right)} \left| H_{k'}^{(J)} \right|^2} = \frac{(1+\lambda_{N/2}) \sum_{k' \in \Psi_{N/2}^{(3)}} \left| H_{k'}^{(J)} \right|^2}{\alpha + \sum_{k' \in \left(\Psi_{N/2}^{(1)} \cup \Psi_{N/2}^{(3)} \right)} \left| H_{k'}^{(J)} \right|^2}. \tag{3.54}$$

which is $\lambda_{N/2} = (C_{N/2} - D_{N/2})/(C_{N/2} + D_{N/2})$.

3.3.4 Performance Results

The performance results of the different receiver designs are presented in this section. Here, as well as for other performance results of this chapter, we consider blocks of $N = 512$ data symbols, plus an appropriate cyclic prefix. The channel spans over 128 symbols and is characterized by the HIPERLAN/2 power delay profile type C [ETS98], with uncorrelated Rayleigh fading on each tap (similar results were observed for other

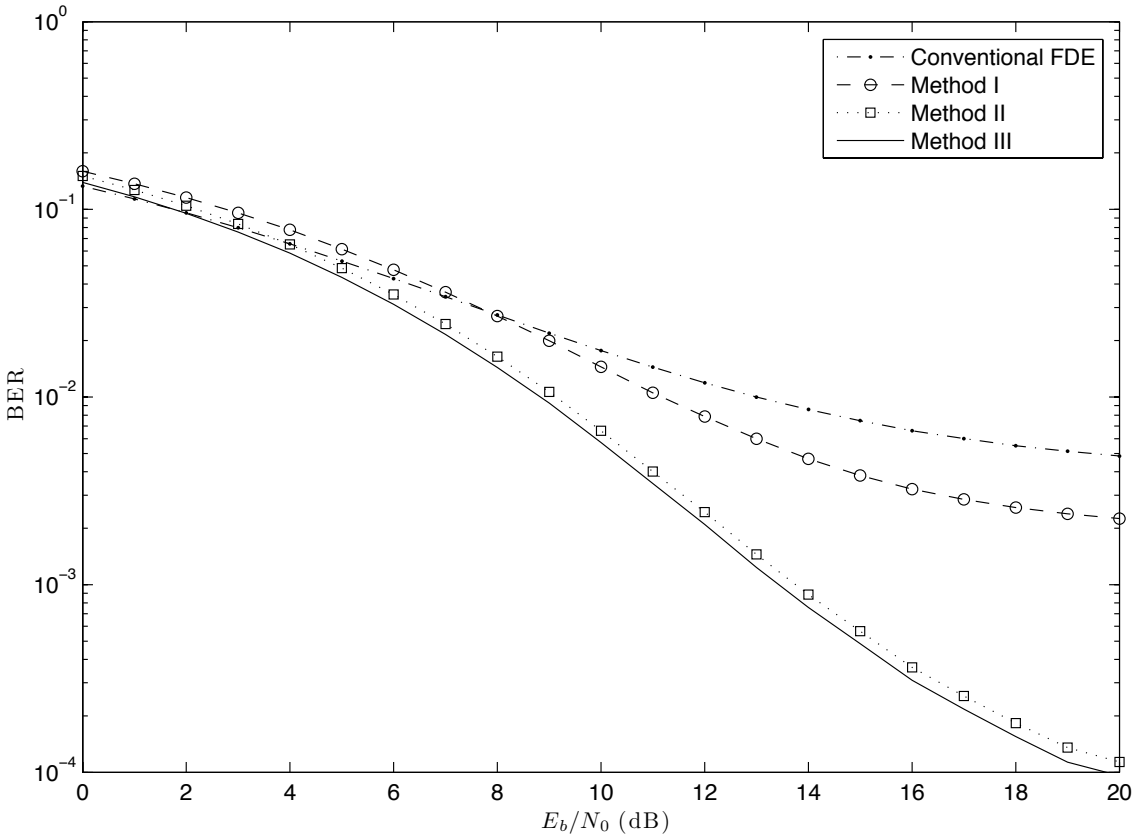

Figure 3.5: BER for linear FDE.

severely time-dispersive channels). We also assume perfect synchronization and channel estimation at the receiver.

From Figure 3.5, we can perceive the performance results obtained by these presented methods while comparing it with either the conventional FDE [Sar+94a]. As stated before, there is an increased performance when the number of constraints decrease (method I has JN constraints, method II has $2N$ constraints, and method III has N constraints). The results show that Method III gives the best overall performance, closely followed by method II. Both of them reduce the BER from 10^{-2} (in the conventional FDE) to 10^{-4} for $E_b/N_0 = 20$dB, showing a significant performance increase in the linear frequency domain equalization of offset modulations.

3.4 Linear FDE with Reduced Overall Residual Interference

It was shown that the introduction of the λ_k factor in the linear equalization, removes the IQI. However, as drawback, this method increases residual ISI, due to the added constraints in the FDE. Therefore, a better approach would be to minimize the overall interference instead of just eliminating IQI and accepting the consequent increase of ISI values. A simple way to minimize the overall interference is to replace the Lagrangian

multipliers λ_k by

$$\lambda_k^{clip} = \begin{cases} \lambda_k & , \quad |\lambda_k| < \lambda^{clip} \\ \frac{\lambda_k}{|\lambda_k|}\lambda^{clip} & , \quad |\lambda_k| > \lambda^{clip} \end{cases} \tag{3.55}$$

which means that we are limiting the effort of the λ_k factor on F_k. In fact, we can improve the performance by limiting the effect of λ_k in the equalization. This increases IQI, losing the constraint from (3.41) and therefore its odd symmetry, but also reduces the residual ISI, allowing to obtain an optimal value.

To obtain the optimum value of λ^{clip}, let us analyze the SIR from both ISI and IQI. Considering $P_k^{eq} = \sum_{q=0}^{J-1} P_{k+qN}^{(J)}$ as the equivalent equalized channel for a signal with N samples, the effective power of this signal can be written as

$$\sum_{k=0}^{N-1} \left|P_k^{eq}\right|^2. \tag{3.56}$$

Its residual ISI, in the frequency domain, will be defined as $I_k = P_k^{eq} - \frac{1}{N}\sum_{k=0}^{N-1} P_k^{eq}$. Therefore, being the residual ISI power proportional to

$$\sum_{k=0}^{N-1} |I_k|^2, \tag{3.57}$$

the signal to inter-symbol interference ratio can then be defined as

$$\text{SIR}_{\text{ISI}} = \frac{\sum_{k=0}^{N-1} \left|P_k^{eq}\right|^2}{\sum_{k=0}^{N-1} |I_k|^2}. \tag{3.58}$$

To obtain the residual IQI, let us look at condition (3.41). From (3.41), $P_k^{Q,eq} = \sum_{q=0}^{J-1} (-1)^q P_{k+qN}^{(J)}$, which means that the equivalent equalized channel, for the quadrature component, needs to have odd symmetry regarding to $N/2$. When we apply (3.55) to F_k, in linear equalization, this symmetry is lost and we can define $P_k^{Q,eq}$ as

$$P_k^{Q,eq} = P_k^{Q,\text{even}} + P_k^{Q,\text{odd}}, \tag{3.59}$$

where $P_k^{Q,\text{even}} = (P_k^{Q,eq} + P_{N-k}^{Q,eq})/2$, and $P_k^{Q,\text{odd}} = (P_k^{Q,eq} - P_{N-k}^{Q,eq})/2$ (without clipping the value of λ_k, $P_k^{Q,\text{even}} = 0$ and $P_k^{Q,\text{odd}} = P_k^{Q,eq}$). The residual IQI is associated with $P_k^{Q,\text{even}}$, and its power is proportional to

$$\sum_{k=0}^{N-1} \left|P_k^{Q,\text{even}}\right|^2. \tag{3.60}$$

Therefore, the signal to IQI ratio can be defined as

$$\text{SIR}_{\text{IQI}} = \frac{\sum_{k=0}^{N-1} \left|P_k^{eq}\right|^2}{\sum_{k=0}^{N-1} \left|P_k^{Q,\text{even}}\right|^2}. \tag{3.61}$$

Finally, the total SIR can be written as

$$\text{SIR} = \frac{\sum_{k=0}^{N-1} \left|P_k^{eq}\right|^2}{\sum_{k=0}^{N-1} \left|P_k^{Q,\text{even}}\right|^2 + \sum_{k=0}^{N-1} |I_k|^2}. \tag{3.62}$$

Figure 3.6 shows the values of SIR_{ISI}, SIR_{IQI} and total SIR versus λ^{clip}. To be able to obtain reliable results, it was assumed a noise-free system. Figure 3.7 shows the obtained BER versus λ^{clip}, for the same system with different E_b/N_0 values. From Figure 3.6 and 3.7 we can perceive that the optimum value of λ^{clip} is 0.5. In the next sections the adopted value of λ^{clip} will be always the optimum value: $\lambda^{clip} = 0.5$.

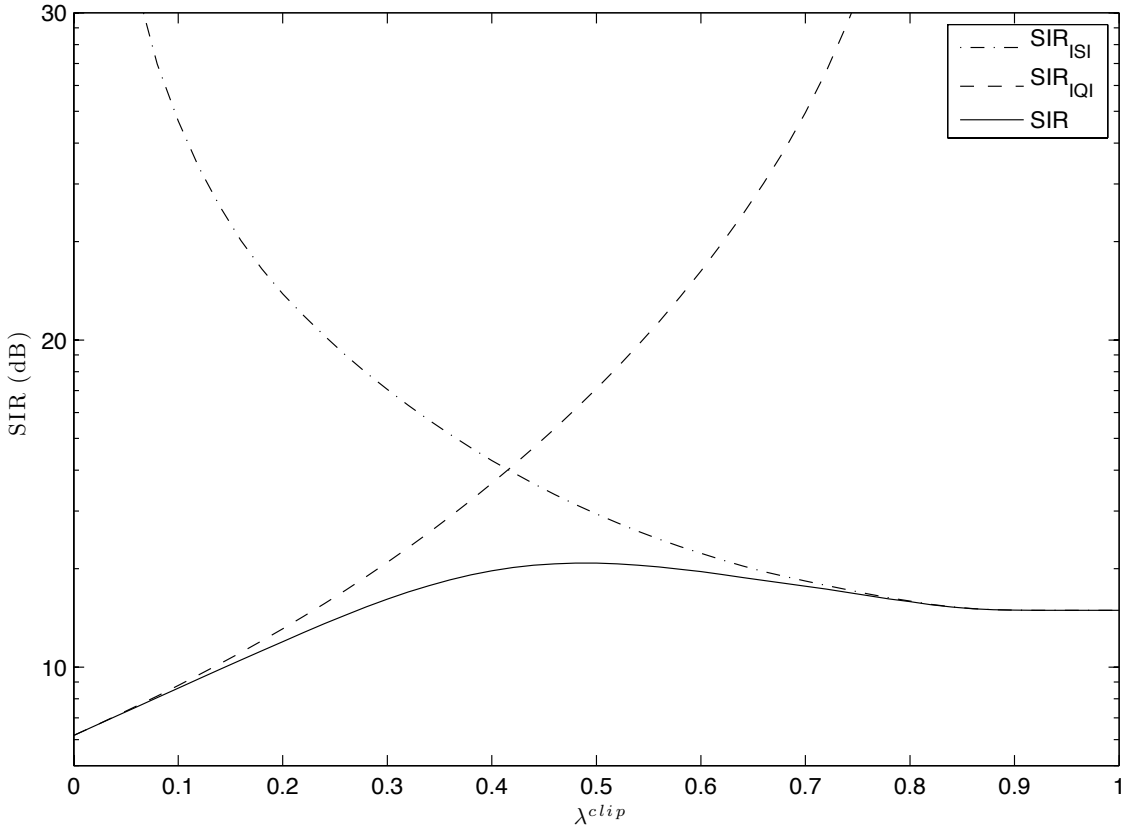

Figure 3.6: SIR_{ISI}, SIR_{IQI} and total SIR versus λ^{clip}.

In Figure 3.8 and 3.9 we compare the performance with this new method with either the conventional FDE [Sar+94a] and method III. Figure 3.8 refers to an OQPSK system, while the performance results of Figure 3.9 are for a 16-OQAM system. Clearly, there is an overall performance improvement (10 times in the OQPSK). These results show that the linear FDE with reduced overall residual interference gives the best performance for linear frequency domain equalization of offset modulations.

3.5 Iterative FDE with IQI Cancellation

As an alternative to an FDE coefficient specially designed to avoid IQI, we could optimize the FDE coefficients without any restrictions (as for QPSK schemes) and modify the receiver to cancel the resulting interference. This approach is particularly interesting when we employ iterative FDE receivers as the IB-DFE, since we can use the iterations to obtain

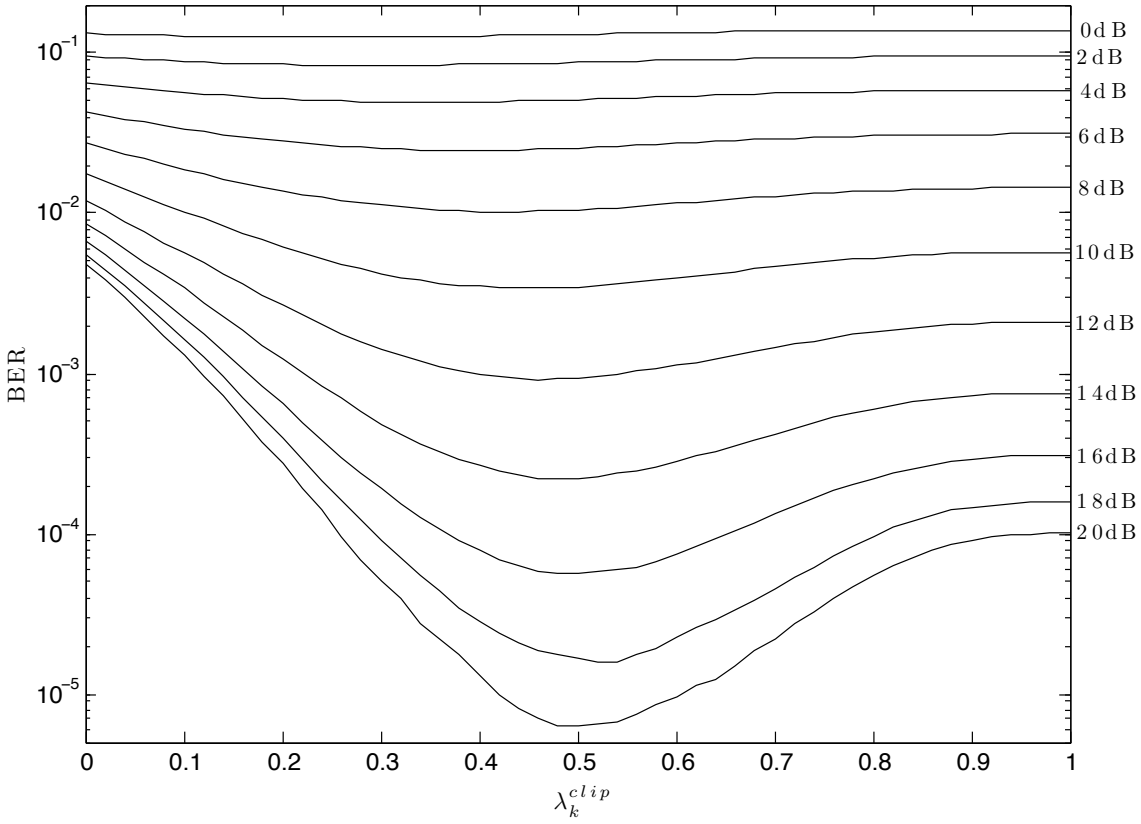

Figure 3.7: λ^{clip} impact on the BER performance of a linear FDE.

enhanced estimates of the I and Q components and cancel them when detecting the other component (see Fig. 3.10, where the middle feedback loop is used for IQI cancellation).

When employing an IB-DFE, the performance of a given system is greatly enhanced. To use the IB-DFE in OQPSK and OQAM schemes, some modifications ought to be done. Taking into account frequency multiplicity the output samples for a given iteration can be defined as

$$\widetilde{A}_k^I = \sum_{q=0}^{J/2-1} \left[F_{k+qN}^{(J)} \left(Y_{k+qN}^{(J)} - \overline{Y}_{k+qN}^{Q(J)} \right) - B_{k+qN}^{(J)} \overline{A}_{k+qN}^{I(J)} \right] \tag{3.63}$$

and

$$\widetilde{A}_k^Q = \sum_{q=0}^{J/2-1} \left[F_{k+qN}^{(J)} \left(Y_{k+qN}^{(J)} - \overline{Y}_{k+qN}^{I(J)} \right) - B_{k+qN}^{(J)} \overline{A}_{k+qN}^{Q(J)} \right], \tag{3.64}$$

where $\{k = 0, \ldots, 2N-1\}$. For the in-phase block, $\{\widetilde{A}_k^I; k = 0, \ldots, 2N-1\} = \text{DFT}\{\widetilde{a}_n^I; n = 0, \ldots, 2N-1\}$ only the even data bits are relevant, whereas for the quadrature block $\{\widetilde{A}_k^Q; k = 0, \ldots, 2N-1\} = \text{DFT}\{\widetilde{a}_n^Q; n = 0, \ldots, 2N-1\}$ the odd data bits are relevant for detection[5]. Note as well that the feedback data bits are, in this case, from soft bit decisions, and therefore more precise (roughly $\overline{A}_k \approx \rho \widehat{A}_k$).

[5] This is due to the time offset between in-phase and quadrature components in OQPSK.

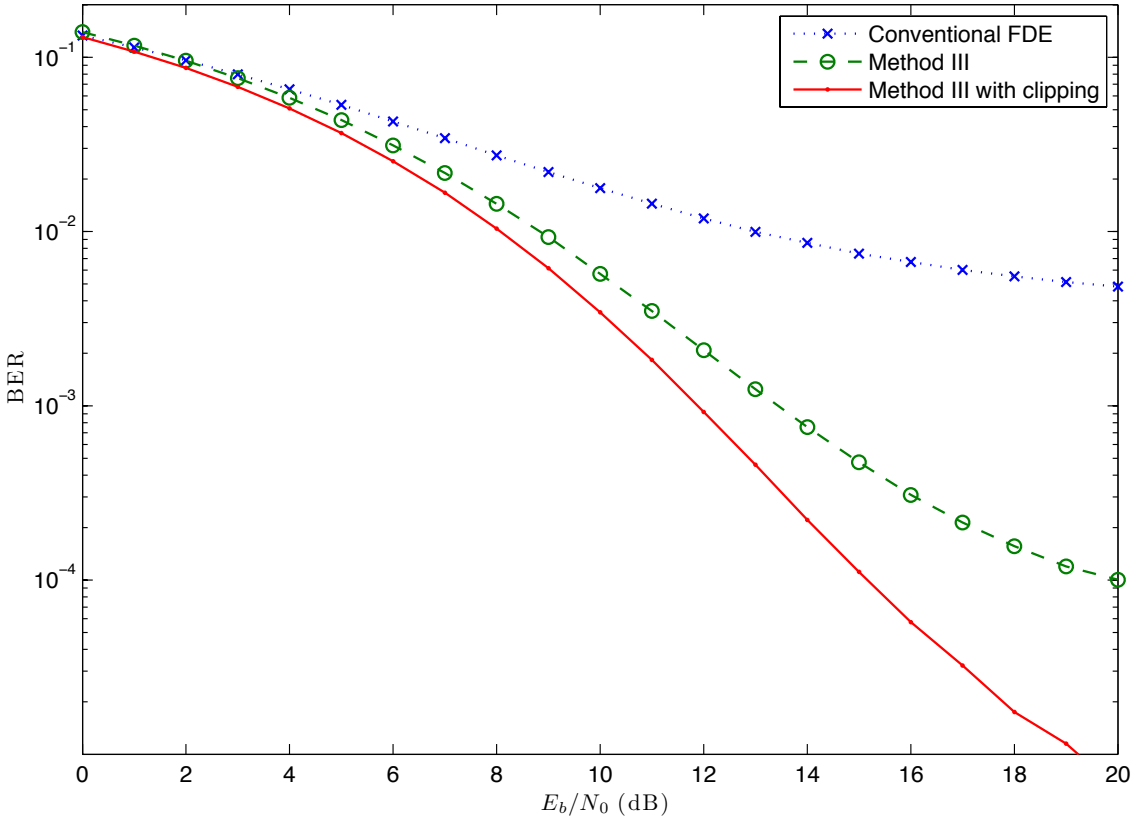

Figure 3.8: BER performance of OQPSK with different linear FDE receivers.

Since the first iteration of this method is, in fact, a linear equalization, where $\rho = 0$ and $\overline{a}_k$ is unknown, we can use any of the presented linear F_k throughout this chapter to minimize both ISI and IQI from the received signal. Nevertheless, the best performances will be obtained when the method with reduced overall residual interference is used. For the subsequent iterations we use the feedforward and feedback coefficients given by (3.16) and (3.17), i.e., we use the same values of the FDE designed for non-offset modulations.

The values of the overall average received frequency values for In-phase $\overline{Y}_k^{I(J)}$ and Quadrature $\overline{Y}_k^{Q(J)}$ signal, that cancel the IQI over the successive iterations are given by

$$\overline{Y}_k^{I(J)} = H_k^{(J)} \overline{A}_k^{I(J)} \tag{3.65}$$

and

$$\overline{Y}_k^{Q(J)} = H_k^{(J)} \Theta_k \overline{A}_k^{Q(J)}. \tag{3.66}$$

Figure 3.11 and 3.12, show the performance results regarding the Iterative FDE with IQI cancellation where the channel spans over 128 symbols and is characterized by the HIPERLAN/2 power delay profile type C [ETS98], with uncorrelated Rayleigh fading on each tap (similar results were observed for other severely time-dispersive channels). Again, perfect synchronization and channel estimation is assumed at the receiver. Figure 3.11 gives the results for an OQPSK system while Figure 3.12 shows the results for a 16-OQAM

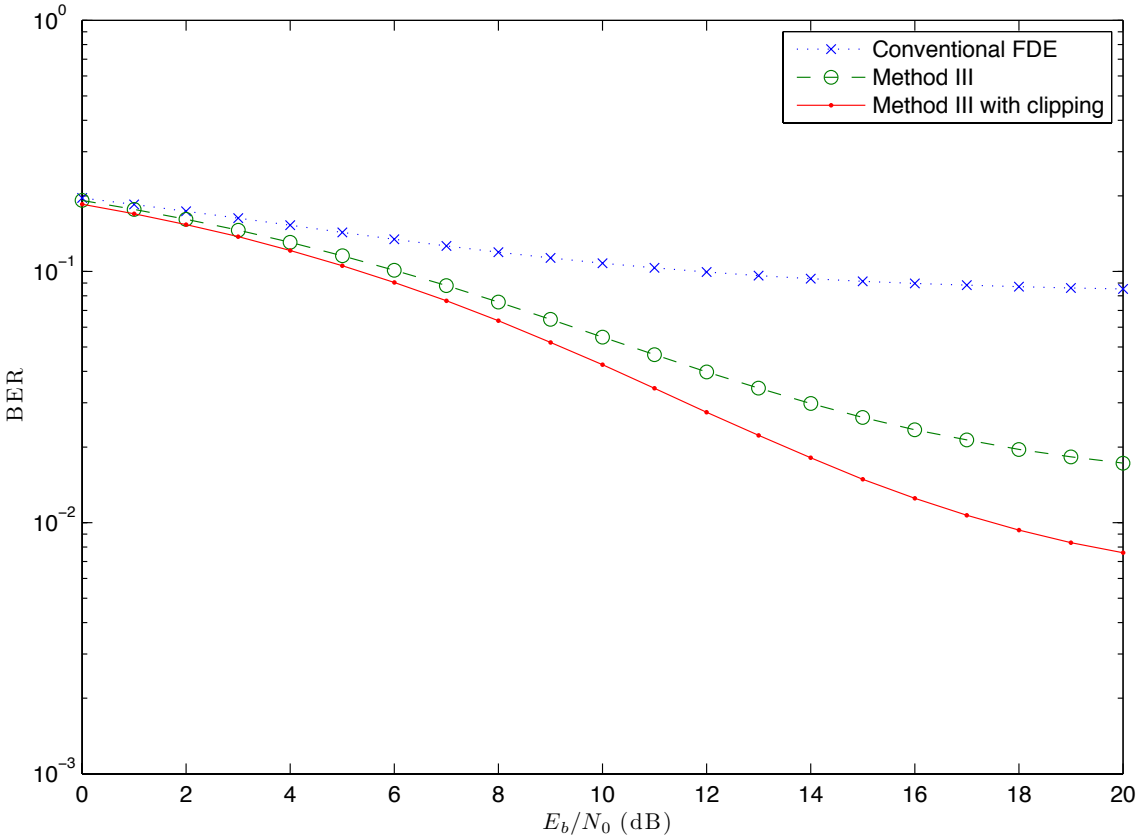

Figure 3.9: BER performance of 16-OQAM with different linear FDE receivers.

system. Each figure evaluates the impact on the number of iterations over the performance results with different equalization methods for the first iteration: conventional, method III, and method III with clipping.

As it can be seen from the results of Figure 3.11, despite the performance difference of the first iteration, all methods converge at the same pace close to the MFB. On the other hand, the 16-OQAM system (see Fig. 3.12) has a clear advantage with the method III with clipping over all the others. If we choose the conventional method over the proposed, one more iteration is needed to obtain similar results. This reduces processing power and energy in the overall equalization.

The results for the conventional IB-DFE without IQI cancellation were not shown since they only have slight performance increase within each iteration, following closely the results of the Linear FDE.

3.6 Performance Results with Multiple Unbalanced Nonlinear Amplifiers

This section considers the impact of phase and gain unbalance between different amplifiers due to an efficient amplification of M^2-OQAM signals.

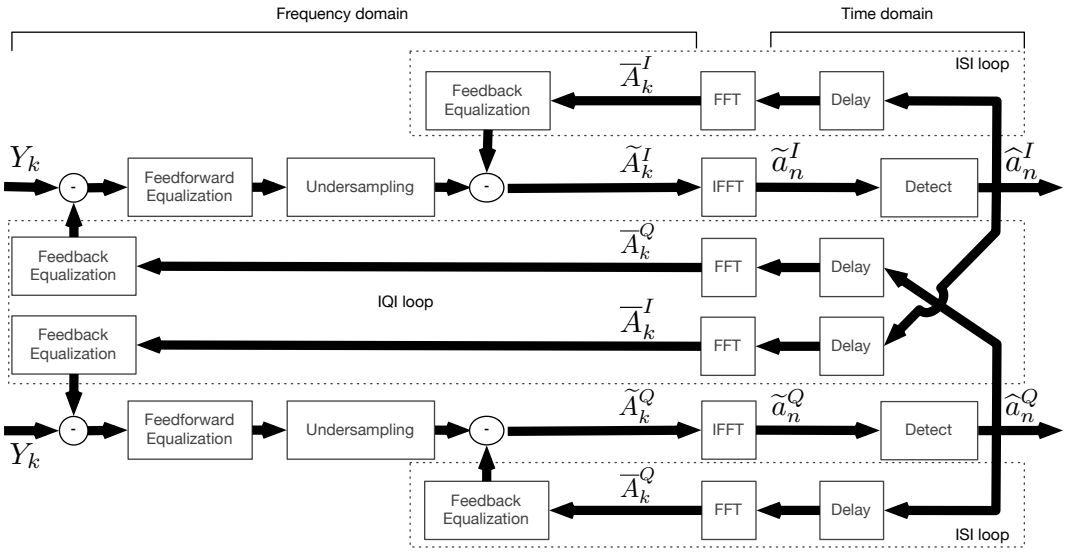

Figure 3.10: Proposed Iterative Receiver Structure.

To obtain high spectral efficiency, large constellations need to be employed. It is well known that QAM schemes have better power efficiency when compared with PSK schemes with the same number of constellation points. However, with QAM constellations the absolute value of the constellation points is not constant, contrarily to the PSK case. This means that QAM signals have significant envelope fluctuations, which lead to amplification constraints. In fact, even typical PSK schemes still require linear amplifiers since the envelope of the corresponding analog signal have envelope fluctuations (it can even be zero when we have transitions from one constellation point to the symmetrical one). OQPSK schemes have been proposed to overcome this problem and the most popular OQPSK scheme is the MSK modulation, where the transmitted signals have constant envelope, allowing a very efficient power amplification based on a grossly nonlinear amplifier.

This concept can be extended to QAM schemes. In fact, the envelope of OQAM signals do not have zero-crossing. However, OQAM signals are not suitable for nonlinear amplifiers because they still have envelope fluctuations. It is known that an OQAM signal can be written as a sum of OQPSK signals that can have constant envelope when a proper pulse shape is selected. In such conditions, these signals allow efficient high power amplification using grossly nonlinear amplifiers. To produce the corresponding OQAM signal we just need to combine the different OQPSK components with a passive combiner before sending them to the transmit antenna. Alternatively, we can employ separate antennas.

Nevertheless, the different amplifiers need to be perfectly balanced and the design of frequency-domain receivers for offset signals is more difficult than with the non-offset case due to the residual interference levels between I and Q components [Din+10b; Luz+10b]. This problem is more serious in the OQAM case [Luz+10a].

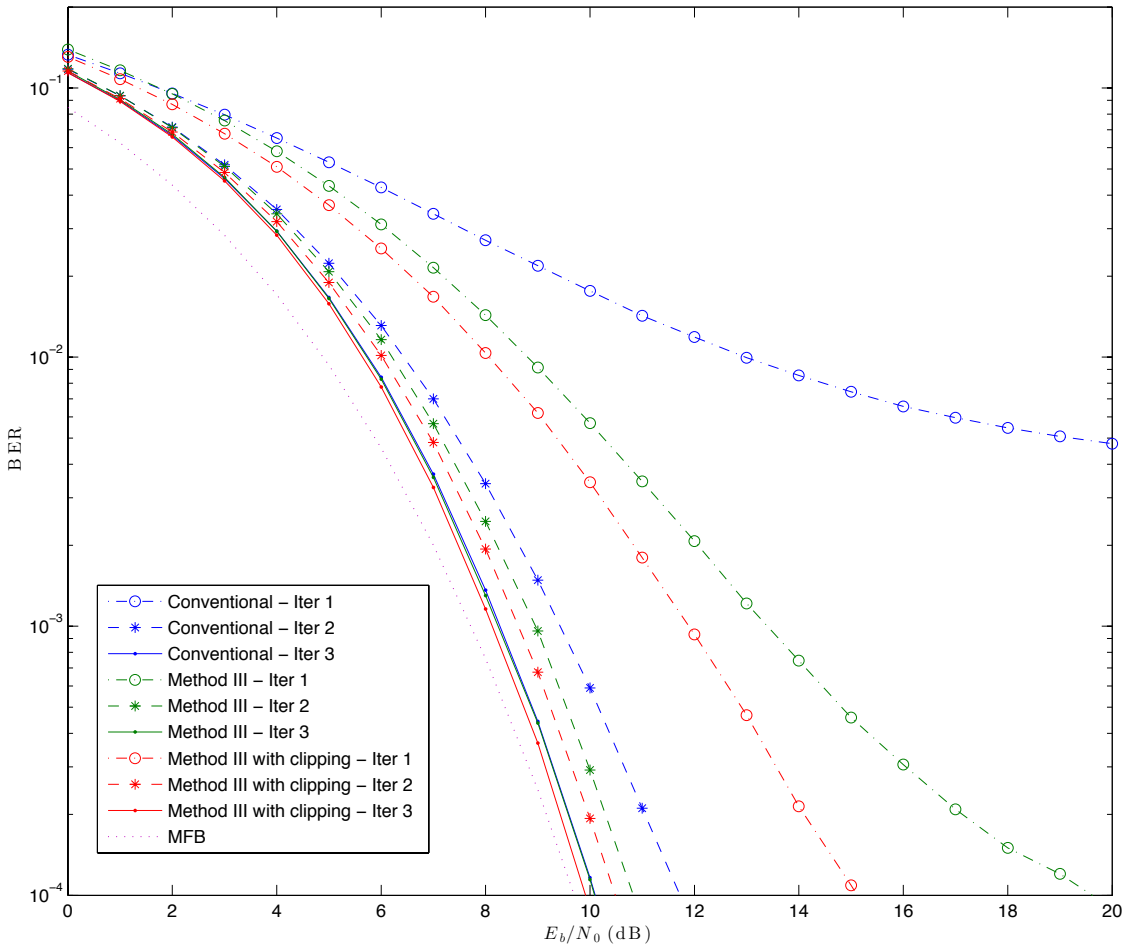

Figure 3.11: BER performance of OQPSK with iterative FDE receivers.

3.6.1 Unbalanced system description

Let us consider an SC-FDE scheme where the data is transmitted in blocks and a suitable cyclic prefix is append to each block. The length-N data block to be transmitted is $\{a_n; n = 0, 1, ..., N-1\}$, where $a_n = a_n^I + ja_n^Q$ is the nth data symbol. For a M^2-OQAM constellation, a_n^I and a_n^Q, take the values ± 1, ± 3, ..., and $\pm M - 1$. The complex envelope of these transmitted signals are

$$x(t) = \sum_{n=-N_{cp}}^{N-1} a_n^I r(t - nT_s) + \sum_{n=-N_{cp}}^{N-1} a_n^Q r(t - nT_s - T_o), \tag{3.67}$$

where $r(t)$ is the adopted pulse shape, T_o is the time offset between both I and Q components (usually $T_s/2$) and N_{cp} is the length of the cyclic prefix required for an efficient FDE implementation [Fal+02]. The block $\{a_n; n = 0, 1, ..., N-1\}$ is periodic with period N, therefore, $a_{-n} = a_{N-n}$.

It is clear that the complex envelope, $x(t)$, has envelope fluctuations due to the different values of a_n^I and a_n^Q. Therefore, it is not possible to apply highly nonlinear power

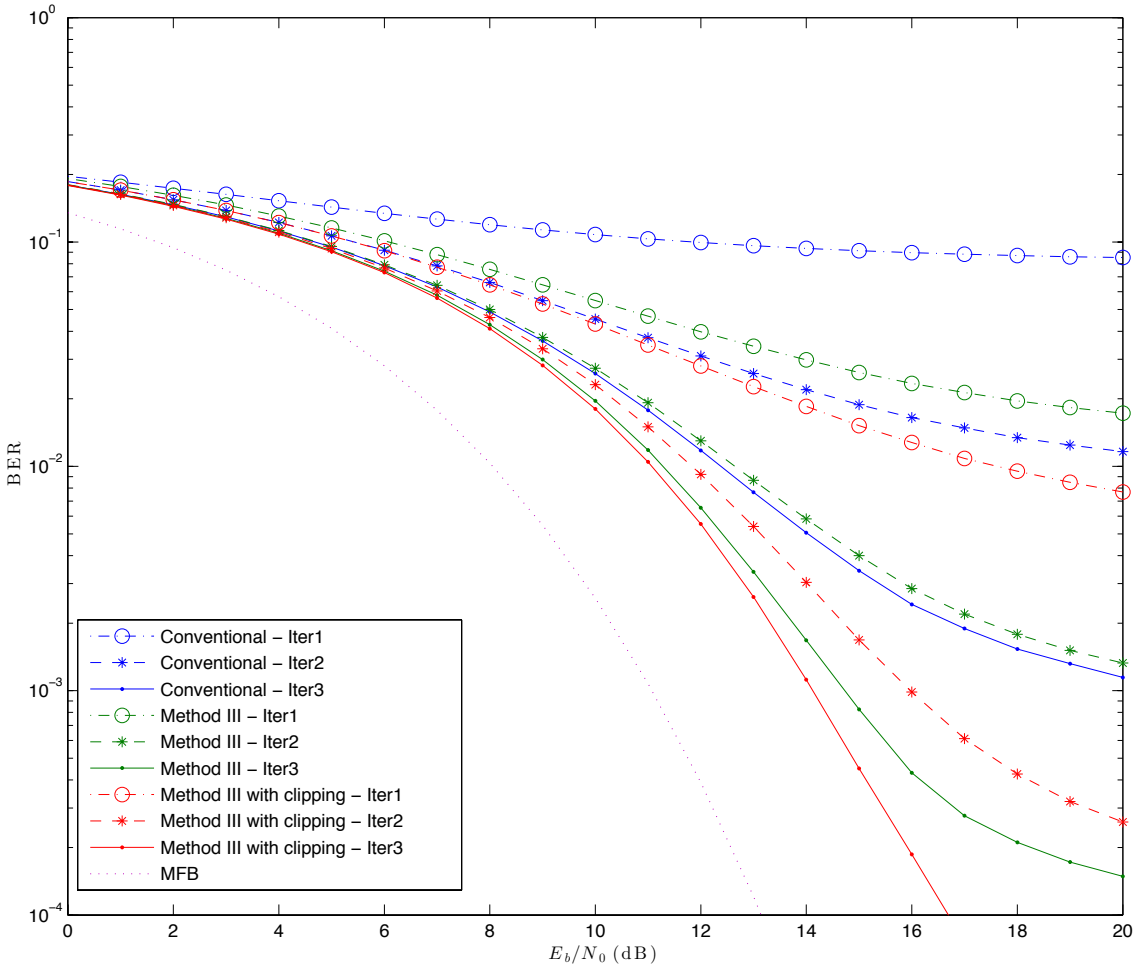

Figure 3.12: BER performance of 16-OQAM with iterative FDE receivers.

amplification directly to this scheme, since constant or quasi-constant envelope is needed. Nevertheless, it is possible to decompose $x(t)$ into $G = log_2(M)$ different components that have constant or quasi-constant envelope, depending on the adopted pulse shape[6]. To decompose $x(t)$ lets consider that the constellation symbols for M^2-QAM can be expressed as a function of the corresponding bits as follows [Din+10a]:

$$a_n^I = \sum_{g=1}^{G} \varphi^{(g)} \prod_{m=1}^{g} b_n^{I(m)}, \tag{3.68}$$

and

$$a_n^Q = \sum_{g=1}^{G} \varphi^{(g)} \prod_{m=1}^{g} b_n^{Q(m)}. \tag{3.69}$$

Merging (3.67), (3.68) and (3.69) it is possible to write $x(t)$ in the following way

$$x(t) = \sum_{g=1}^{G} x_g(t), \tag{3.70}$$

[6]For a MSK support pulse the signals will have constant envelope.

where

$$x_g(t) = \varphi^{(g)} \sum_{n=-N_{cpa}}^{N-1} \left(\prod_{m=1}^{g} b_n^{I(m)} r(t - nT_s) + \prod_{m=1}^{g} b_n^{Q(m)} r(t - nT_s - T_o) \right). \tag{3.71}$$

Now, every $x_g(t)$ component can be regarded as an OQPSK signal, which in fact has constant or quasi-constant envelope, allowing highly efficient nonlinear amplification. The main problem with this scheme is that G balanced power amplifiers are needed (Fig. 2.9).

3.6.2 Performance Results

This section presents a set of performance results concerning the impact of unbalanced transmitter power amplifiers with different gains and phases. The transmitted symbols are selected from a 16-OQAM signal constellation, that can be decomposed into two OQPSK signals, more specifically, MSK signals due to the pulse selection. For the iterative receiver we assumed four iterations and blocks of $N = 256$ data symbols. Two scenarios were approached: when the power amplifier G_2 (fig. 2.9) has a phase deviation ($\Delta\theta$), and when it has a gain deviation (ΔG_2). Mathematically these deviations can be expressed as

$$x(t)^{16OQAM} = \Delta G_2 e^{j\Delta\theta}\, x_1(t) + x_2(t), \tag{3.72}$$

with $x_1(t)$, by definition, being the signal with highest amplitude. As an example we considered a severely time dispersive propagation channel characterized by the power delay profile type C for High Performance Local Area Lan [ETS98], with uncorrelated Rayleigh fading in different taps (similar results were observed for other severely time-dispersive channels with rich multi-path propagation). The duration of the useful part of the data block (N symbols) is $4\mu s$. It is also assumed perfect synchronization and channel estimation.

In Figure 3.13 and 3.14 are shown the BER for two different values of E_b/N_0: 14dB (red) and 18dB (blue). It can be seen how the performance decreases with the unbalance between the amplifiers, either Figure 3.13 for the phase deviation or Figure 3.14 for the gain deviation. It is clear that a phase or gain deviation higher than 0.15 will greatly hinder the success of the transmission.

In Figure 3.15 it is shown the BER versus E_b/N_0 for three different values of $\Delta\theta$: 0 (perfectly balanced amplifiers), 0.1 and 0.2 rad, and Figure 3.16 shows the BER versus E_b/N_0 for three different values of ΔG_2: 1 (perfectly balanced amplifiers), 1.1, and 1,2. As we can see, this receiver performs well even for strong levels of amplifier unbalance.

3.7 Computational Complexity

3.7.1 Linear method

The computational complexity per data block of the equalizer structures resumes to a pair of FFT/IFFT, whose complexity is of the order $2JN\log_2(JN)$, plus JN multiplications by

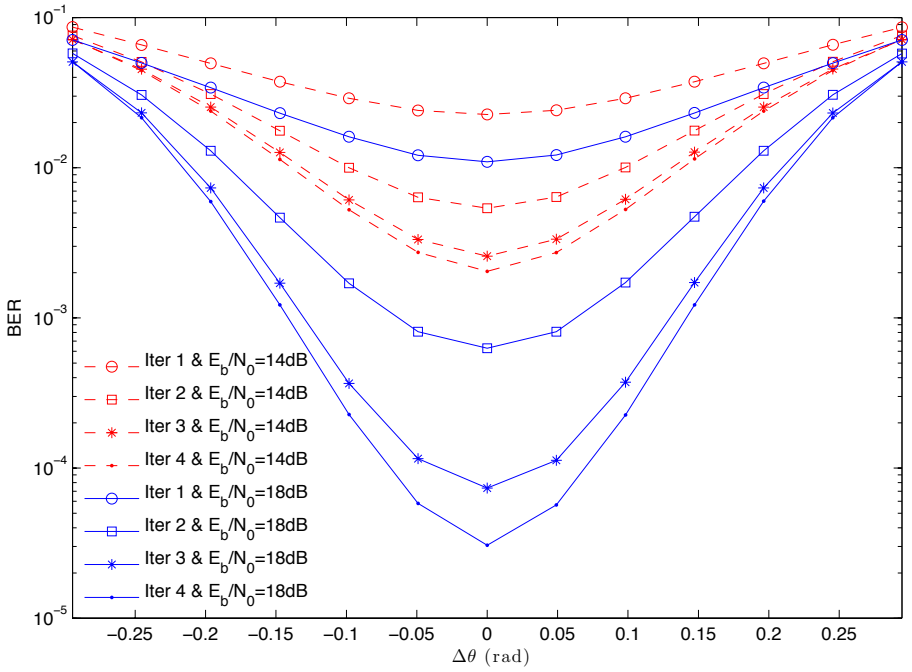

Figure 3.13: BER performance versus $\Delta\theta$ for the four iteration with an E_b/N_0 of 14 and 18dB.

the F_k coefficients and N additions of J replicas. Therefore, the overall FDE complexity is

$$O(JN\ \log(JN)) + O(JN) \propto O(JN\ \log(JN)). \tag{3.73}$$

This means that the receiver runs in quasi-linear time [Nai+94]. The overall complexity per data symbol is $O(J\ \log(JN))$.

The complexity required to obtain the F_k is $O(JN)$

3.7.2 Iterative method

For the iterative method we need a pair of FFT/IFFT, with complexity of the order $2JN\log_2(JN)$, plus $2JN$ multiplications (JN for the F_k and JN for the B_k), for each iteration. We also need to perform the I-Q cancellation (JN operations) for each iteration. If the receiver has N_I iterations, the overall receiver complexity is $O(N_I JN\ \log(JN))$ and the complexity per detected symbol is $O(N_I J\ \log(JN))$.

For each iteration, the complexity required to obtain the F_k and B_k is $O(JN)$

3.8 Conclusions and Final Remarks

In this chapter we considered frequency domain receiver designs for OQPSK and OQAM schemes. It was shown that conventional non-offset receivers are not suitable for offset schemes since they lead to significant interference between in-phase and quadrature components. These effects can be especially serious for OQAM schemes. To overcome this

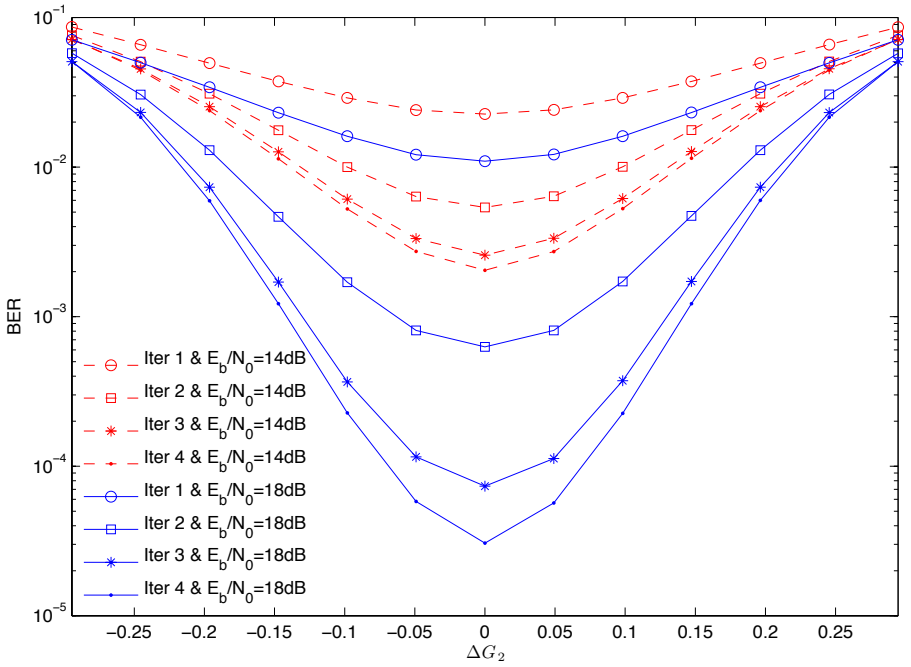

Figure 3.14: BER performance versus ΔG_2 for the four iteration with an E_b/N_0 of 14 and 18dB.

problem we proposed FDE designs that mitigate IQI at the sampling instants, as well as iterative FDE schemes with IQI cancellation. It was shown that our receivers are suitable to these schemes and are able to cope with IQI.

Our receivers significantly outperform FDE receivers designed for QPSK modulations. It was also demonstrated that the linear designs significantly outperform the linear FDE for non-offset modulations. Moreover, the iterative FDE can have performances close to the MFB, as it can be seen from the performance results.

It should be pointed out that the complexity of the different linear or iterative FDE receiver designs, proposed in this chapter, is not significantly higher than the complexity of the corresponding linear or iterative FDE receivers for conventional, non-offset modulations. For the linear receivers we need a few additional operations to obtain the Lagrange multipliers required for the computation of the FDE coefficients, but the FDE receiver complexity is identical. For the iterative receiver the FDE coefficients are the same; we only need to include the IQI removal block for each iteration.

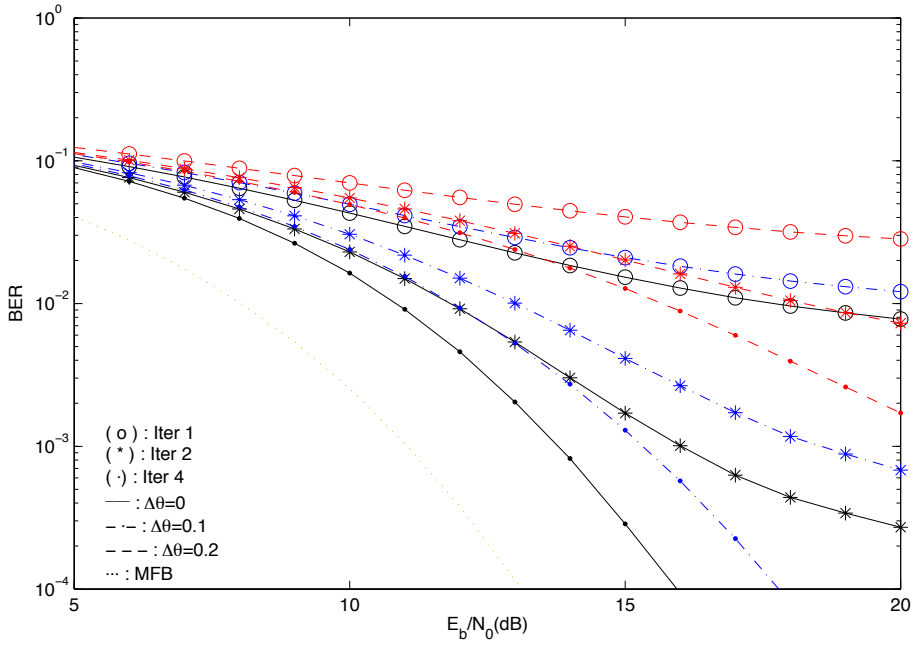

Figure 3.15: BER performance versus E_b/N_0 for $\Delta\theta = 0, 0.1$ and 0.2 rad.

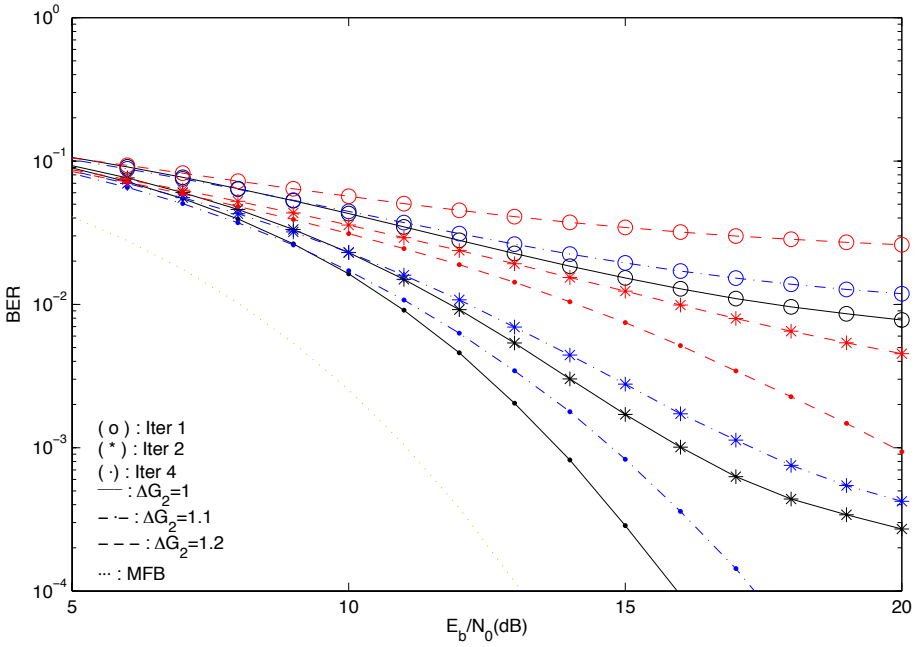

Figure 3.16: BER performance versus E_b/N_0 for $\Delta G_2 = 1, 1.1$ and 1.2.

CHAPTER 4

PRAGMATIC RECEIVER DESIGNS FOR OFFSET MODULATIONS

4.1 Introduction

Offset signals designed to have reduced envelope fluctuations allow high amplification efficiency. When combined with SC-FDE schemes, they become excellent candidates for broadband wireless systems with severe power constraints. However, the performance of these modulations with conventional FDE receivers is sub-par, even for receivers specifically designed for offset modulations. This is especially serious when large offset QAM constellations are used. In this chapter we consider SC-FDE schemes combined with offset modulations and study the reason behind the poor performance of conventional FDE implementations. We also present pragmatic FDE receivers for offset modulations that have low complexity and excellent performance.

To achieve a low cost and highly efficient power amplification we should employ grossly nonlinear power amplifiers. These amplifiers are only recommendable for signals with constant or quasi-constant envelope. As referred before offset modulations are particularly interesting in this context because both the envelope fluctuations and dynamic range of the transmitted signals are typically much lower than those of their corresponding non-offset signals. However, this is achieved at the expense of bandwidths wider than the minimum Nyquist band. Modulations like MSK [GM76], GMSK and other CPM schemes [Sun95] can be decomposed as the sum of OQPSK components [Ga+97], and we can design OQPSK-type signals with good trade-offs between power efficiency, spectral efficiency and reduced envelope fluctuations [DGa95; Mon06]. Offset modulations based on larger constellations such as OQAM [MG99], while having much higher envelope fluctuations, can also be written as a sum of OQPSK components with very low envelope fluctuations. These components can then be separately amplified, without added distortion, by several

grossly nonlinear amplifiers [Luz+11], allowing efficient power amplification.

SC-FDE schemes [Sar+94a] are excellent candidates for the uplink of broadband wireless systems where MTs have strict power constraints. In fact, the achievable performance and and overall signal processing complexity are similar to OFDM systems, but the transmitted signals have much lower envelope fluctuations and the signal processing load is shifted to the receiver (the BS in the uplink case). The performance can be further improved when SC-FDE schemes are combined with efficient nonlinear equalization techniques [BT02b]. However, when conventional FDE receivers (designed for non-offset modulations) are employed with offset modulations, the performance is very poor due to the residual interference between the in-phase and quadrature components at the sampling instants [Din+10b]. For this reason, FDE receivers specially designed for offset modulations were proposed in [Din+10b]. The basic idea behind these schemes is to design the FDE in such a way that the overall impulse response at its output (including the channel and transmit and receive filters) becomes real, avoiding IQI. Since these schemes can have very high residual ISI, modified FDE receivers were proposed in [Luz+10b] that minimize the overall residual ISI plus IQI levels, allowing an improved performance. Unfortunately, even the best FDE receivers for offset modulations have a somewhat disappointing performance when large offset constellations are employed [Luz+10a].

Contrary to what could be expected, the performance of offset modulations with conventional FDE receivers improves when we employ raised-cosine pulses with close to zero roll-off (i.e. with the minimum Nyquist bandwidth) [Luz+12a]. In this chapter, we take advantage of this particular property to define pragmatic FDE receivers for offset modulations that can take full advantage of the multi-path diversity. To decrease the complexity of the feedback loop, the oversampling and offset procedures are treated separately from the equalization process in a special block pair. The proposed FDE schemes can equalize oversampled and non-oversampled, offset and non-offset signals alike, allowing good performance, even for high order constellations.

This chapter is organized as follows: section 4.2 explains both QAM and OQAM signals and their respective oversampling. Section 4.3 describes several linear receiver designs for offset modulations. A set of performance results is shown in section 4.4. Section 4.5 shows the designs' adaptation to iterative receivers and devises a less complex iterative method. A series of simulations were conducted to evaluate the performance of the proposed iterative receivers. The corresponding BER performance results are then presented in section 4.6. A complexity analysis is made in section 4.7 and section 4.8 gives the final remarks for this chapter.

4.2 Offset QAM Signals

Let us consider an SC-FDE scheme where the data is transmitted in blocks of N symbols with a suitable cyclic prefix of N_{cp} samples appended to the beginning of each block. The data block to be transmitted is $\{a_n; n = 0, 1, ..., N-1\}$, where $a_n = a_n^I + ja_{n'}^Q$ is the nth data

symbol, a_n^I for the in-phase component and a_n^Q for the quadrature component. The data bits of an M^2-OQAM constellation with no zero crossings and low envelope fluctuations with a general grey mapping can be described as,

$$a_n^I = \sum_{g=1}^{G} \varphi^{(g)} \prod_{m=1}^{g} b_n^{I(m)}, \tag{4.1}$$

for the in-phase component and

$$a_n^Q = \sum_{g=1}^{G} \varphi^{(g)} \prod_{m=1}^{g} b_n^{Q(m)}, \tag{4.2}$$

for the quadrature component, where $b_n^{I(m)} = \pm 1$ and $b_n^{Q(m)} = \pm 1$ are the m's in-phase and quadrature sent data bits [Din+10a; Din+10c],

$$G = \log_2(M), \tag{4.3}$$

and $\{\varphi^{(g)}; g = 1, ..., G\}$ is the resolution block ($\varphi^{(1)}$ is the highest order resolution bit and $\varphi^{(G)}$ the lowest). For uniform constellations, $\varphi^{(g)} = 2^{G-g}$. This implies that the values associated to a_n^I and a_n^Q for an 4-OQAM constellation are ± 1, for 16-OQAM ± 1 and ± 3, for 64-OQAM ± 1, ± 3, ± 5, and ± 7 and so forth.

Assuming that the complex envelope of the transmitted signal is

$$x(t) = \sum_{n=-N_{cp}}^{N-1} a_n^I \, r(t - nT_s) \; + \; j a_n^Q \, r(t - nT_s - T_o), \tag{4.4}$$

where $r(t)$ is the adopted pulse shape, T_s is the sampling time, $T_o = T_s\phi$ is the time offset between both I and Q components, usually with $\phi = 0.5$, and N_{cp} is the length of the cyclic prefix required for an efficient FDE implementation [Fal+02]. The block $\{a_n; n = 0, 1, ..., N-1\}$ is periodic with period N. Therefore, the cyclic prefix is a repetition of the last N_{cp} data symbols of the data block, $a_{-n} = a_{N-n}$.

At the receiver side, if the received block is sampled at T_s/J rate, with $J \in \mathbb{N}$ samples per symbol, the samples associated to the useful part of the block, without cyclic prefix, will be $\{x_n^{(J)}; n = 0, 1, \ldots, JN-1\}$, with $x_n^{(J)} \triangleq x(n\,T_s/J)$[1]. Since $x(t)$ is cyclostationary [Gar91], $E\left[x(t)x(t-\tau)\right]$ is periodic in t, with period T_s for non-offset modulations, and $T_s/2$ for offset modulations.

The frequency-domain block associated to $\{x_n^{(J)}; n = 0, 1, \ldots, JN-1\}$, can be defined as $\{X_k^{(J)}; k = 0, 1, \ldots, JN-1\}$, and

$$X_k^{(J)} = A_k^{(J)} R_k^{(J)}, \tag{4.5}$$

where

$$\left\{R_k^{(J)}; k = 0, 1, \ldots, JN-1\right\} = \text{DFT}\left\{r_n^{(J)} \triangleq r(n\,T_s/J); n = 0, 1, \ldots, JN-1\right\}, \tag{4.6}$$

[1] J is assumed to be large enough to avoid aliasing effects.

and

$$\left\{A_k^{(J)}; k = 0, 1, \ldots, JN-1\right\} = \text{DFT}\left\{a_n^{(J)}; n = 0, 1, \ldots, JN-1\right\}, \tag{4.7}$$

as the oversampled data symbols. The relation of the oversampled data symbols to the regular data symbol block is distinct, whether we consider offset or non-offset modulations.

4.2.1 Non-offset Modulations

If we consider a non-offset modulation ($\phi = 0$), the relation of the oversampled data symbols to the regular data symbol block, as we can see in Fig. 4.1, is

$$a_n^{(J)} = \begin{cases} a_{n'} & , \quad n = Jn' \\ 0 & , \quad \text{otherwise} \end{cases}, \tag{4.8}$$

with $n = 0, 1, \ldots, JN-1$ and $n' = 0, 1, ..., N-1$. In the frequency domain, the correspondent oversampled data symbol block is

$$A_k^{(J)} = A_{k \bmod N}, \tag{4.9}$$

with x mod y as the remainder of division of x by y. The process to obtain the regular data

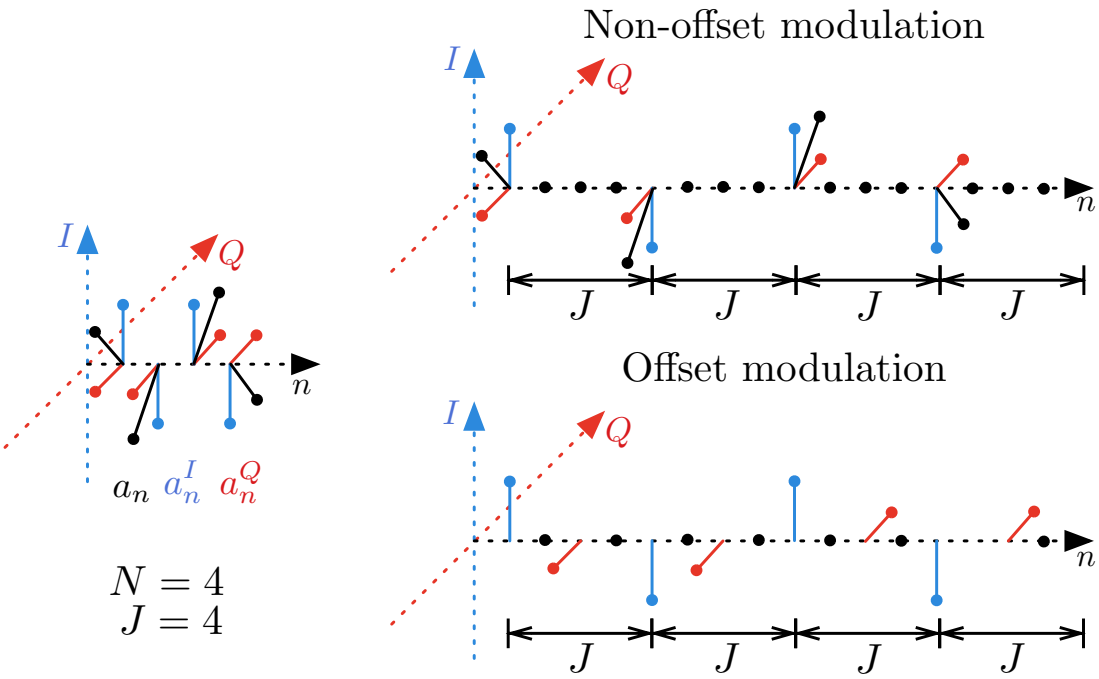

Figure 4.1: Data symbols' oversampling (regular data symbols in the left, oversampled data symbols in the right).

symbols from an non-offset oversampled frequency data block is

$$\left\{a_n; n = 0, 1, \ldots, N-1\right\} = \text{IDFT}\left\{\sum_{q=0}^{J-1} A_{k+qN}^{(J)}; k = 0, 1, \ldots, N-1\right\} \tag{4.10}$$

This means that an implicit multiplicity exists in the frequency-domain block when the adopted pulse shape has a bandwidth higher than the Nyquist band[2] [Oba+09]. Therefore, the frequency-domain sample A_k, can be repeated in several $X_k^{(J)}$ samples, separated by multiples of N, as shown in Figure 4.2.

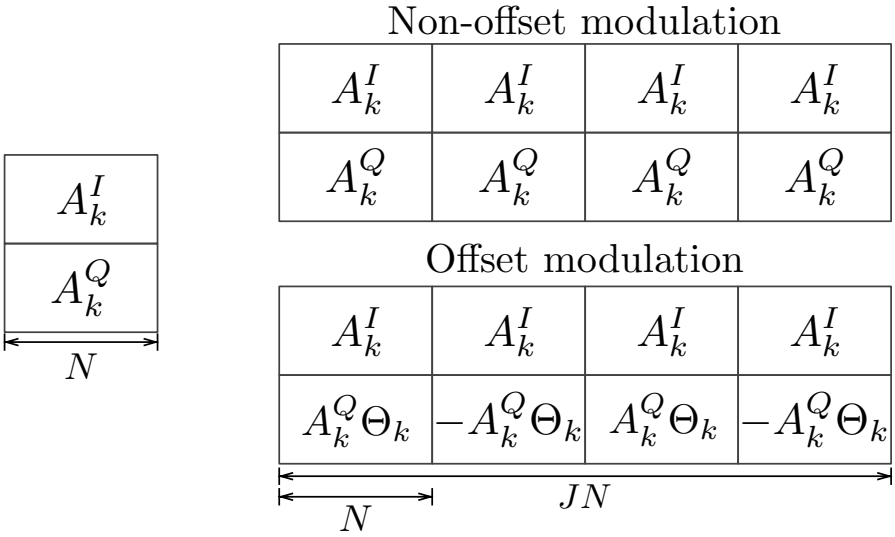

Figure 4.2: Frequency data symbols block oversampling (regular data symbols in the left, oversampled data symbols in the right).

4.2.2 Offset Modulations

On the other hand, in offset modulations (usually with $\phi = 0.5$ or $T_o = T_s/2$) the relation of the oversampled data symbols to the regular data symbol block is

$$a_n^{(J)} = \begin{cases} a_{n'}^I & , \quad n = Jn' \\ j\,a_{n'}^Q & , \quad n = Jn' + J\phi\,, \\ 0 & , \quad \text{otherwise} \end{cases} \tag{4.11}$$

where the symbol from in-phase component appears separated from the quadrature component, as depicted in Fig. 4.1. Furthermore, the oversampling procedure needs J as a multiple of $1/\phi$ and can be represented in the frequency domain as

$$A_k^{(J)} = A^I_{k \bmod N} + A^Q_{k \bmod N}\Theta_k, \tag{4.12}$$

where

$$\left\{A_k^I; k = 0, 1, \ldots, N-1\right\} = \text{DFT}\left\{a_n^I; n = 0, 1, \ldots, N-1\right\} \tag{4.13}$$

and

$$\left\{A_k^Q; k = 0, 1, \ldots, N-1\right\} = \text{DFT}\left\{a_n^Q; n = 0, 1, \ldots, N-1\right\}. \tag{4.14}$$

[2] R_k is not restricted to N non-zero samples.

The correspondent frequency domain phase deviation, from the quadrature component relatively to the in-phase component, can be described as

$$\Theta_k = j \exp\left(-\frac{j2\pi\phi k}{N}\right). \tag{4.15}$$

In regular offset modulations, where $\phi = 0.5$, there is a key difference when compared with non-offset modulation: $\Theta_{k+N} = -\Theta_k$. Therefore a sign shift occurs every N samples (see Fig. 4.2). To obtain the regular data symbols from an oversampled frequency data block taking into account the implicit multiplicity, we need to process the oversampled frequency domain data symbols by performing undersampling,

$$A_k = \frac{1}{J}\sum_{q=0}^{J-1} A^{(J)}_{k+qN} + j\,\frac{1}{J}\sum_{q=0}^{J-1} \frac{A^{(J)}_{k+qN}}{\Theta_{k+qN}}, \tag{4.16}$$

followed by the usual Inverse Discrete Fourier Transform (IDFT)

$$\left\{a_n; n = 0, 1, \ldots, N-1\right\} = \text{IDFT}\left\{A_k; k = 0, 1, \ldots, N-1\right\}. \tag{4.17}$$

4.3 Linear FDE Design for OQAM

In FDE, the received signal is sampled at J/T_s rate (oversampling the signal at rate J), the cyclic prefix is removed and the resulting block $\{y^{(J)}_n; n = 0, 1, \ldots, JN-1\}$ is transformed into the frequency domain, leading to the block $\{Y^{(J)}_k; k = 0, 1, \ldots, JN-1\}$. If the cyclic prefix is longer than the overall channel impulse response length then

$$Y^{(J)}_k = A^{(J)}_k H^{(J)}_k + N^{(J)}_k, \tag{4.18}$$

where $N^{(J)}_k$ is the corresponding noise component and

$$H^{(J)}_k = \breve{H}^{(J)}_k R^{(J)}_k \tag{4.19}$$

is the overall channel impulse response associated to the kth subcarrier, which includes the adopted pulse shape $R^{(J)}_k$ and the channel impulse response $\breve{H}^{(J)}_k$, as shown in Fig. 4.3.

From Fig. 4.4 it is clear that the inherent time offset T_o produces high level interference between both I and Q components of OQAM signals. Since the I and Q symbols are associated to the real and imaginary parts of the transmitted signals, there is no interference between the I and Q components at the sampling instants, when the adopted pulse shape is real. However, it is not enough to employ a real-valued pulse shape $r(t)$, because the channel can make the equivalent pulse shape at the receiver[3]

$$p(t) = r(t) * h(t) * f(t), \tag{4.20}$$

[3] $h(t)$ is the channel impulse response, $f(t)$ the corresponding feedforward equalization filter and $*$ denotes the convolution operator.

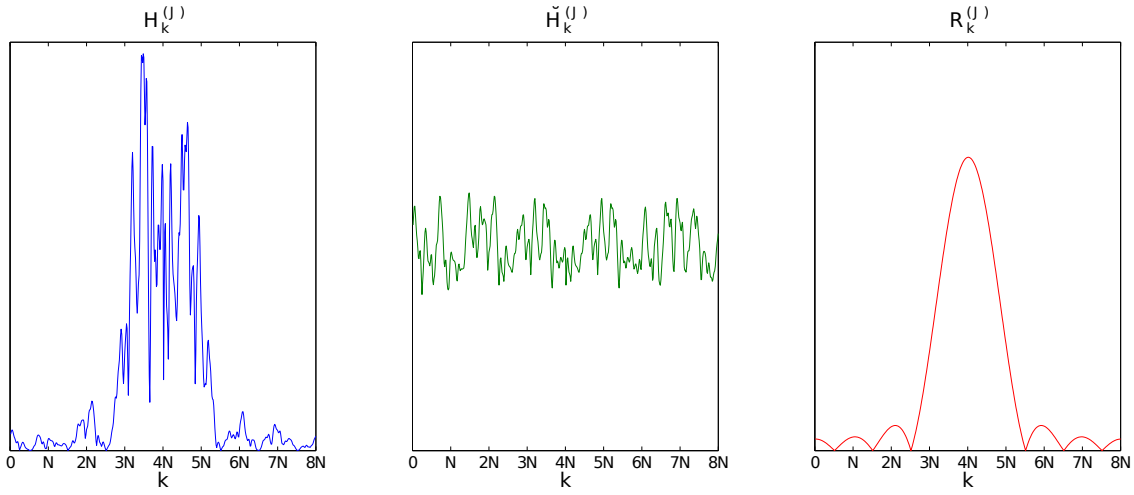

Figure 4.3: Overall channel impulse response ($H_k^{(J)}$), channel impulse response ($\breve{H}_k^{(J)}$) and adopted pulse shape ($R_k^{(J)}$) for $N = 64$ and $J = 8$.

complex-valued, where the received symbols after the feedforward filter become

$$\sum_n a_n^I p(t - nTs) + j \sum_n a_n^Q p(t - nTs - To). \tag{4.21}$$

This is the case of typical time-dispersive multi-path channels such as the ones inherent to broadband wireless systems.

Fig. 4.5 represents the equalization process for a linear FDE that can be expressed as

$$\widetilde{A}_k^{(J)} = F_k^{(J)} Y_k^{(J)}, \tag{4.22}$$

where $\{F_k^{(J)}; k = 0, ..., JN - 1\}$ are the feedforward coefficients, responsible for the performance of the linear FDE that will be discussed in the following subsections. Finally, to obtain the corresponding time domain data symbols' estimate $\widetilde{a}_{n'}$, it is necessary to remove the oversampling and the offset from $\widetilde{A}_k^{(J)}$ (4.16), and apply the IDFT to the resulting $\widetilde{A}_k$ (4.17).

4.3.1 Conventional FDE

The conventional linear FDE for non-offset modulations taking into account oversampled signals under the MMSE criteria is characterized by the following feedforward coefficients [Ga+03]:

$$F_k^{(J)} = \frac{\kappa \, H_k^{(J)\,*}}{\alpha + \sum_{q=0}^{J-1} \left| H_{(k \bmod N)+qN}^{(J)} \right|^2}, \tag{4.23}$$

with α denoting the inverse of the SNR and κ selected to ensure

$$\frac{1}{JN} \sum_{q=0}^{JN-1} F_k^{(J)} H_k^{(J)} = 1. \tag{4.24}$$

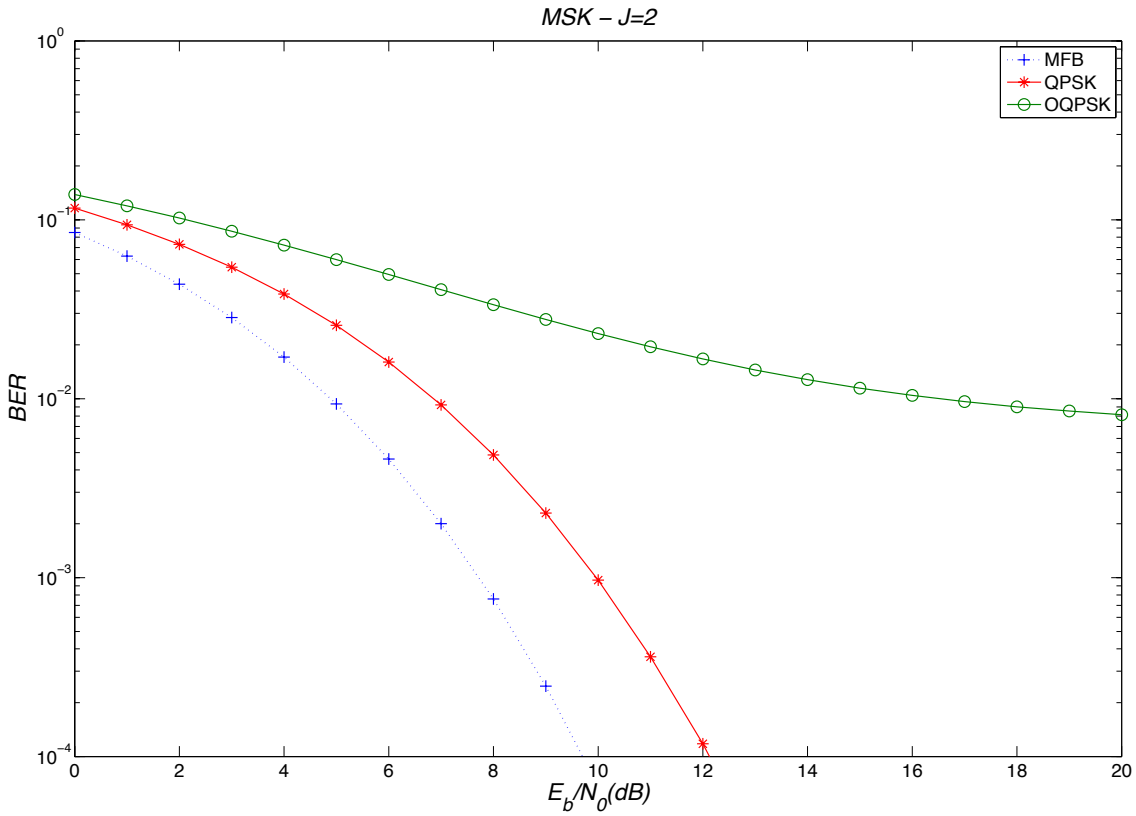

Figure 4.4: BER performance for QPSK and OQPSK with conventional FDE.

4.3.2 Interference minimization FDE

It was demonstrated in [Din+10b] that conventional MMSE FDE for non-offset modulations had very poor performance under offset scenarios. In chapter 3 we presented a solution using feedforward coefficient values that minimize both IQI and ISI under the MMSE criteria

$$F_k^{(J)} = \begin{cases} \dfrac{\kappa(1-\lambda_{k'}^{clip})H_k^{(J)*}}{\alpha+\sum_{(k \bmod N)\in\left(\Psi_{k'}^{(1)} \cup \Psi_{k'}^{(3)}\right)}\left|H_k^{(J)}\right|^2} & , \quad k \in \Psi_{k'}^{(1)} \\ \dfrac{\kappa(1+\lambda_{k'}^{clip})H_k^{(J)*}}{\alpha+\sum_{(k \bmod N)\in\left(\Psi_{k'}^{(1)} \cup \Psi_{k'}^{(3)}\right)}\left|H_k^{(J)}\right|^2} & , \quad k \in \Psi_{k'}^{(3)} \\ \dfrac{\kappa(1-\lambda_{k'}^{clip})H_k^{(J)*}}{\alpha+\sum_{(k \bmod N)\in\left(\Psi_{k'}^{(2)} \cup \Psi_{k'}^{(4)}\right)}\left|H_k^{(J)}\right|^2} & , \quad k \in \Psi_{k'}^{(2)} \\ \dfrac{\kappa(1+\lambda_{k'}^{clip})H_k^{(J)*}}{\alpha+\sum_{(k \bmod N)\in\left(\Psi_{k'}^{(2)} \cup \Psi_{k'}^{(4)}\right)}\left|H_k^{(J)}\right|^2} & , \quad k \in \Psi_{k'}^{(4)} \end{cases}, \tag{4.25}$$

with $k' = 0, 1, \ldots, N-1$ and

$$\lambda_{k'}^{clip} = \begin{cases} \lambda_{k'} & , \quad |\lambda_{k'}| < 0.5 \\ \frac{\lambda_{k'}}{|\lambda_{k'}|}\,0.5 & , \quad |\lambda_{k'}| > 0.5 \end{cases}, \tag{4.26}$$

where

$$\lambda_{k'} = \frac{\left(Z^{-}_{(1,2)}\right)\left(\alpha + Z^{+}_{(3,4)}\right) + \left(Z^{-}_{(3,4)}\right)\left(\alpha + Z^{+}_{(1,2)}\right)}{\left(Z^{+}_{(1,2)}\right)\left(\alpha + Z^{+}_{(3,4)}\right) + \left(Z^{+}_{(3,4)}\right)\left(\alpha + Z^{+}_{(1,2)}\right)}, \tag{4.27}$$

with

$$Z^{-}_{(i,j)} = \sum_{k \in \Psi^{(i)}_{k'}} \left|H^{(J)}_k\right|^2 - \sum_{k \in \Psi^{(j)}_{k'}} \left|H^{(J)}_k\right|^2, \tag{4.28}$$

$$Z^{+}_{(i,j)} = \sum_{k \in \Psi^{(i)}_{k'}} \left|H^{(J)}_k\right|^2 + \sum_{k \in \Psi^{(j)}_{k'}} \left|H^{(J)}_k\right|^2, \tag{4.29}$$

and

$$\Psi^{(1)}_{k'} = \left\{k' + q2N; q = 0, 1, ..., J/2 - 1\right\}, \tag{4.30}$$

$$\Psi^{(2)}_{k'} = \left\{N - k' + q2N; q = 0, 1, ..., J/2 - 1\right\}, \tag{4.31}$$

$$\Psi^{(3)}_{k'} = \left\{N + k' + q2N; q = 0, 1, ..., J/2 - 1\right\}, \tag{4.32}$$

$$\Psi^{(4)}_{k'} = \left\{2N - k' + q2N; q = 0, 1, ..., J/2 - 1\right\}. \tag{4.33}$$

This method was shown to have significantly better performance over the conventional MMSE FDE [Luz+10b].

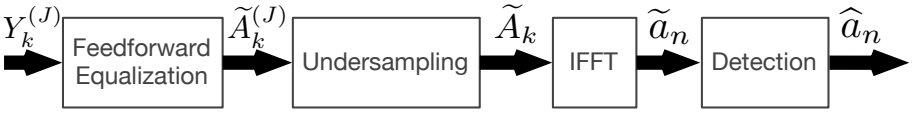

Figure 4.5: Linear frequency domain equalization.

4.3.3 Minimum-band FDE

The motivation for this method started with the BER performance comparison between raised cosine support pulses with different roll-off factors. From the observation of the right side of Fig. 4.6, it is possible to conclude that using the conventional linear FDE equalization, characterized by (4.23), with an extremely selective channel impulse response, the best performance is only achieved by raised cosine support pulses with a null roll-off factor. From Fig. 4.6 we can perceive that the IQI levels are lower when the support pulse bandwidth shrinks.

Therefore we can define, a very simple FDE where the received signal is filtered to remove all frequency multiplicity, leaving only the N sample signal (Φ) that has the highest power at the transmitter (see Fig. 4.7) [Luz+12a]. Mathematically, this operation can be expressed as

$$H^{(\mathrm{MB})(J)}_k = \begin{cases} H^{(J)}_k & , \quad k \in \Phi \\ 0 & , \quad \text{otherwise} \end{cases}. \tag{4.34}$$

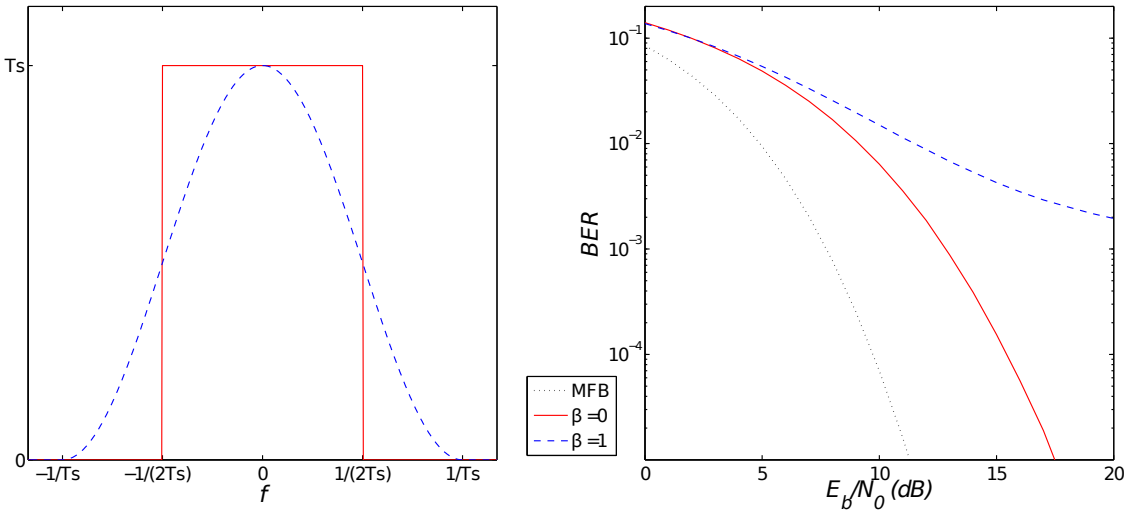

Figure 4.6: Frequency spectrum of raised cosine support pulse (left) and BER performance vs. E_b/N_0 for conventional FDE using raised cosine support pulses (right), for different β (roll-off) factors.

Further on, the equalizer coefficients are obtained by the traditional MMSE criteria,

$$F_k^{(J)} = \frac{\kappa \left(H_k^{(\mathrm{MB})(J)} \right)^*}{\alpha + \left| H_k^{(\mathrm{MB})(J)} \right|^2}, \tag{4.35}$$

but take into account the filtered channel response $H_k^{(\mathrm{MB})(J)}$, instead of the overall channel impulse response $H_k^{(J)}$. However, there is a drawback in this method, since it neglects all the power sent by the transmitter outside of the filtered region and therefore, all of the signals' diversity. In fact, the total power loss, considering an MSK support pulse is

$$\frac{\sum_{k=0}^{JN-1} \left| R_k^{(\mathrm{MB})(J)} \right|^2}{\sum_{k=0}^{JN-1} \left| R_k^{(J)} \right|^2} \approx -1.5\mathrm{dB}, \tag{4.36}$$

with

$$R_k^{(\mathrm{MB})(J)} = \begin{cases} R_k^{(J)} & , \quad k \in \Phi \\ 0 & , \quad \text{otherwise} \end{cases}. \tag{4.37}$$

Therefore, this method starts off hindered, compared to the other ones.

4.3.4 Full-band FDE

This method implements a pragmatic equalization algorithm that uses the full band of the oversampled received signal already represented in Fig. 4.2. The transmitted signal given by (4.5) is divided in two parts: the data symbols $A_k^{(J)}$ and the support pulse $R_k^{(J)}$. Since the support pulse has a fixed given value, the receiver will be able to know a priori, its value without any kind of estimation.

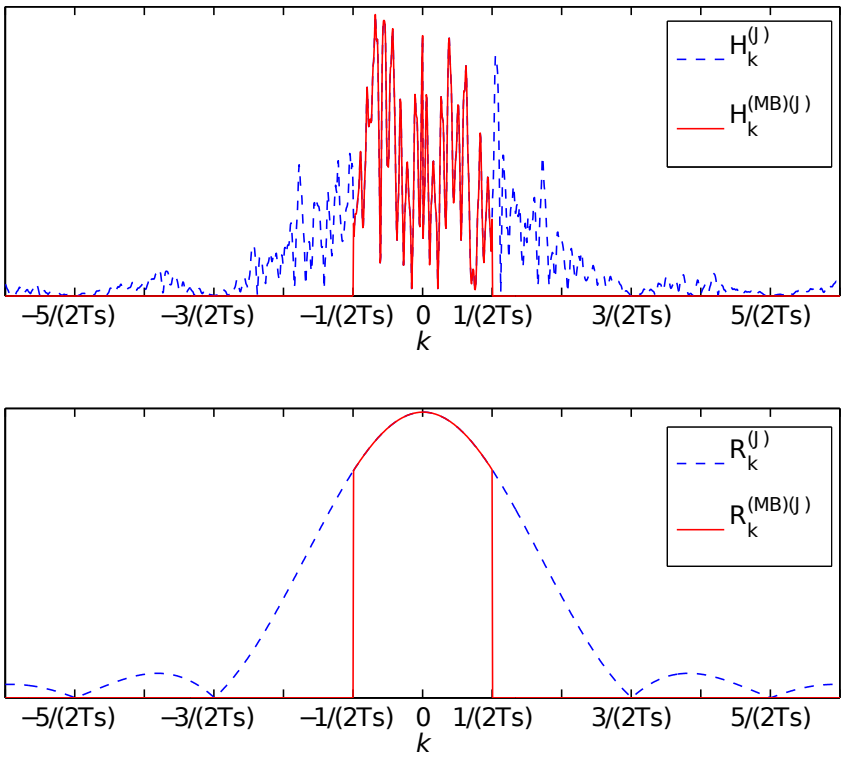

Figure 4.7: Frequency spectrum of $H_k^{(J)}$, $H_k^{(\mathrm{MB})(J)}$ (up) and $R_k^{(J)}$, $R_k^{(\mathrm{MB})(J)}$ (down) for an MSK support pulse.

For the sake of simplicity, let us assume that the support pulse $r(t)$ is selected to ensure that the output of the matched filter, i.e. $r(t) * r^*(-t)$, fulfills the first Nyquist criterion. Therefore, there is neither ISI nor IQI at the time-domain symbol sampling associated to the signal $A_k^{(J)} \left|R_k^{(J)}\right|^2$ since the time-domain samples associated to $\left|R_k^{(J)}\right|^2$ are, in fact, real. The same would remain true if a ZF equalizer (i.e., $F_k = 1/H_k$) was to be employed at the receiver before the equivalent matched filter operation[4]. Since a ZF is not recommendable in SC-FDE communication due to noise enhancement effects, we can employ a "full-band" MMSE equalizer to invert channel effects. The feedforward coefficients values for this equalization are

$$F_k^{(J)} = \kappa\, E_k^{(J)} R_k^{(J)^*}, \tag{4.38}$$

with

$$E_k^{(J)} = \frac{\breve{H}_k^{(J)^*}}{\alpha + \left|\breve{H}_k^{(J)}\right|^2} \tag{4.39}$$

as the MMSE equalizer.

In this way, for a high enough SNR ($\alpha \to 0$), when E_k is applied to $\breve{H}_k^{(J)}$, the result will be

$$\frac{1}{JN} \sum_{k=0}^{JN-1} E_k^{(J)} \breve{H}_k^{(J)} \approx 1. \tag{4.40}$$

[4]In the frequency domain, the matched filter can be regarded as multiplying the "full-band" signal samples (i.e. the samples associated to the oversampled received) by $R_k^{(J)^*}$.

Therefore, when the values for the feedforward coefficients $F_k^{(J)}$ are applied to $H_k^{(J)}$,

$$F_k^{(J)} H_k^{(J)} = \left(\frac{\breve{H}_k^{(J)*}}{\alpha + \left|\breve{H}_k^{(J)}\right|^2} R_k^{(J)*} \right) \left(\breve{H}_k^{(J)} R_k^{(J)} \right) \approx \left| R_k^{(J)} \right|^2, \tag{4.41}$$

and

$$F_k^{(J)} Y_k^{(J)} \approx A_k^{(J)} \left| R_k^{(J)} \right|^2, \tag{4.42}$$

mitigating both ISI and IQI.

4.4 Performance Results for Linear Equalization

In this section we present a set of performance results concerning linear receivers for 16-OQAM and 64-OQAM signal constellations with blocks of $N = 256$ data symbols and an MSK support pulse. We considered severely time dispersive propagation channels, with uncorrelated Rayleigh fading in different taps. The duration of the useful part of the data block (N symbols) is $4\mu s$ and perfect synchronization and channel estimation is assumed. Oversampled and non oversampled regular modulations (16-QAM and 64-QAM) with linear conventional FDE were added to the results for comparison purposes. Fig. 4.8 presents the BER performance of these three methods against the conventional FDE and the MFB for a 16-OQAM constellation. The MFB can be defined as

$$P_{\text{MFB}}\left(\frac{E_b}{N_0}\right) = \frac{2}{\log_2(M)}\left(1 - \frac{1}{M}\right) \cdot Q\left(\sqrt{\frac{6\log_2(M)}{(M^2-1)} \cdot \frac{E_b}{N_0} \cdot \frac{\sum_k \left|H_k^{(J)}\right|^2}{\sum_k \left|R_k^{(J)}\right|^2}} \right), \tag{4.43}$$

where E_b denotes the average bit energy and N_0 the one-sided power spectral length of the channel noise.

From these results we can verify that all the methods achieve better performance than the conventional FDE except the minimum-band method for E_b/N_0 values below 10 dB (mainly due to the specific 1.5 dB power loss of the method). Nevertheless, for $E_b/N_0 > 20$ dB, this method surpasses the interference minimization method, becoming the second best. It's clear that the method with the best performance is the full-band FDE, reaching the lowest BER for any given E_b/N_0 value. This behavior becomes more obvious when the constellation order is increased, as we can see from the comparison of Fig. 4.9 with Fig. 4.8. Due to the high interference values of 64-OQAM constellation, conventional and IQI-free methods have increasingly reduced performance. In higher order constellations, the advantage of the minimum-band and full-band FDE is more distinct, with the latter still acquiring the best performance result of all the methods. When compared to non-offset modulations, the full-band FDE has better performance than non-oversampled 16-QAM and 64-QAM but falls behind the oversampled 16-QAM and 64-QAM results.

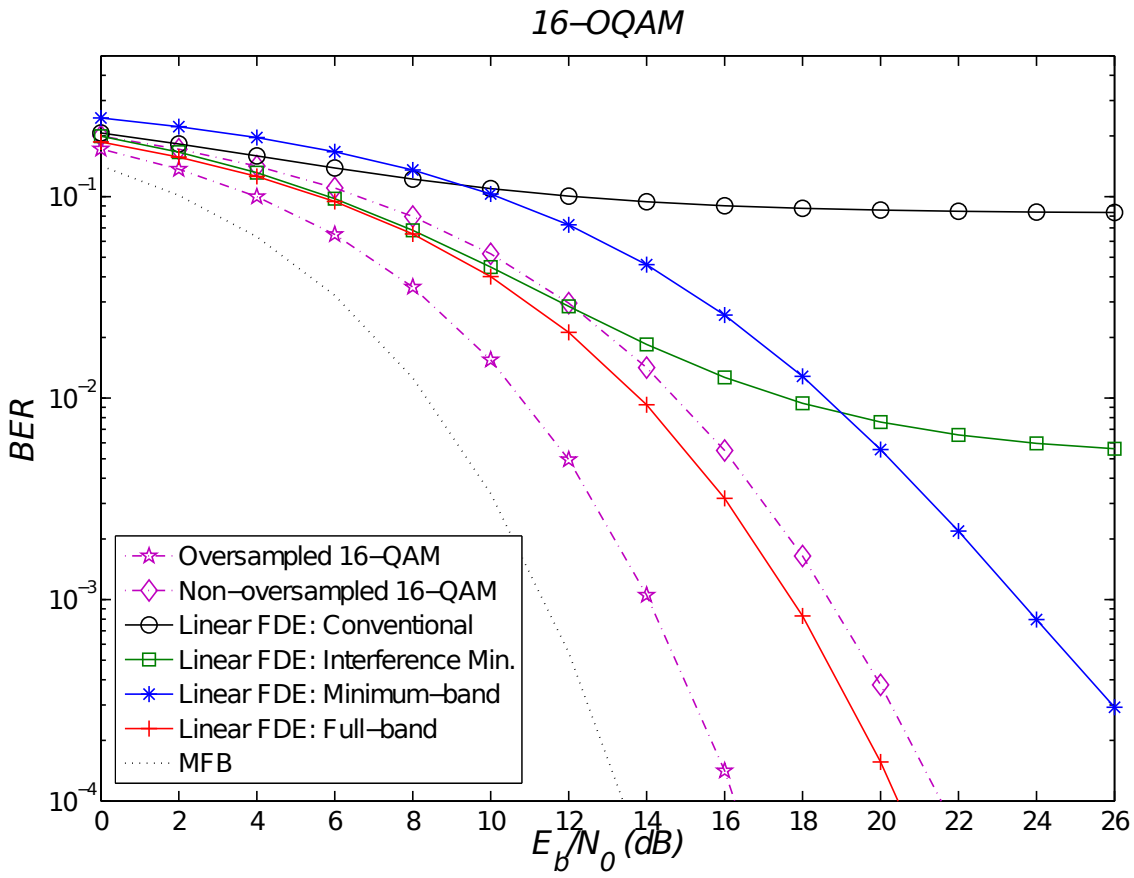

Figure 4.8: BER performance versus E_b/N_0 for a 16-OQAM constellation.

4.5 Iterative FDE design

4.5.1 Iterative FDE with IQI cancellation

Further improvements over the performance of linear equalization can be obtained through iterative equalization. The objective of the iterative receiver of [Luz+12b], whose structure is depicted in Fig. 4.10, is to mitigate the residual ISI from the feedforward equalization, and at the same time cancel the IQI by removing the signal's quadrature component from the in-phase detection and vice versa. This method can be regarded as

$$\widetilde{A}_k^I = \sum_{q=0}^{J/2-1} \left[F_{k+qN}^{(J)} \left(Y_{k+qN}^{(J)} - \overline{Y}_{k+qN}^{Q^{(J)}} \right) - B_{k+qN}^{(J)} \overline{A}_{k+qN}^{I^{(J)}} \right] \tag{4.44}$$

for the in-phase component and

$$\widetilde{A}_k^Q = \sum_{q=0}^{J/2-1} \left[F_{k+qN}^{(J)} \left(Y_{k+qN}^{(J)} - \overline{Y}_{k+qN}^{I^{(J)}} \right) - B_{k+qN}^{(J)} \overline{A}_{k+qN}^{Q^{(J)}} \right] \tag{4.45}$$

for the quadrature component, with $\{B_k^{(J)}; k = 0, 1, \ldots, JN-1\}$ as the feedback equalization coefficients and where $\{k = 0, \ldots, 2N-1\}$. For the in-phase block,

$$\left\{ \widetilde{A}_k^I; k = 0, \ldots, 2N-1 \right\} = \text{DFT} \left\{ \widetilde{a}_n^I; n = 0, \ldots, 2N-1 \right\} \tag{4.46}$$

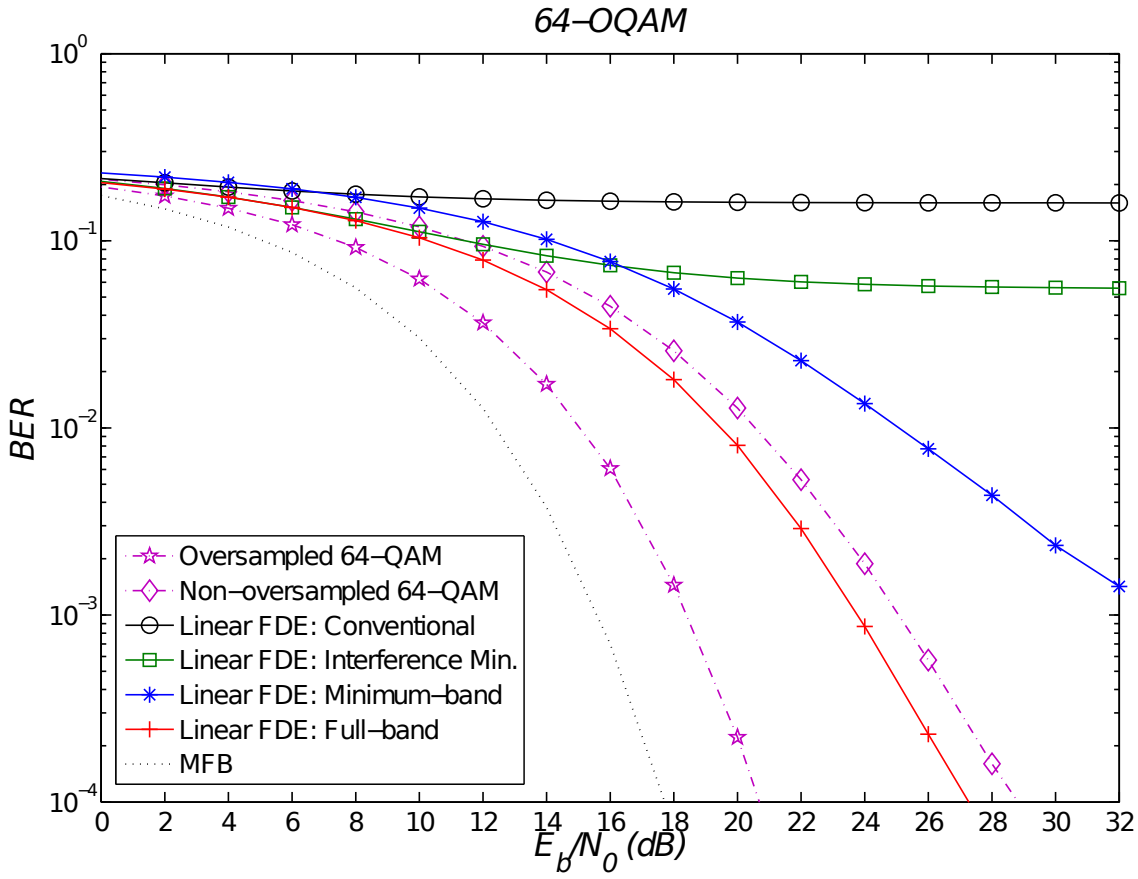

Figure 4.9: BER performance versus E_b/N_0 for a 64-OQAM constellation.

only the even data bits are relevant, whereas for the quadrature block

$$\left\{\widetilde{A}_k^{Q}; k = 0, \ldots, 2N-1\right\} = \text{DFT}\left\{\widetilde{a}_n^{Q}; n = 0, \ldots, 2N-1\right\} \tag{4.47}$$

only the odd data bits are relevant for detection.

The first iteration of this method is, in fact, a linear equalization, where $\overline{A}_k$ are non existent and $\rho = 0$. Therefore, we can use any linear method (namely those from subsection 4.3.1, 4.3.2, 4.3.3 and 4.3.4) as the first iteration of the IB-DFE. For all the following iterations, the values of the feedforward and feedback coefficients are calculated in the following way:

$$F_k^{(J)} = \frac{\kappa H_k^{(J)*}}{\alpha + (1-\rho^2)\sum_{q=0}^{J-1}\left|H^{(J)}_{(k \bmod N)+qN}\right|^2}, \tag{4.48}$$

$$B_k^{(J)} = F_k^{(J)} H_k^{(J)} - 1, \tag{4.49}$$

with the feedback data reliability, ρ, defined by (4.62). The overall average received frequency values for the in-phase and quadrature that cancel IQI through the successive iterations are

$$\overline{Y}_k^{I(J)} = H_k^{(J)} \overline{A}_k^{I(J)} \tag{4.50}$$

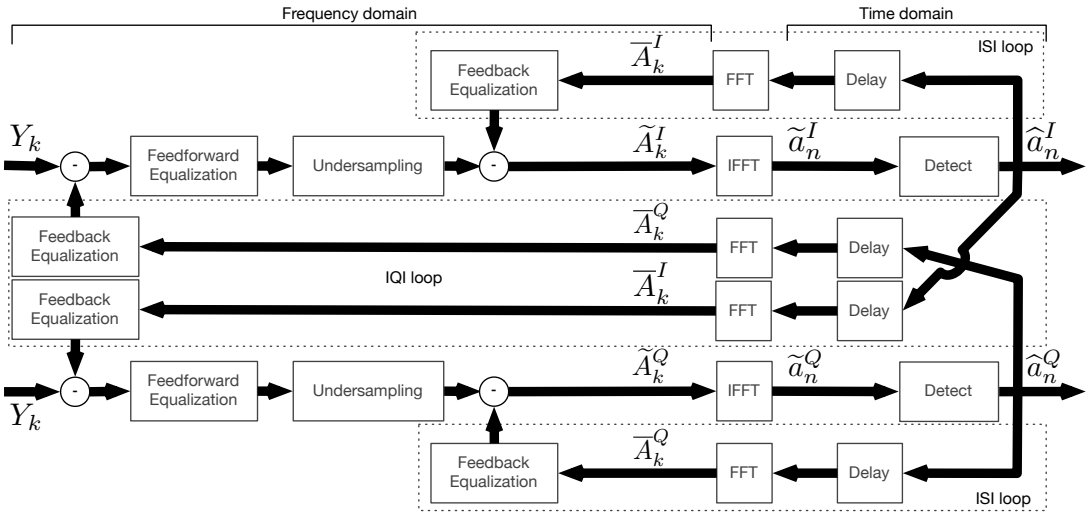

Figure 4.10: Regular Iterative Receiver Structure.

for the in-phase component and

$$\overline{Y}_k^{Q(J)} = H_k^{(J)} \Theta_k \overline{A}_k^{Q(J)} \tag{4.51}$$

for the quadrature component, where $\overline{A}_k^{I(J)}$ and $\overline{A}_k^{Q(J)}$ are the oversampled frequency domain data bits for the in-phase and quadrature component, respectively, defined in section 4.5.3.

4.5.2 Proposed Iterative Receiver

The complexity of the previous iterative receiver, with different equalization for each signal component, was significant. To reduce its complexity, we combine the feedback data symbols in such a way that there is no need to separately equalize the in-phase and quadrature components of the received signal. The structure of this new iterative receiver is depicted in Fig. 4.11, and the FDE's output for a given iteration can be defined as

$$\widetilde{A}_k^{(J)} = F_k^{(J)} Y_k^{(J)} - B_k^{(J)} \overline{A}_k^{(J)}. \tag{4.52}$$

Note that the feedback data bits are more precise due to soft bit decisions (explained in the next subsection) [Ben+10]. After applying the undersample (4.16) and IDFT (4.17) we obtain the non-offset estimated data bits $\widetilde{a}_n$. The values of $B_k^{(J)}$ are given by (4.49) and $F_k^{(J)}$ can either by obtained by (4.48) or by a slightly different version of (4.38), the Full-Band FDE, that takes into account the feedback data reliability

$$F_k^{(J)} = \frac{\kappa \breve{H}_k^{(J)^*} R_k^{(J)^*}}{\alpha + (1-\rho^2)\left|\breve{H}_k^{(J)}\right|^2}. \tag{4.53}$$

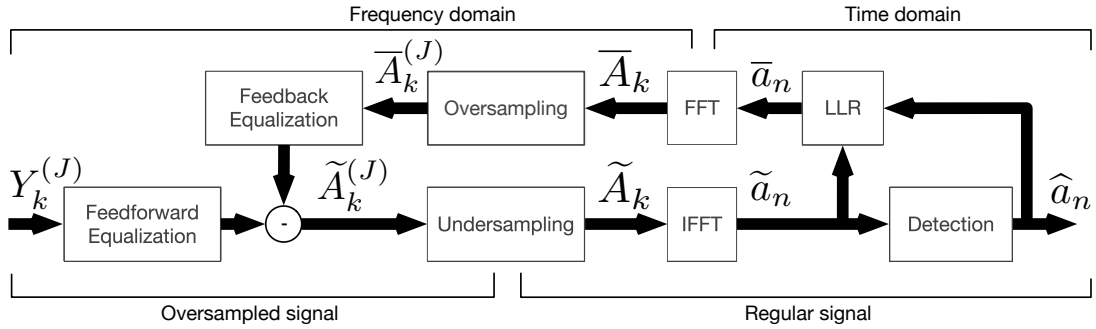

Figure 4.11: Proposed Iterative Receiver Structure.

4.5.3 Feedback Data Symbols

Considering the general M^2-QAM mapping in (4.1) and (4.2), and assuming uncorrelated bits due to the usage of a suitable interleaver, we can obtain $\{\overline{A}_k^{I(J)}; k = 0, \ldots, JN-1\}$ and $\{\overline{A}_k^{Q(J)}; k = 0, \ldots, JN-1\}$ (for the Iterative FDE design of section 4.5.1) from $\{\overline{a}_n^I; k = 0, \ldots, JN-1\}$ and $\{\overline{a}_n^Q; k = 0, \ldots, JN-1\}$, by using (4.8) and applying the DFT. To obtain $\{\overline{A}_k^{(J)}; k = 0, \ldots, JN-1\}$ we apply (4.8) and the DFT in the same way, but with

$$\overline{a}_n = \overline{a}_n^I + j\,\overline{a}_n^Q, \tag{4.54}$$

where

$$\overline{a}_n^I = \sum_{g=1}^{G} \varphi^{(g)} \prod_{m=1}^{g} \overline{b}_n^{I(m)}, \tag{4.55}$$

and

$$\overline{a}_n^Q = \sum_{g=1}^{G} \varphi^{(g)} \prod_{m=1}^{g} \overline{b}_n^{Q(m)}. \tag{4.56}$$

To obtain $\overline{a}_n$, the average symbol values conditioned to the FDE output [Din+10a; Din+10c], we need to compute the average bit values conditioned to the FDE output, i.e. $\overline{b}_n^{I(m)}$ and $\overline{b}_n^{Q(m)}$. The mth bit of the nth transmitted symbol component can be obtained by

$$\overline{b}_n^{I(m)} = \tanh\left(\frac{\Lambda_n^{I(m)}}{2}\right) \tag{4.57}$$

for the in-phase component and

$$\overline{b}_n^{Q(m)} = \tanh\left(\frac{\Lambda_n^{Q(m)}}{2}\right) \tag{4.58}$$

for the quadrature component. The log-likelihood ratio of the mth bit of the nth transmitted symbol component, $\Lambda_n^{I(m)}$ for the in-phase component and $\Lambda_n^{Q(m)}$ for the quadrature component, are given by

$$\Lambda_n^{I(m)} = \log\left(\frac{\sum_{a^I \in \Phi_1^{(m)}} \exp\left(-\frac{\left|\widetilde{a}_n^I - a^I\right|^2}{2\sigma_N^2}\right)}{\sum_{a^I \in \Phi_{-1}^{(m)}} \exp\left(-\frac{\left|\widetilde{a}_n^I - a^I\right|^2}{2\sigma_N^2}\right)}\right), \tag{4.59}$$

and

$$\Lambda_n^{Q(m)} = \log\left(\frac{\sum_{a^Q\in\Phi_1^{(m)}} \exp\left(-\frac{\left|\widetilde{a}_n^Q - a^Q\right|^2}{2\sigma_N^2}\right)}{\sum_{a^Q\in\Phi_{-1}^{(m)}} \exp\left(-\frac{\left|\widetilde{a}_n^Q - a^Q\right|^2}{2\sigma_N^2}\right)}\right), \tag{4.60}$$

where $\Phi_1^{(m)}$ and $\Phi_{-1}^{(m)}$ are the constellation's subsets associated to the symbols with the mth bit at 1 or -1, respectively [Din+10a]. The estimated data bits values $\widetilde{a}_n^I$ and $\widetilde{a}_n^Q$ are obtained by (4.52), after applying the undersample and IFFT operations characterized by (4.16) and (4.17). σ_N^2 denotes the variance of the real and imaginary part of the overall noise (plus residual ISI and IQI) at the FDE output. In practice it can be estimated by

$$\sigma_N^2 = \frac{1}{2N}\sum_{n=0}^{N-1} E[|\widetilde{a}_n - a_n|^2] \approx \frac{1}{2N}\sum_{n=0}^{N-1} E[|\widetilde{a}_n - \overline{a}_n|^2]. \tag{4.61}$$

Finally, the reliability of the estimated average data symbols' soft decision $\overline{a}_n$, to be used in the feedback loop, taking into account the use of a general M^2-OQAM mapping in (4.1) and (4.2), are obtained by

$$\begin{aligned}\rho &= \frac{E\left[\overline{a}_n a_n^*\right]}{E\left[\left|a_n\right|^2\right]} \approx \\ &\approx \frac{1}{2N}\sum_{n=0}^{N-1}\sum_{g=1}^{G}\frac{\left|2^{\varphi(g)}\prod_{m=1}^{g}\left(\rho_n^{I(m)}\right)\right|}{2^{\varphi(g)}} + \\ &\quad + \frac{1}{2N}\sum_{n=0}^{N-1}\sum_{g=1}^{G}\frac{\left|2^{\varphi(g)}\prod_{m=1}^{g}\left(\rho_n^{Q(m)}\right)\right|}{2^{\varphi(g)}},\end{aligned} \tag{4.62}$$

with $\rho_n^{I(m)}$ and $\rho_n^{Q(m)}$ as the reliability of the estimated in-phase and quadrature data given by

$$\rho_n^{I(m)} = \tanh\left(\frac{\left|\Lambda_n^{I(m)}\right|}{2}\right) \tag{4.63}$$

and

$$\rho_n^{Q(m)} = \tanh\left(\frac{\left|\Lambda_n^{Q(m)}\right|}{2}\right). \tag{4.64}$$

4.6 Performance Results for Iterative Equalization

In this section we present a set of performance results concerning iterative receivers for 16-OQAM, uniform 64-OQAM and non-uniform 64-OQAM signal constellations. The assumptions are the same from the linear receivers' performance results. Oversampled non-offset modulations (16-QAM and 64-QAM) with linear conventional FDE were added to the results for comparison purposes. In this case (Fig. 4.12), with the proposed receiver and four iterations, all the methods obtain similar performance results, except for the conventional FDE. This means that the proposed iterative receiver has substantial interference cancellation power, with performance results close to the MFB for all the other three

methods. Nevertheless, when we increase the constellation order to 64-OQAM (Fig. 4.13),

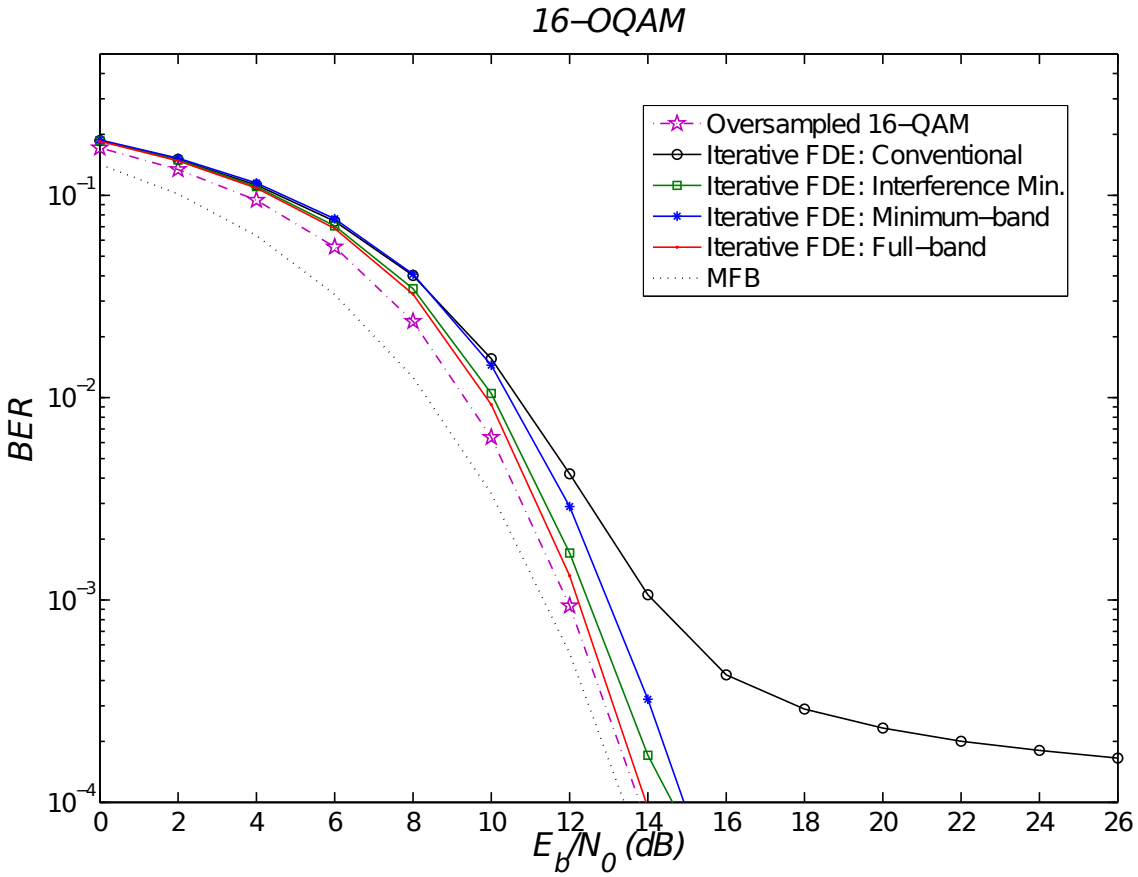

Figure 4.12: BER performance versus E_b/N_0 for 16-OQAM constellation for 4 iterations.

both the conventional and interference minimization methods reach a BER floor of 10^{-2} and 10^{-3}, respectively, due to being unable to mitigate all of the 64-OQAM interference. Only the minimum and full-band FDE are able to cope with the interference sensitivity of a 64-OQAM signal constellation, with the full-band maintaining the closest results to the MFB, and similar to that of a conventional iterative FDE for an oversampled non-offset modulation (this remains valid even for the case of a 64-OQAM constellation with a severely time dispersive propagation channel).

If we increase the overall SIR, by using a non-uniform 64-OQAM constellation, with High Protected Bits (HPBs) $\varphi^{(3)} = 4$, Medium Protected Bits (MPBs) $\varphi^{(2)} = 1$ and Low Protected Bitss (LPBs) $\varphi^{(1)} = 1/4$ (see Fig. 4.14), the results show that for linear receivers there is a significant performance difference between the full-band and min-band FDE, with the former having always higher rates. On the other hand, for the iterative receivers, only the least protected bits of the full-band FDE have significantly higher performance than for the min-band FDE. In the higher protected bits, while full-band FDE outperforms min-band FDE in all simulated results, the performance of both methods is similar. The conventional FDE and interference minimization FDE methods were unable to mitigate the high levels of SIR, making data transmission unfeasible.

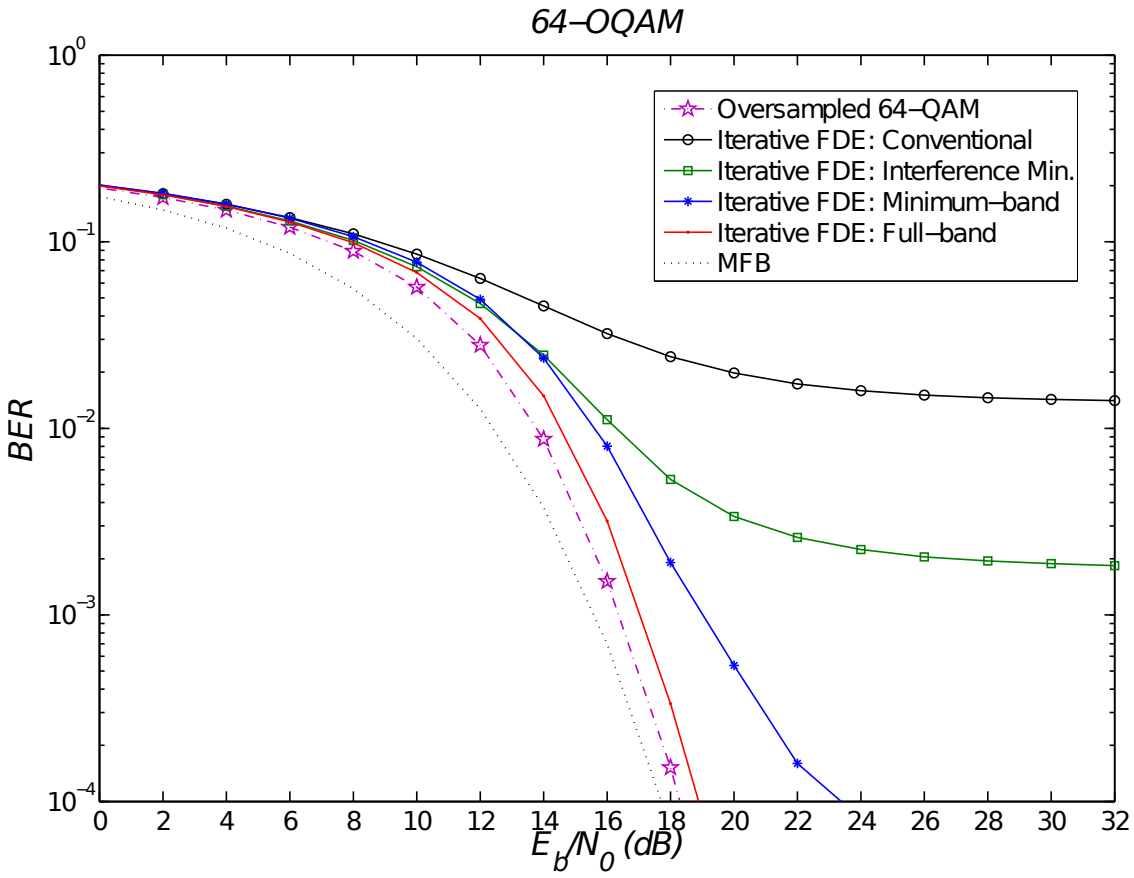

Figure 4.13: BER performance versus E_b/N_0 for 64-OQAM constellation for 4 iterations.

4.7 Computational Complexity

The receiver complexity is mainly a function of the oversampling factor and the number of iterations, for both offset and non-offset modulations. In fact, for a given oversampling factor and number of FDE iterations, the receiver complexity is similar with both modulations since the number of FFT operations are similar. When we employ Nyquist filtering with zero or near zero roll-off factor (i.e., we have minimum bandwidth), the oversampling is not an issue and the resulting complexity for either modulation is also similar. However, for a signal with wider bandwidth, it is recommendable to employ oversampling to take full advantage of its diversity effects.

The computational complexity per data block of the equalizer structures resumes to a pair of FFT/IFFT, whose complexity is of the order $2JN\log_2(JN)$, plus JN multiplications by the F_k coefficients and N additions of J replicas. Therefore, the overall FDE complexity is

$$O(JN\ \log(JN)) + O(JN) \propto O(JN\ \log(JN)). \tag{4.65}$$

The overall complexity per data symbol is $O(J\ \log(JN))$ and the complexity required to obtain the F_k is $O(JN)$

For the iterative method we need a pair of FFT/IFFT, with complexity of the order

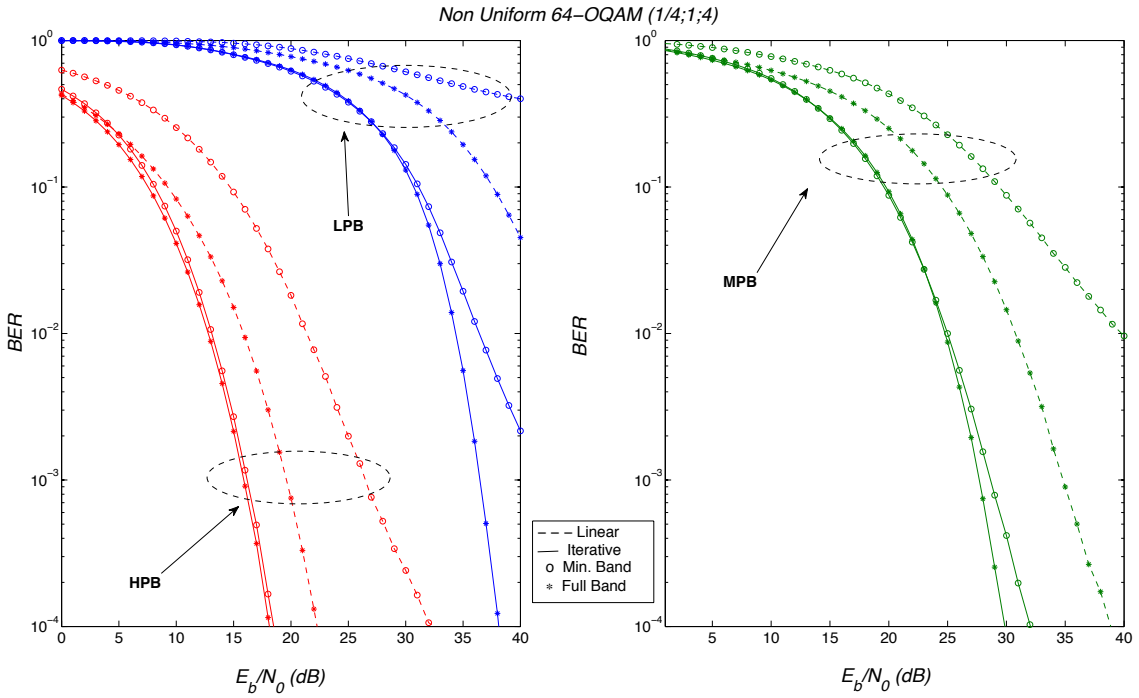

Figure 4.14: BER performance versus E_b/N_0 for Non-uniform 64-OQAM constellation (4;1;1/4) for linear and iterative (4 iterations) equalization.

$2JN\log_2(JN)$, plus $2JN$ multiplications (JN for the F_k and JN for the B_k), for each iteration. If the receiver has I iterations, the overall receiver complexity is $O(IJN\ \log(JN))$ and the complexity per detected symbol is $O(IJ\ \log(JN))$. For each iteration, the complexity required to obtain the F_k and B_k is also $O(JN)$.

4.8 Conclusions

In this chapter we considered the use of offset modulations with SC-FDE schemes and we presented pragmatic receiver designs suitable for signals with bandwidth above the Nyquist band. The oversampled OQAM signal was demystified and we presented both linear and iterative FDE designs that are able to cope with the high interference generated by an oversampled 64-OQAM signal, reaching values close to the MFB for the iterative full-band FDE. In this way we were able to develop both linear and iterative FDE designs that are easily interchangeable for offset, non-offset, oversampled and non-oversampled signals, requiring only a pair of "Oversampling/Undersampling" blocks that take into account whether the received signal is an offset or non-offset signal, and a different feedforward coefficient calculation, from their conventional FDE counterpart.

Our performance results show that the pragmatic FDE receivers have excellent performance and are a promising method for offset modulations with high order constellations.

CHAPTER 5

MULTIPLE USER RECEIVER DESIGNS FOR OFFSET MODULATIONS

5.1 Introduction

It is widely accepted that SC-FDE is a good candidate for broadband wireless communications, due to his lower PAPR when compared with OFDM. Nevertheless, to obtain a SC signal without envelope fluctuations, capable of handling a highly nonlinear amplification, its spectral occupation becomes several times higher than its minimum value, resulting in low spectral efficiency. In this chapter we consider a Frequency Division Multiple Access (FDMA) system employing OQPSK modulations with quasi-constant envelope that increases the overall spectral efficiency, by considering spectral overlapping between several different frequency channels, reducing its spectral occupation. To mitigate the overall interference, we present two iterative frequency-domain receivers with parallel multiple user detection. These systems are capable to cope with ISI, strong ACI or CCI levels inherent to spectral overlapping, and IQI, the interference between the I and Q components of the OQPSK signals, for severely time-dispersive channels.

A common drawback of the signals with reduced envelope fluctuations is the increased spectral occupation, much higher than the minimal spectral occupation for QPSK signals with the same rate (achieved for Nyquist pulses with roll-off zero)[1]. To avoid ACI the channel separation has to become several times the symbol rate[2], resulting in a very small spectral efficiency for the overall system. To improve the system's spectral efficiency we can overlap adjacent carriers. This leads to strong ACI levels, or even CCI if we put two or more carriers in the same frequency. By jointly detecting all the channels in a Serial

[1] In fact, the spectral occupation for MSK signals is infinity, with relevant side lobes for frequencies several times above the symbol rate.

[2] For Nyquist pulses the minimum separation between frequency channels, achieved for zero roll-off, is equal to the symbol rate.

Iterative Cancellation (SIC) fashion, it is possible to cope with the strong ACI levels for non offset modulations [Din+05]. Another approach, aimed to increase the spectral efficiency, is to merge different users into the same frequency and try to recover the sent signal at the receiver. These approaches are possible due to the inherent severe time-dispersion effect associated to the multi-path propagation of systems with high bit rates. Therefore, the highly selective channel can be used as an orthogonal medium to separate the co-channel users, much like CDMA does with orthogonal codes.

This chapter aims to increase the spectral efficiency by reducing channel separation and developing receivers able to cope with the high ACI, considering an extension of the receiver proposed in [Din+05] to OQPSK signals and to a Parallel Interference Cancellation (PIC) approach that has lower delay and allow a parallel receiver implementation. From another point of view, to drastically reduce the channel separation, we will put two carriers in the same frequency. This produces incredibly high CCI levels since more users coexist in the same frequency channel. For such a scenario it is developed a method to retrieve the data from such an high interference transmission.

This chapter is organized as follows: section 5.2 considers a high complexity SC-FDE system employing OQPSK modulations with quasi-constant envelope that increases the overall spectral efficiency by overlapping adjacent channels and section 5.3 considers a low complexity pragmatic SC-FDE system employing OQPSK modulations with quasi-constant envelope that increases the overall spectral efficiency by considering total spectral overlapping of two different users. Due to the high complexity of the equations in the following sections, the symbols from both sections will overlap, but they will only regard each section, and are not always interchangeable.

5.2 Receiver design for strong ACI levels

In this section we consider a high complexity SC-FDE system employing OQPSK modulations with quasi-constant envelope that increases the overall spectral efficiency by overlapping adjacent channels. To mitigate the overall interference, we present an iterative frequency-domain receiver with parallel multiple user detection capable to cope with ISI, ACI levels inherent to the spectral overlapping, and IQI, for severely time-dispersive channels.

5.2.1 System Description

Let us consider a FDMA system employing an SC-FDE scheme with an OQPSK modulation for each frequency channel. Under these conditions, U frequency channels are adopted, with the carrier frequency denoted by f_u, $u = 1, 2, ...U$. It is also assumed equally spaced frequency channels: $f_u - f_{u-1} = \Delta f$ and transmitted blocks with the same length

for all the carriers (Figure 5.1). The data block transmitted by the uth frequency channel is

$$x_u(t) = \sum_{n=-N_{cp}}^{N-1} a_{n,u}^{I} r(t - nT_s) + j \sum_{n=-N_{cp}}^{N-1} a_{n,u}^{Q} r(t - nT_s - T_s/2), \tag{5.1}$$

where $a_{n,u}^{I} = \pm 1$ and $a_{n,u}^{Q} = \pm 1$ are, respectively, the nth in-phase and quadrature data symbol of the uth frequency channel. T_s denotes the symbol duration, $r(t)$ is the transmitted pulse shape and N_{cp} denotes the number of samples at the cyclic prefix (longer than the overall channel impulse response length) appended to each block where $a_{-n,u}^{Q} = a_{N-n,u}^{Q}$ and $a_{-n,u}^{I} = a_{N-n,u}^{I}$.

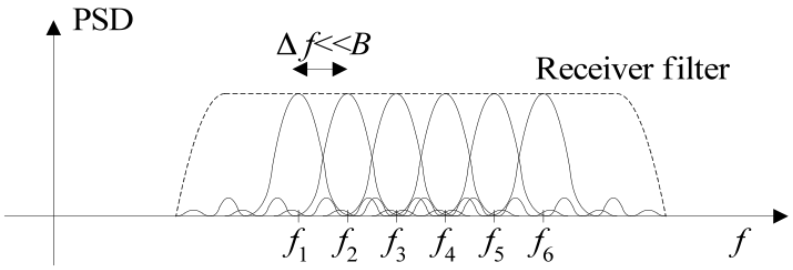

Figure 5.1: System with strong ACI levels

It is assumed that the bandwidth B of $x_u(t)$, i.e., the bandwidth associated to $r(t)$, is larger than the symbol rate $1/T_s$[1]. Clearly, ACI will be present whenever $\Delta f < B$.

The frequency separation between channels is Δf. Given Δf, the ACI-free conditions are only valid for raised-cosine pulses with roll-off zero, which means that the highest spectral efficiency can be achieved.

To cope with strong ACI levels, all channels will be detected simultaneously. Therefore, it is necessary to employ a wide-band receiver filter and sample the overall received signal with a rate of $J/T_s >> 1/T_s$, large enough to avoid aliasing effects. This implies an oversampling factor of J. Given the implicit frequency multiplicity [Gar91] on the FDE for oversampled signals, after removing the samples associated to the cyclic prefix and computing its size-JN DFT, the corresponding frequency-domain received block can represented as a J-sized vector containing the J multiplicity blocks

$$\boldsymbol{Y}_k = \boldsymbol{H}_k \boldsymbol{A}_k + \boldsymbol{N}_k, \tag{5.2}$$

where $k = 0, 1, \ldots, N-1$. The corresponding channel noise for the kth frequency is $\boldsymbol{N}_k = \left[N_k \; N_{k+N} \; \ldots \; N_{k+(J-1)N} \right]^T$. The overall channel frequency response for the kth frequency which includes the adopted pulse shape, the channel impulse response for the different frequency users in its U columns and the frequency oversampling factor in its J

[1]For a raised-cosine pulse the two-sided bandwidth is $(1+\beta)/T_s$. For OQPSK signals with almost constant envelope $B >> 1/T_s$.

rows is defined as

$$\boldsymbol{H}_k = \begin{bmatrix} \boldsymbol{H}_{k,0} & \cdots & \boldsymbol{H}_{k,u} & \cdots & \boldsymbol{H}_{k,U} \end{bmatrix} = \begin{bmatrix} H_{k,1} & \cdots & H_{k,U} \\ H_{k+N,1} & \cdots & H_{k+N,U} \\ \vdots & & \vdots \\ H_{k+(J-1)N,1} & \cdots & H_{k+(J-1)N,U} \end{bmatrix}. \tag{5.3}$$

The frequency domain data symbols, $\boldsymbol{A}_k = [A_{k,0}\ A_{k,1}\ \ldots\ A_{k,U}]^T$, are also a J-sized vector where

$$A_{k,u} = A^I_{k,u} + A^Q_{k,u}\Theta_k. \tag{5.4}$$

The frequency domain time offset inherent to these modulations is $\Theta_k = je^{-j\pi k/N}$, and the frequency domain data symbols can be obtained from their time domain counterparts with the DFT operation

$$\{A^I_{k,u}, k = 0, 1, \ldots, N-1\} = \text{DFT}\left\{a^I_{n,u}, n = 0, 1, \ldots, N-1\right\}, \tag{5.5}$$

and

$$\{A^Q_{k,u}, k = 0, 1, \ldots, N-1\} = \text{DFT}\left\{a^Q_{n,u}, n = 0, 1, \ldots, N-1\right\}. \tag{5.6}$$

Consequently, the FDE will be able to use the periodic frequency blocks associated to the data, to correctly detect the different frequency users. Besides the ACI problem, this system will also suffer from IQI inherent to all Offset systems, as shown in Figure 5.2.

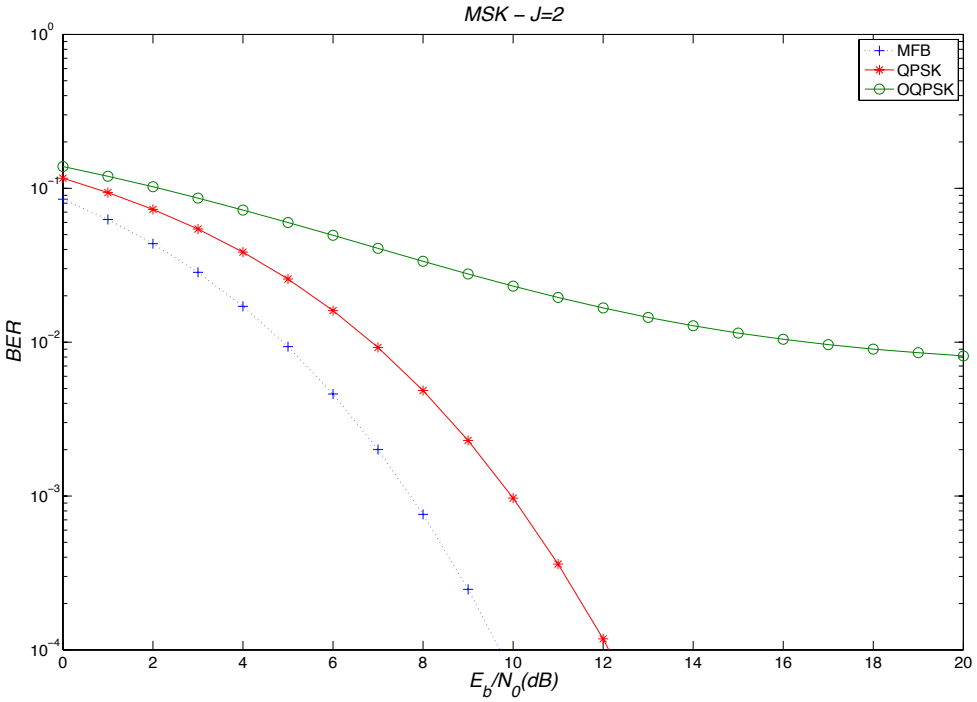

Figure 5.2: BER performance for QPSK and OQPSK with raised cosine ($\beta = 1$) support pulse and conventional FDE.

5.2.2 Parallel FDE Design with ACI and IQI Cancellation

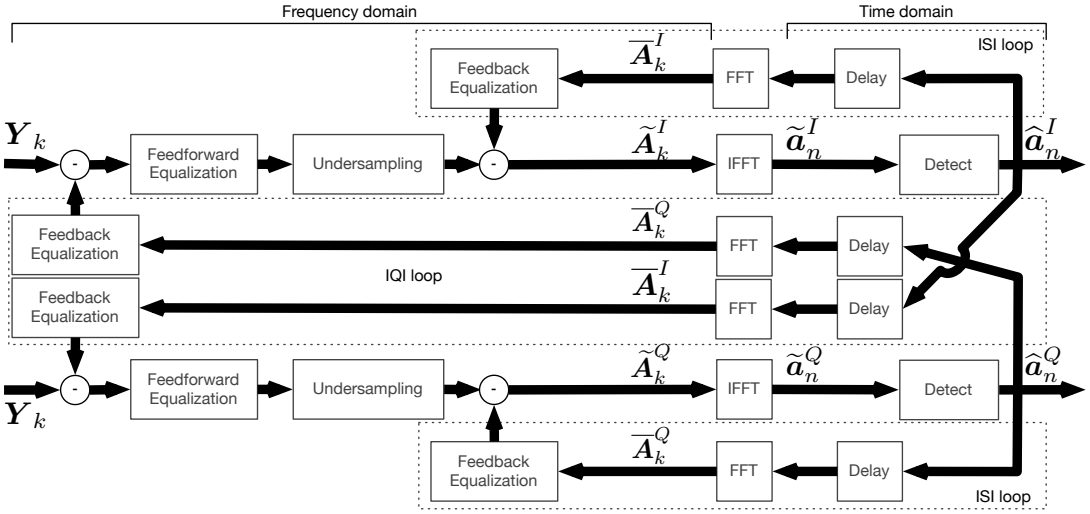

Figure 5.3: Proposed receiver structure.

In this section, an iterative receiver with separated estimations of the I and Q components is presented. After the first iteration, $i = 0$, the information from one component is fed back to remove its interference from the other. Figure 5.3 shows the proposed receiver structure. Therefore, for any given iteration, the outputs for the components I and Q are described by the relations

$$\widetilde{\boldsymbol{A}}_k^{I(i)} = \boldsymbol{F}_k^{(i)} \left(\boldsymbol{Y}_k - \overline{\boldsymbol{Y}}_k^{Q(i-1)} \right) - \boldsymbol{B}_k^{(i)} \overline{\boldsymbol{A}}_k^{I(i-1)}, \tag{5.7}$$

and

$$\widetilde{\boldsymbol{A}}_k^{Q(i)} = \boldsymbol{F}_k^{(i)} \, \boldsymbol{\Theta}_k^{-1} \left(\boldsymbol{Y}_k - \overline{\boldsymbol{Y}}_k^{I(i-1)} \right) - \boldsymbol{B}_k^{(i)} \overline{\boldsymbol{A}}_k^{Q(i-1)}. \tag{5.8}$$

We may note that the first iteration, $i = 0$, is similar to a linear equalization, where the data estimation from I and Q components is nonexistent, and therefore $\overline{\boldsymbol{Y}}_k^{I(-1)}$, $\overline{\boldsymbol{Y}}_k^{Q(-1)}$, $\overline{\boldsymbol{A}}_k^{I(1)}$ and $\overline{\boldsymbol{A}}_k^{Q(-1)}$ are null vectors. The parallel feedforward coefficient matrix that mitigates ISI and ACI is obtained by

$$\boldsymbol{F}_k^{(i)} = \begin{bmatrix} F_{k,1}^{(i)} & F_{k+N,1}^{(i)} & \cdots & F_{k+(J-1)N,1}^{(i)} \\ \vdots & \vdots & & \vdots \\ F_{k,U}^{(i)} & F_{k+N,U}^{(i)} & \cdots & F_{k+(J-1)N,U}^{(i)} \end{bmatrix} = \boldsymbol{K}^{(i)} \boldsymbol{H}_k^H \left[\alpha \boldsymbol{I}_J + \boldsymbol{H}_k^* \, \boldsymbol{\Omega}^{(i-1)} \, \boldsymbol{H}_k^T \right]^{-1} \tag{5.9}$$

with α as the inverse of the SNR,

$$\boldsymbol{\Omega}^{(i)} = \operatorname{diag} \left(1 - {\rho_1^{(i)}}^2 \, ; \, 1 - {\rho_2^{(i)}}^2 \, ; \, \cdots \, ; \, 1 - {\rho_U^{(i)}}^2 \right), \tag{5.10}$$

with the correlation coefficient that provides a block wise reliability measure of the estimates used in the feedback loop $\rho_u^{(i)}$ given by

$$\rho_u^{(i)} = \frac{E\left[\widehat{a}_{n,u}a_{n,u}^*\right]}{E\left[\left|a_{n,u}^2\right|\right]} \approx \frac{1}{2N}\sum_{n=0}^{N-1}\left(\mathrm{Re}\left\{\overline{a}_{n,u}^{I(i)}\right\} + \mathrm{Re}\left\{\overline{a}_{n,u}^{Q(i)}\right\}\right). \tag{5.11}$$

$\boldsymbol{K}^{(i)}$ is a normalization factor that will be deduced in the next subsection. The U-by-U feedback coefficient matrix, given by

$$\boldsymbol{B}_k^{(i)} = \begin{bmatrix} B_{k,1,1}^{(i)} & \cdots & B_{k,U,1}^{(i)} \\ \vdots & \ddots & \vdots \\ B_{k,1,U}^{(i)} & \cdots & B_{k,U,U}^{(i)} \end{bmatrix} = \boldsymbol{F}_k^{(i)}\boldsymbol{H}_k - \boldsymbol{I}_U, \tag{5.12}$$

is needed to mitigate IQI and remove the residual ACI and ISI after the feedforward filtering. It should be noted that the values of $\boldsymbol{F}_k^{(i)}$ and $\boldsymbol{B}_k^{(i)}$ are the same for both I and Q components and $\boldsymbol{\Theta}_k$ is a diagonal matrix defined as

$$\boldsymbol{\Theta}_k = \mathrm{diag}\left(\Theta_k\,;\,\cdots\,;\,\Theta_{k+(J-1)N}\right), \tag{5.13}$$

that relates to the time offset of the quadrature component. The fed back matrices

$$\overline{\boldsymbol{A}}_k^{I(i)} = \left[\overline{A}_{k,1}^{I(i)}\ \overline{A}_{k,2}^{I(i)}\ \ldots\ \overline{A}_{k,U}^{I(i)}\right]^T, \tag{5.14}$$

and

$$\overline{\boldsymbol{A}}_k^{Q(i)} = \left[\overline{A}_{k,1}^{Q(i)}\ \overline{A}_{k,2}^{Q(i)}\ \ldots\ \overline{A}_{k,U}^{Q(i)}\right]^T, \tag{5.15}$$

denote the soft decision frequency block vector taken from

$$\{\overline{A}_{k,u}^{I(i)}, k = 0,1,\ldots,N-1\} = \mathrm{DFT}\left\{\overline{a}_{n,u}^{I(i)}, n = 0,1,\ldots,N-1\right\} \tag{5.16}$$

and

$$\{\overline{A}_{k,u}^{Q(i)}, k = 0,1,\ldots,N-1\} = \mathrm{DFT}\left\{\overline{a}_{n,u}^{Q(i)}, n = 0,1,\ldots,N-1\right\}, \tag{5.17}$$

where $\overline{a}_{n,u}^{I(i)}$ and $\overline{a}_{n,u}^{Q(i)}$ are the soft decisions values obtained from $\widetilde{a}_{n,u}^{I(i)}$ and $\widetilde{a}_{n,u}^{Q(i)}$, associated to the previous iteration. They can be obtained by

$$\overline{a}_{n,u}^{I(i)} = \tanh\left(\frac{\mathrm{Re}\{\widetilde{a}_{n,u}^{(i)}\}}{\sigma_{N,u}^{(i)^2}}\right), \tag{5.18}$$

and

$$\overline{a}_{n,u}^{Q(i)} = \tanh\left(\frac{\mathrm{Im}\{\widetilde{a}_{n,u}^{(i)}\}}{\sigma_{N,u}^{(i)^2}}\right), \tag{5.19}$$

where

$$\sigma_{N,u}^{(i)^2} = \frac{1}{2}E[|a_{n,u} - \widetilde{a}_{n,u}^{(i)}|^2] \approx \frac{1}{2N}\sum_{n=0}^{N-1}|\widehat{a}_{n,u}^{(i)} - \widetilde{a}_{n,u}^{(i)}|^2. \tag{5.20}$$

Finally, the overall averaged received frequency values for in-phase and quadrature components that cancel the IQI over the successive iterations can be obtained from $\overline{A}_{k,u}^{I(i)}$ and $\overline{A}_{k,u}^{Q(i)}$ and are defined as

$$\overline{\boldsymbol{Y}}_k^{I(i)} = \boldsymbol{H}_k \overline{\boldsymbol{A}}_k^{I(i)}, \tag{5.21}$$

$$\overline{\boldsymbol{Y}}_k^{Q(i)} = \boldsymbol{H}_k \boldsymbol{\Theta}_k \overline{\boldsymbol{A}}_k^{Q(i)}. \tag{5.22}$$

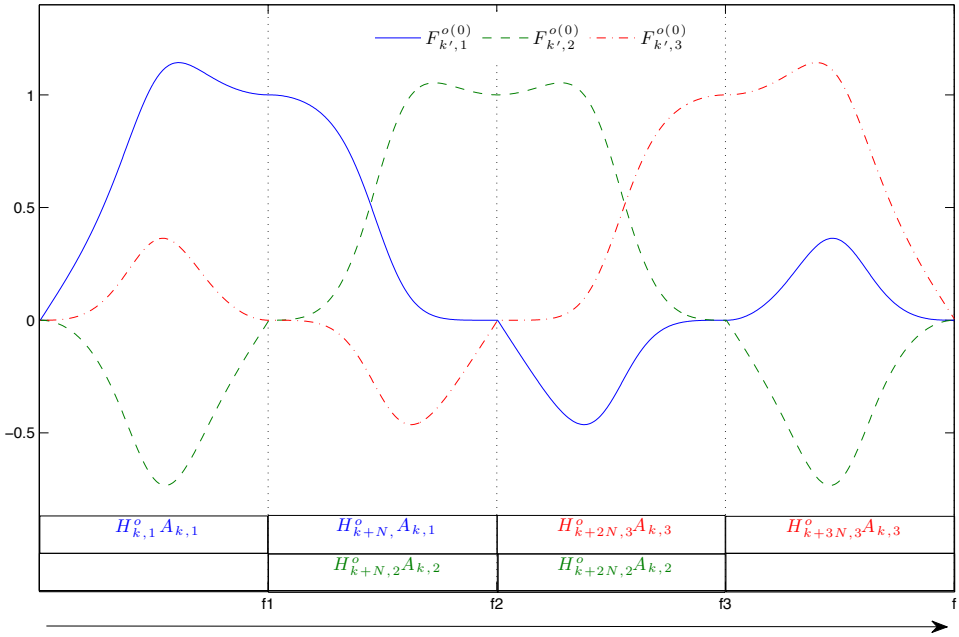

Figure 5.4: Frequency spectrum of $F_{k,u}^{(i)}$ and $H_{k,u}.A_{k,u}$ for $U = 3$, a noise-free flat-fading channel and a raised cosine support pulse with roll-off = 1.

Figure 5.4 shows the obtained values of $F_{k,u}^{(i)}$ for $B = 2/T_s$, $U = 3$, $J = 4$ and a flat fading channel. For the first user ($u = 1$), the value of $F_{k,1}^{(i)}$ is positive over the first two N blocks, where the desired signal, $A_{k,1}$, exists. The second N block, has ACI from the second user ($u = 2$), and as it can be seen from Figure 5.4, on the third N block the ACI interference from the second user is removed ($F_{k+2N,1}^{(i)} \leq 0, k = 0, 1, \ldots, N-1$). Unfortunately, the removed ACI contains information from third user as well. For a correct equalization, it is also needed to mitigate the interference from the third user, which is what happens in the fourth Nth block. This method is extendable to any other value of U.

5.2.3 Computation of Receiver Parameters

In this subsection we will show how to compute the receiver parameters for a system with U users with partially overlapping spectrum. To obtain the feedforward and feedback coefficients, we need to minimize the expected value for each individual user

$$\mathrm{E}\left[\left|\widetilde{A}_{k,u}^{(i)} - A_{k,u}\right|^2\right], \tag{5.23}$$

where $\widetilde{A}_{k,u}^{(i)}$ are the frequency domain estimated data symbols for the ith iteration of the uth user and $A_{k,u}$ the data symbols in the frequency domain. These data symbols can be regarded to those of (5.2) in the following way

$$A_{k,u} = \mathbf{\Gamma}_u^{(i)} \boldsymbol{A}_k, \tag{5.24}$$

where

$$\mathbf{\Gamma}_u^{(i)} = \begin{bmatrix} 0 & \cdots & \gamma_u^{(i)} & \cdots & 0 \end{bmatrix}. \tag{5.25}$$

is the operation that shapes $\boldsymbol{A}_k$ in a single u user format.

For the sake of computation simplicity for this particular situation, we will use hard decisions $\widehat{\boldsymbol{A}}_k^{(i)}$ instead of the soft decisions $\overline{\boldsymbol{A}}_k^{(i)}$ in the feedback loop, and since the IQI is removed before the feedforward equalization (5.8), the FDE design assumes a QPSK constellation. Under these assumptions, the output for the FDE is

$$\widetilde{\boldsymbol{A}}_k^{(i)} = \boldsymbol{F}_k^{(i)} \boldsymbol{Y}_k - \boldsymbol{B}_k^{(i)} \widehat{\boldsymbol{A}}_k^{(i-1)}, \tag{5.26}$$

or in a single u user format

$$\widetilde{A}_{k,u}^{(i)} = \boldsymbol{F}_{k,u}^{(i)} \boldsymbol{Y}_k - \boldsymbol{B}_{k,u}^{(i)} \widehat{\boldsymbol{A}}_k^{(i-1)}, \tag{5.27}$$

where $\boldsymbol{F}_{k,u}^{(i)} = \mathbf{\Gamma}_u^{(i)} \boldsymbol{F}_k^{(i)}$ and $\boldsymbol{B}_{k,u}^{(i)} = \mathbf{\Gamma}_u^{(i)} \boldsymbol{B}_k^{(i)}$.

The frequency domain hard decisions obtained from the estimated data symbols can be assumed to be divided into two components

$$\widehat{\boldsymbol{A}}_k^{(i)} = \boldsymbol{\rho}^{(i)} \boldsymbol{A}_k + \boldsymbol{\Delta}_k^{(i)} \tag{5.28}$$

where

$$\boldsymbol{\rho}^{(i)} = \operatorname{diag}\left(\rho_1^{(i)} \; ; \; \rho_2^{(i)} \; ; \; \cdots \; ; \; \rho_U^{(i)} \right), \tag{5.29}$$

represents the correlation coefficient that provides a block wise reliability measure of the estimates used in the feedback loop and

$$\boldsymbol{\Delta}_k^{(i)} = \begin{bmatrix} \Delta_{k,1}^{(i)} & \Delta_{k,2}^{(i)} & \cdots & \Delta_{k,U}^{(i)} \end{bmatrix}^T, \tag{5.30}$$

that denotes a zero-mean error term with the expected value

$$\mathrm{E}\left[\left| \Delta_{k,u}^{(i)} \right|^2 \right] \approx \left(1 - {\rho_u^{(i)}}^2 \right) \mathrm{E}\left[\left| A_{k,u}^{(i)} \right|^2 \right]. \tag{5.31}$$

Similarly, the estimated data bits can be written as

$$\widetilde{\boldsymbol{A}}_k^{(i)} = \mathbf{\Gamma}^{(i)} \boldsymbol{A}_k + \boldsymbol{\Delta}_k^{(i)} \tag{5.32}$$

with $\boldsymbol{e}_k^{(i)}$ as the estimation error,

$$\mathbf{\Gamma}^{(i)} = \operatorname{diag}\left(\gamma_1^{(i)} \; ; \; \gamma_2^{(i)} \; ; \; \cdots \; ; \; \gamma_U^{(i)} \right), \tag{5.33}$$

and

$$\gamma_u^{(i)} = \frac{1}{JN} \sum_{k=0}^{JN-1} F_{k,u}^{(i)} \, H_{k,u}. \tag{5.34}$$

After some straightforward manipulation of (5.27) we can obtain

$$\widetilde{A}_{k,u}^{(i)} = \mathbf{\Gamma}_u^{(i)} \boldsymbol{A}_k + \left(\boldsymbol{F}_{k,u}^{(i)} \boldsymbol{H}_k - \boldsymbol{B}_{k,u}^{(i)} \boldsymbol{\rho}^{(i-1)} - \mathbf{\Gamma}_u^{(i)} \right) \boldsymbol{A}_k - \boldsymbol{B}_{k,u}^{(i)} \mathbf{\Delta}_k^{(i-1)} + \boldsymbol{F}_{k,u}^{(i)} \boldsymbol{N}_k. \tag{5.35}$$

At this point we can say that $\mathbf{\Gamma}_u^{(i)} \boldsymbol{A}_k$ is the useful signal and everything else is either noise or interference. Using the Lagrangian multipliers method we get

$$L = \mathrm{E}\left[\left| \widetilde{A}_{k,u}^{(i)} - \mathbf{\Gamma}_u^{(i)} \boldsymbol{A}_k \right|^2 \right] + \lambda_u^{(i)} \left(\gamma_u^{(i)} - 1 \right), \tag{5.36}$$

where $\lambda_u^{(i)}$ is the Lagrangian multiplier for an optimization carried out under $\gamma_u^{(i)} = 1$. The optimum feedforward coefficients are obtained by solving the following set of equations:

$$\begin{aligned} \boldsymbol{\nabla}_{\boldsymbol{F}_{k,u}^{(i)}} L = 0 \quad \Leftrightarrow \quad & \boldsymbol{F}_{k,u}^{(i)} \boldsymbol{H}_k \boldsymbol{R}_S \boldsymbol{H}_k^H - \boldsymbol{B}_{k,u}^{(i)} \boldsymbol{\rho}^{(i-1)} \boldsymbol{R}_S \boldsymbol{H}_k^H - \mathbf{\Gamma}_u^{(i)} \boldsymbol{R}_S \boldsymbol{H}_k^H + \\ & + \boldsymbol{F}_{k,u}^{(i)} \boldsymbol{R}_N + \frac{\lambda_u^{(i)}}{N} \boldsymbol{H}_{k,u}^H = 0 \\ \Leftrightarrow \quad & \boldsymbol{F}_{k,u}^{(i)} \boldsymbol{H}_k \boldsymbol{H}_k^H - \boldsymbol{B}_{k,u}^{(i)} \boldsymbol{\rho}^{(i-1)} \boldsymbol{H}_k^H - \mathbf{\Gamma}_u^{(i)} \boldsymbol{H}_k^H + \\ & + \alpha \boldsymbol{F}_{k,u}^{(i)} + \frac{\lambda_u^{(i)}}{2\sigma_S^2 N} \boldsymbol{H}_{k,u}^H = 0, \end{aligned} \tag{5.37}$$

$$\nabla_{\boldsymbol{B}_{k,u}^{(i)}} L = 0 \quad \Leftrightarrow \quad \boldsymbol{B}_{k,u}^{(i)} \left(\boldsymbol{R}_S \boldsymbol{\rho}^{(i-1)^2} + \boldsymbol{R}_\Delta^{(i)} \right) = \boldsymbol{F}_{k,u}^{(i)} \boldsymbol{H}_k \boldsymbol{R}_S \boldsymbol{\rho}^{(i-1)} - \mathbf{\Gamma}_u^{(i)} \boldsymbol{R}_S \boldsymbol{\rho}^{(i-1)}, \tag{5.38}$$

and

$$\nabla_{\lambda_u^{(i)}} = 0 \Leftrightarrow \gamma_u^{(i)} = 1 \tag{5.39}$$

with

$$\boldsymbol{R}_S = \mathrm{E}\left[\boldsymbol{A}_k^* \, \boldsymbol{A}_k^T \right] = 2\sigma_S^2 \boldsymbol{I}_U, \tag{5.40}$$

$$\boldsymbol{R}_N = \mathrm{E}\left[\boldsymbol{N}_k^* \, \boldsymbol{N}_k^T \right] = 2\sigma_N^2 \boldsymbol{I}_J \tag{5.41}$$

and

$$\boldsymbol{R}_\Delta^{(i-1)} = \mathrm{E}\left[\boldsymbol{\Delta}_k^{(i)^*} \, \boldsymbol{\Delta}_k^{(i)^T} \right] = 2\sigma_S^2 \, \mathrm{diag}\left(1 - \rho_1^{(i-1)^2}, \cdots, 1 - \rho_U^{(i-1)^2} \right) = 2\sigma_S^2 \mathbf{\Omega}^{(i-1)}. \tag{5.42}$$

As expected, (5.39) is the condition under which the optimization is carried out.

Rewriting (5.38) by noting that $\boldsymbol{\rho}^{(i-1)^2} \boldsymbol{R}_S + \boldsymbol{R}_\Delta^{(i)} = \boldsymbol{R}_S$, the optimum feedback vector is given by

$$\boldsymbol{B}_{k,u}^{(i)} = \left(\boldsymbol{F}_{k,u}^{(i)} \boldsymbol{H}_k - \mathbf{\Gamma}_u^{(i)} \right) \boldsymbol{\rho}^{(i-1)}. \tag{5.43}$$

By replacing (5.43) in (5.37) we obtain the feedforward coefficients

$$\boldsymbol{F}_{k,u}^{(i)} = \boldsymbol{K}_u^{(i)} \boldsymbol{H}_k^H \left[\alpha \boldsymbol{I}_J + \boldsymbol{H}_k^* \, \mathbf{\Omega}^{(i-1)} \boldsymbol{H}_k^T \right]^{-1} \tag{5.44}$$

where $\boldsymbol{K}_u^{(i)}$ represents a constant normalization vector given by

$$\boldsymbol{K}_u^{(i)} = \begin{bmatrix} 0 & \cdots & \kappa_u^{(i)} & \cdots & 0 \end{bmatrix} = \boldsymbol{\Omega}_u^{(i-1)} \boldsymbol{\Gamma}_u^{(i)} - \frac{\boldsymbol{\lambda}_u^{(i)}}{2\sigma_S^2 N} \tag{5.45}$$

with

$$\boldsymbol{\lambda}_u^{(i)} = \begin{bmatrix} 0 & \cdots & \lambda_u^{(i)} & \cdots & 0 \end{bmatrix} \tag{5.46}$$

being the Lagrangian multipliers vector associated to the u^{th} user and since $\gamma_u^{(i)} = 1$,

$$\boldsymbol{\Gamma}_u^{(i)} = \begin{bmatrix} 0 & \cdots & 1 & \cdots & 0 \end{bmatrix} \tag{5.47}$$

Considering the detection of all users (i.e. PIC receiver), the optimum forward and backward matrices, can also be obtained by employing the Lagrangian multipliers method, with

$$\boldsymbol{F}_k^{(i)} = \boldsymbol{K}^{(i)} \boldsymbol{H}_k^H \left[\alpha \boldsymbol{I}_J + \boldsymbol{H}_k^* \, \boldsymbol{\Omega}^{(i-1)} \, \boldsymbol{H}_k^T \right]^{-1}. \tag{5.48}$$

Taking into consideration that the optimization is carried out with $\gamma^{(i)} = 1$, we may write

$$\boldsymbol{K}^{(i)} = \boldsymbol{\Omega}^{(i-1)} - \frac{\boldsymbol{\lambda}^{(i)}}{2\sigma_S^2 N}, \tag{5.49}$$

$$\boldsymbol{\lambda}^{(i)} = \text{diag}\left(\lambda_1^{(i)} \, ; \, \cdots \, ; \, \lambda_u^{(i)} \, ; \, \cdots \, ; \, \lambda_U^{(i)} \right) \tag{5.50}$$

and

$$\boldsymbol{B}_k^{(i)} = \left(\boldsymbol{F}_k^{(i)} \boldsymbol{H}_k - \boldsymbol{I}_U \right) \boldsymbol{\rho}^{(i-1)}. \tag{5.51}$$

Since we are using soft bit decisions, the vector $\boldsymbol{\rho}^{(i-1)}$ is no longer needed[3] and the feedback coefficients remain only

$$\boldsymbol{B}_k^{(i)} = \boldsymbol{F}_k^{(i)} \boldsymbol{H}_k - \boldsymbol{I}_U. \tag{5.52}$$

5.2.4 Performance Results

In this section we present a set of performance results concerning both linear and iterative receivers for OQPSK signal constellations with blocks of $N = 256$ data symbols and three different users $U = 3$. Both raised cosine support pulses with roll off value of 1 and MSK pulses with a Gaussian filtering with standard deviation $0.09T_s$. As an example we considered a severely time dispersive propagation channel characterized by the power delay profile type C for High Performance Local Area Network [ETS98], with uncorrelated Rayleigh fading in different taps. The duration of the useful part of the data block (N symbols) is $4\mu s$. It is also assumed perfect synchronization and channel estimation.

In Figure 5.5 we present the frequency spectrum of the used support pulses. As we can see, both have a higher frequency occupation than the Nyquist bandwidth (N samples). Raised cosine support pulses have a $B = 2N$ and MSK has $B > 5N$, therefore ACI will

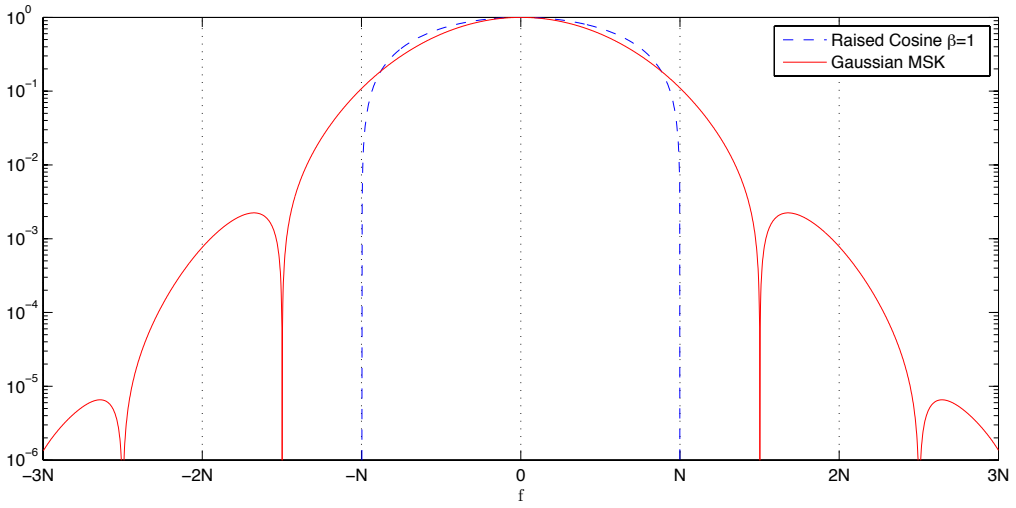

Figure 5.5: Frequency spectrum of raised cosine (dashed blue line) and MSK with Gaussian filtering (red line) support pulses.

be present in systems with multiple users. In Figure 5.6 we can perceive the level of ACI existent in this system for both support pulses.

In Figure 5.7 the values of $\boldsymbol{F}_k^{(i)}$ for a power delay profile type C for HIPERLAN/2 channel [ETS98] are presented. As expected, the $\boldsymbol{F}_k^{(i)}$ follows the behavior observed for flat fading channels (Figure 5.4), naturally, with the fluctuations inherent to the channel selectivity.

Figure 5.8 show the BER results for the four iterations of three different users for raised cosine support pulse. Due to the inherent system design, there are two separate results for each iteration: one for the lower ACI users: the leftmost and rightmost user (solid lines) and the higher ACI users: the inward users (dashed lines). As expected, the lower ACI users have better performance, but after the fourth iteration these differences can be neglected. The results also show that after three or four iterations, the BER is near the MFB in spite of the strong IQI and ACI levels.

Figure 5.9 show the BER results for the four iterations of three different users for MSK with Gaussian filtering with standard deviation $0.09T_s$. These results follow the same pattern as the previous ones, demonstrating an initial performance advantage for the lower ACI users. Nevertheless, despite the higher overall ACI level of this particular support pulse, the results show similar performance of the receiver, implying that with proper support pulse shaping this receiver is able to cope with high ACI (and IQI) level, reaching results close to the BER after just four iterations.

[3] In fact, $\overline{A}_k^{(i)} \approx \boldsymbol{\rho}^{(i)} \hat{A}_k^{(i)}$.

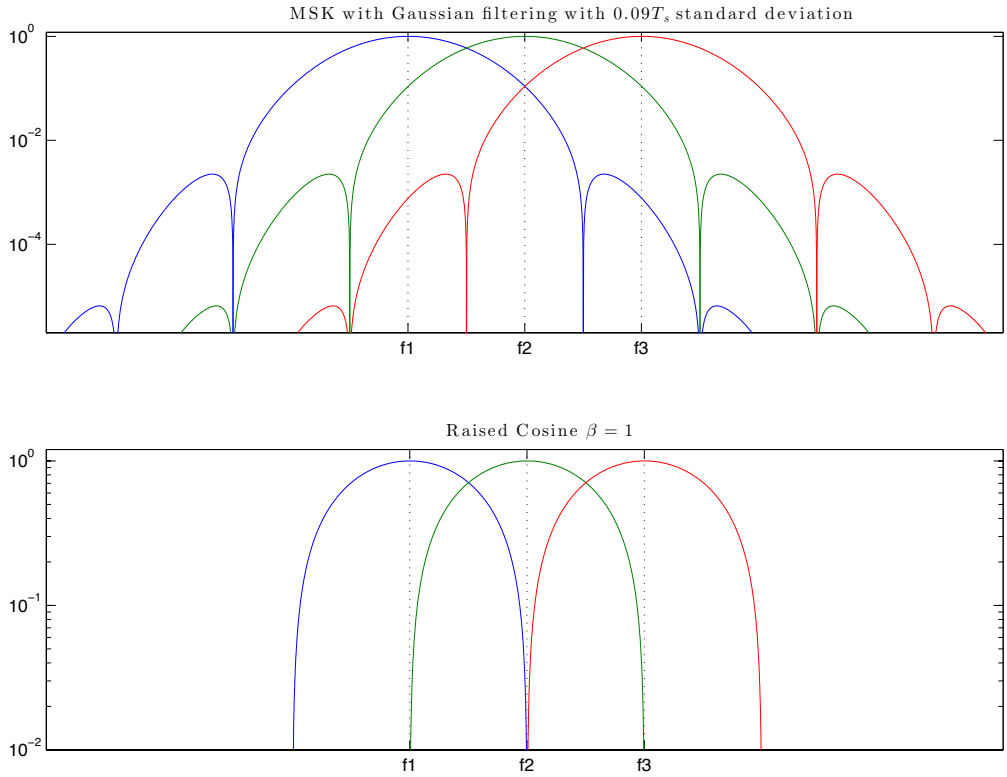

Figure 5.6: Frequency overlap of three different users: raised cosine (up) and MSK with Gaussian filtering (down).

5.2.5 Conclusions

In this section we considered a FDMA system employing SC-FDE schemes with OQPSK modulations and significant spectral overlapping between different frequency channels. This system had two major problems: IQI and ACI. It was shown that conventional FDE designs lead to significant performance degradation due to the interference between in-phase and quadrature components. We proposed an iterative receiver able to cope with strong ACI levels and especially designed to remove the interference between in-phase and quadrature components. It was shown that the proposed method was able to mitigate both IQI and ACI. Moreover, this system achieves high power efficiency due to the OQPSK modulation, and high spectral efficiency due to the spectral overlapping of adjacent users. Our performance results show that this receiver needs only 3 or 4 iterations to remove IQI and ACI, obtaining remarkable BER performance for scenarios with strong ACI levels.

5.3 Receiver design for strong CCI levels

In this section we consider a simple and low complexity pragmatic SC-FDE system employing OQPSK modulations with quasi-constant envelope that increases the overall spectral efficiency by considering total spectral overlapping of two different users. To

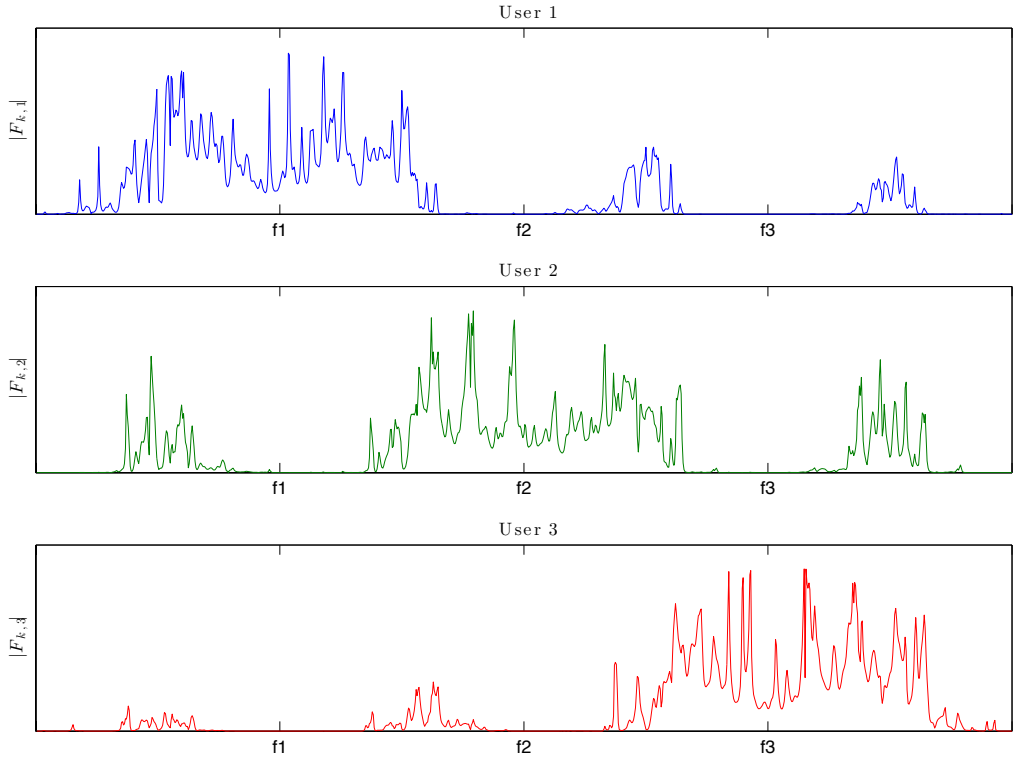

Figure 5.7: Frequency spectrum of $F_{k,u}^{(i)}$ for $U = 3$, $B = 2/T_s$ and a frequency selective fading channel.

mitigate the overall interference, we present an iterative frequency-domain receiver with parallel multiple user detection capable to cope with ISI, CCI levels inherent to the spectral overlapping, and IQI, for severely time dispersive channels.

5.3.1 System Description

Let us consider a simple system employing an SC-FDE scheme with U co-channel users with OQPSK signals for a single frequency channel. Under these conditions, the signal transmitted by the uth frequency channel is

$$s_u(t) = \sum_{n=-N_{cp}}^{N-1} a_{n,u}^I r(t - nT_s) + j \sum_{n=-N_{cp}}^{N-1} a_{n,u}^Q r(t - nT_s - T_s/2), \tag{5.53}$$

with $n = 0, 1, \ldots, N-1$, and where $a_{n,u}^I = \pm 1$ and $a_{n,u}^Q = \pm j$ are, respectively, the nth in-phase and quadrature data symbol of the uth frequency channel. T_s denotes the symbol duration, $r(t)$ is the transmitted pulse shape and N_{cp} denotes the number of samples at the cyclic prefix (longer than the overall channel impulse response length) appended to each block where $a_{-n,u}^Q = a_{N-n,u}^Q$ and $a_{-n,u}^I = a_{N-n,u}^I$. Naturally, the regular data symbols will be $a_{n,u} = a_{n,u}^I + j a_{n,u}^Q$.

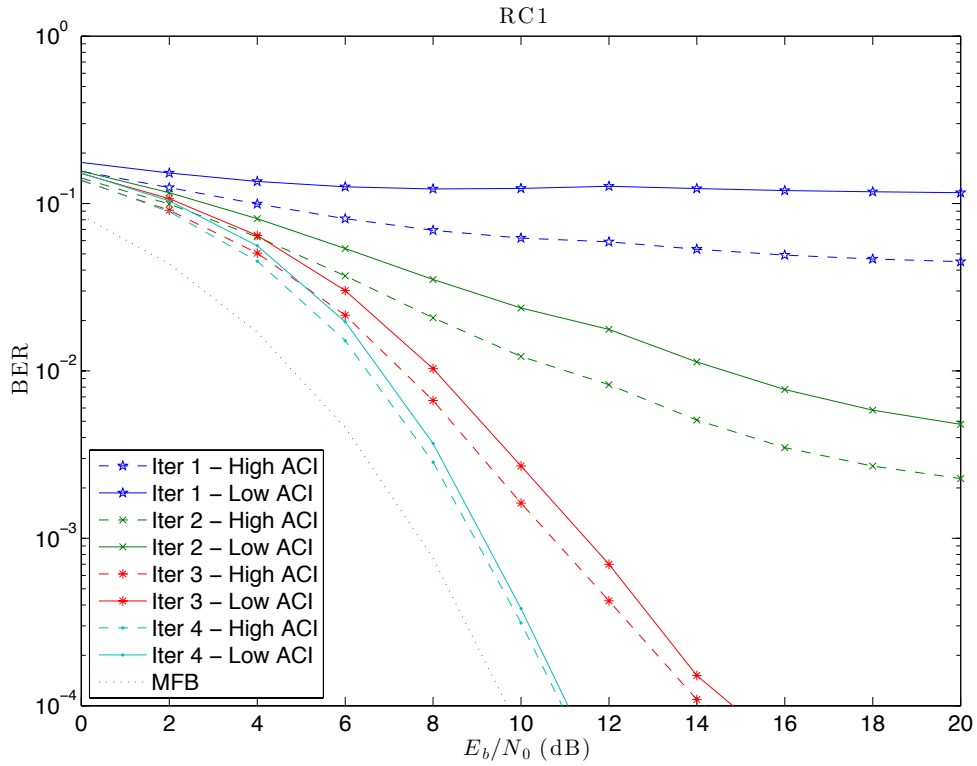

Figure 5.8: BER performance RC1

To cope with the strong CCI levels, all channels will be detected simultaneously. Therefore, it is necessary to employ a reception filter and sample the overall received signal with a J/T_s rate, resulting in an oversampling factor of J.

The relation of the oversampled data symbols $a^{(J)}_{n,u}$ to the regular data symbol block $a_{n,u}$ in an offset modulation is

$$a^{(J)}_{n,u} \begin{cases} a^I_{n',u} & , \quad n = Jn' \\ j\, a^Q_{n',u} & , \quad n = Jn' + J/2\,, \\ 0 & , \quad \text{otherwise} \end{cases} \tag{5.54}$$

with $n = 0, 1, \ldots, JN-1$ where the symbol from the in-phase component appears separated from the quadrature component. Furthermore, the oversampling procedure needs J as a multiple of 2 and can be represented in the frequency domain as

$$A^{(J)}_{k,u} = A^I_{k \bmod N,u} + A^Q_{k \bmod N,u}\Theta_k, \tag{5.55}$$

where

$$\left\{A^I_{k,u}; k = 0, 1, \ldots, N-1\right\} = \text{DFT}\left\{a^I_{n,u}; n = 0, 1, \ldots, N-1\right\}, \tag{5.56}$$

and

$$\left\{A^Q_{k,u}; k = 0, 1, \ldots, N-1\right\} = \text{DFT}\left\{a^Q_{n,u}; n = 0, 1, \ldots, N-1\right\}. \tag{5.57}$$

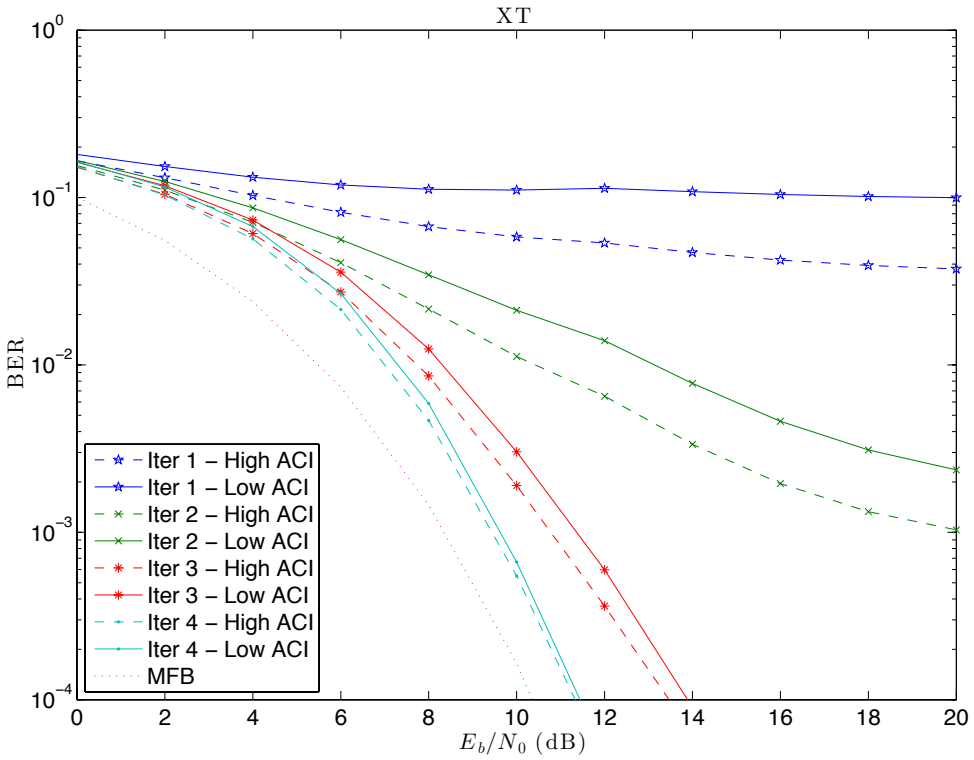

Figure 5.9: BER performance XT

The correspondent frequency domain phase deviation, from the quadrature component relatively to the in-phase component, can be described as

$$\Theta_k = j \exp\left(-\frac{j2\pi k}{2N}\right). \tag{5.58}$$

In offset modulations there is a key difference when compared with non-offset modulation: $\Theta_{k+N} = -\Theta_k$. Therefore a sign shift occurs every N samples (see Figure 5.10).

A_k^I	A_k^I	A_k^I	A_k^I
$A_k^Q\Theta_k$	$-A_k^Q\Theta_k$	$A_k^Q\Theta_k$	$-A_k^Q\Theta_k$

N JN

Figure 5.10: Frequency data symbols block with offset and oversampling.

To obtain the regular data symbols from an oversampled frequency data block, taking into account the implicit multiplicity [Gar91], we need to process the oversampled

frequency domain data symbols by performing undersampling,

$$A_{k,u} = \frac{1}{J}\sum_{q=0}^{J-1} A^{(J)}_{k+qN,u} + j\,\frac{1}{J}\sum_{q=0}^{J-1} \frac{A^{(J)}_{k+qN,u}}{\Theta_{k+qN}}, \tag{5.59}$$

followed by the usual IDFT

$$\left\{a_{n,u}; n = 0,1,\ldots,N-1\right\} = \text{IDFT}\left\{A_{k,u}; k = 0,1,\ldots,N-1\right\}. \tag{5.60}$$

After removing the samples associated to the cyclic prefix and computing its size-JN DFT, the corresponding frequency-domain received block can represented as

$$Y^{(J)}_k = \boldsymbol{H}^{(J)}_k \boldsymbol{A}^{(J)}_k + N^{(J)}_k, \tag{5.61}$$

where $k = 0,1,\ldots,JN-1$, with $N^{(J)}_k$ as the corresponding frequency domain noise for the kth frequency. The overall channel frequency response for the kth frequency which includes the frequency domain adopted pulse shape R^J_k and the channel impulse response $\breve{\boldsymbol{H}}^{(J)}_k$ for the different frequency users in its U columns is defined as

$$\boldsymbol{H}^{(J)}_k = \breve{\boldsymbol{H}}^{(J)}_k R^{(J)}_k = \left[\breve{H}^{(J)}_{k,1} R^{(J)}_k \quad \ldots \quad \breve{H}^{(J)}_{k,U} R^{(J)}_k\right]^T \tag{5.62}$$

and the frequency domain data symbols

$$\boldsymbol{A}^{(J)}_k = \left[A^{(J)}_{k,1} \quad \ldots \quad A^{(J)}_{k,U}\right]. \tag{5.63}$$

Consequently, the FDE will be able to use the periodic frequency blocks associated to the data, to correctly detect the different U frequency users. Besides the CCI problem, this system will also suffer from IQI inherent to all offset systems, as shown in Figure 5.11.

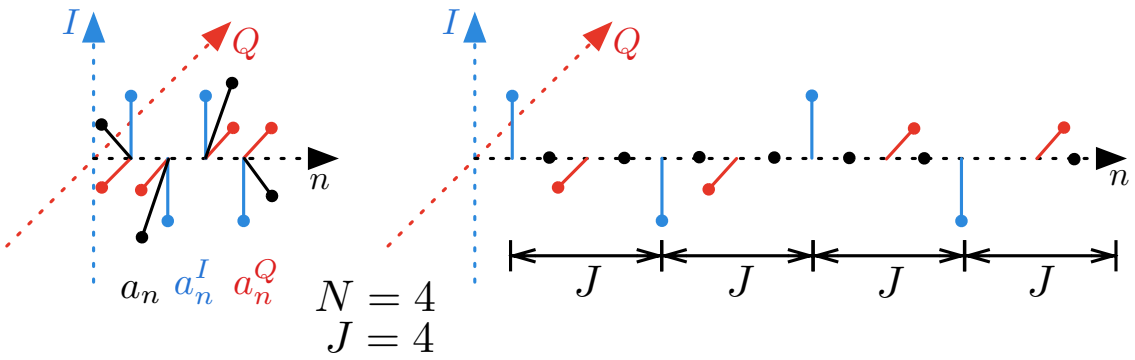

Figure 5.11: Regular data symbols (right) and oversampled offset data symbols' (right).

5.3.2 Low Complexity Parallel FDE Design

This section presents a low complexity iterative receiver capable of mitigating ISI, IQI and CCI. After the first iteration, information from the previous detection is fed back to

improve subsequent equalization procedure, making estimated symbols more reliable. Therefore, for any given iteration, the estimated frequency domain data symbols' block is described by the relation

$$\widetilde{\boldsymbol{A}}_k^{(J)} = \boldsymbol{Y}_k^{(J)} \boldsymbol{F}_k^{(J)} - \overline{\boldsymbol{A}}_k^{(J)} \boldsymbol{B}_k^{(J)}. \tag{5.64}$$

The proposed receiver structure is shown in Figure 5.12.

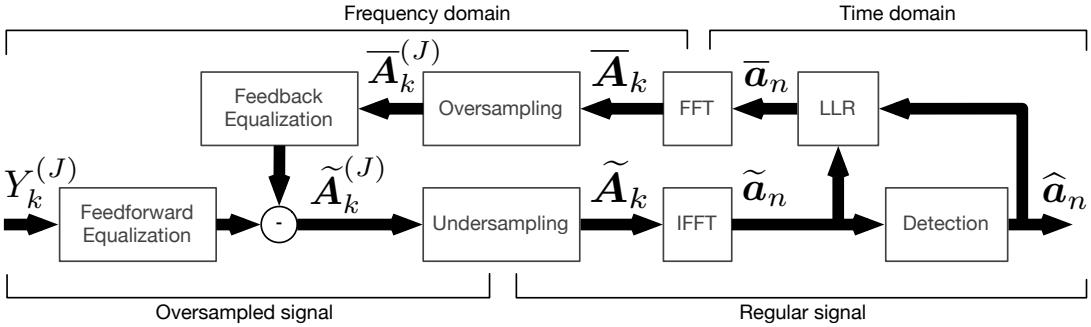

Figure 5.12: Proposed receiver structure.

For the first iteration, there is no information about any detected symbols, therefore it is similar to a linear equalization where $\overline{\boldsymbol{A}}_k^{(J)}$ is a null vector. The feedforward coefficient matrix, derived from the pragmatic method presented in subsection 4.3.4 is obtained by

$$\boldsymbol{F}_k^{(J)} = \begin{bmatrix} F_{k,1}^{(J)} \\ \vdots \\ F_{k,U}^{(J)} \end{bmatrix}^T = \frac{\breve{\boldsymbol{H}}_k^{(J)^H} \left(\boldsymbol{I}_U - \boldsymbol{\rho}\boldsymbol{\rho}^H \right)}{\breve{\boldsymbol{H}}_k^{(J)^H} \left(\boldsymbol{I}_U - \boldsymbol{\rho}\boldsymbol{\rho}^H \right) \breve{\boldsymbol{H}}_k^{(J)} + \boldsymbol{\alpha}} R_k^{(J)^*} \tag{5.65}$$

with $\boldsymbol{\alpha}$ as the inverse of SNR for each user. Note that the denominator of (5.65) is, in fact, not a matrix but just a single number, therefore there is no matrix inversion inherent to this procedure. This approach reduces significantly the complexity of this multiple user detection method.

The U-by-U feedback coefficient matrix, needed to mitigate IQI and remove the residual CCI and ISI after the feedforward filtering is given by

$$\boldsymbol{B}_k^{(J)} = \begin{bmatrix} B_{k,1,1}^{(J)} & \cdots & B_{k,U,1}^{(J)} \\ \vdots & \ddots & \vdots \\ B_{k,1,U}^{(J)} & \cdots & B_{k,U,U}^{(J)} \end{bmatrix} = \boldsymbol{F}_k^{(J)} \boldsymbol{H}_k^{(J)} - \boldsymbol{I}_U. \tag{5.66}$$

The computation of these receiver parameters will be explained in section 5.3.4.

The correlation coefficient matrix that provides a block wise reliability measure of the estimates used in the feedback loop

$$\boldsymbol{\rho} = \text{diag}\left(\rho_1, \ldots, \rho_u, \ldots, \rho_U \right), \tag{5.67}$$

and the fed back matrix denoting the soft decision frequency block vector

$$\overline{\boldsymbol{A}}_k^{(J)} = \left[\overline{A}_{k,1}^{(J)} \cdots \overline{A}_{k,u}^{(J)} \cdots \overline{A}_{k,U}^{(J)} \right], \tag{5.68}$$

will be both explained in the next section.

5.3.3 Feedback Data Symbols

Considering the general OQPSK constellation mapping for every user u, and assuming uncorrelated bits due to the usage of a suitable interleaver, we can obtain $\{\overline{A}_{k,u}^{(J)}; k = 0, \ldots, JN-1\}$ by applying (5.59) and the DFT with

$$\overline{a}_{n,u} = \overline{a}_{n,u}^{I} + j\,\overline{a}_{n,u}^{Q}, \tag{5.69}$$

where $\overline{a}_{n,u}^{I}$ and $\overline{a}_{n,u}^{Q}$, the average symbol values conditioned to the FDE output [BT05] can be obtained by

$$\overline{a}_{n,u}^{I} = \tanh\left(\frac{\Lambda_{n,u}^{I}}{2}\right) \tag{5.70}$$

for the in-phase component and

$$\overline{a}_{n,u}^{Q} = \tanh\left(\frac{\Lambda_{n,u}^{Q}}{2}\right) \tag{5.71}$$

for the quadrature component. The log-likelihood ratio of the nth transmitted symbol component, $\Lambda_{n,u}^{I}$ for the in-phase component and $\Lambda_{n,u}^{Q}$ for the quadrature component, are given by

$$\Lambda_{n,u}^{I} = \frac{2\mathrm{Re}\{\widetilde{a}_{n,u}\}}{\sigma_{N,u}^{2}}, \tag{5.72}$$

and

$$\Lambda_{n,u}^{Q} = \frac{2\mathrm{Im}\{\widetilde{a}_{n,u}\}}{\sigma_{N,u}^{2}}. \tag{5.73}$$

The estimated data bits values $\widetilde{a}_{n,u}^{I}$ and $\widetilde{a}_{n,u}^{Q}$ are obtained by (5.64), after applying the undersample and IFFT operations characterized by (5.59) and (5.60). $\sigma_{N,u}^{2}$ denotes the variance of the real and imaginary part of the overall noise (plus residual ISI and IQI) at the FDE output. In practice it can be estimated by

$$\sigma_{N,u}^{2} = \frac{1}{2N}\sum_{n=0}^{N-1} E[|\widetilde{a}_{n,u} - a_{n,u}|^{2}] \approx \frac{1}{2N}\sum_{n=0}^{N-1} E[|\widetilde{a}_{n,u} - \overline{a}_{n,u}|^{2}]. \tag{5.74}$$

Finally, the reliability of the estimated average data symbols' soft decision $\overline{a}_{n}$, to be used in the feedback loop are obtained by

$$\rho_{u} = \frac{E\left[\overline{a}_{n,u}a_{n,u}^{*}\right]}{E\left[|a_{n,u}|^{2}\right]} \approx \frac{1}{2N}\sum_{n=0}^{N-1}\left[\left|\tanh\left(\frac{|\Lambda_{n,u}^{I}|}{2}\right)\right| + \left|\tanh\left(\frac{|\Lambda_{n,u}^{Q}|}{2}\right)\right|\right]. \tag{5.75}$$

5.3.4 Computation of Receiver Parameters

In this subsection we will show how to compute the receiver parameters for a system with U users with total overlapping spectrum. To obtain the feedforward and feedback coefficients, we need to minimize the expected value for every u user

$$E\left[\boldsymbol{e}^H\boldsymbol{e}\right] = E\left[\left(\widetilde{\boldsymbol{A}}_k - \boldsymbol{A}_k\right)^H\left(\widetilde{\boldsymbol{A}}_k - \boldsymbol{A}_k\right)\right] \tag{5.76}$$

where $\boldsymbol{e}$ is the error matrix associated with the users' errors for each iteration. For the sake of simplicity lets assume that

$$\widetilde{\boldsymbol{A}}_k = \boldsymbol{Y}_k\boldsymbol{F}_k - \widehat{\boldsymbol{A}}_k\boldsymbol{B}_k \tag{5.77}$$

instead of (5.64), given that $\overline{\boldsymbol{A}}_k \approx \widehat{\boldsymbol{A}}_k\boldsymbol{\rho}^H$ and put aside the oversampling symbol $^{(J)}$ (but take into consideration that all these matrices and symbols regard to oversampled symbols). The relation between the hard decisions to the estimated data symbols is

$$\widehat{\boldsymbol{A}}_k = \boldsymbol{A}_k\boldsymbol{\rho} - \boldsymbol{\Delta}_k, \tag{5.78}$$

with $\boldsymbol{\Delta}_k = \left[\Delta_{k,1}\ \cdots\ \Delta_{k,u}\ \cdots\ \Delta_{k,U}\right]$ regarding the error associated to each users' hard decision. It is possible to rewrite (5.77) using (5.61) and (5.78) in the following way

$$\widetilde{\boldsymbol{A}}_k = \boldsymbol{A}_k\boldsymbol{H}_k\boldsymbol{F}_k + \boldsymbol{N}_k\boldsymbol{F}_k - \boldsymbol{A}_k\boldsymbol{\rho}\boldsymbol{B}_k - \boldsymbol{\Delta}_k\boldsymbol{B}_k. \tag{5.79}$$

Taking into account that the following expected values: $E\left[\boldsymbol{A}_k^H\boldsymbol{\Delta}_k\right]$, $E\left[\boldsymbol{\Delta}_k^H\boldsymbol{A}_k\right]$, $E\left[\boldsymbol{N}_k^H\boldsymbol{A}_k\right]$, $E\left[\boldsymbol{A}_k^H\boldsymbol{N}_k\right]$, $E\left[\boldsymbol{N}_k^H\boldsymbol{\Delta}_k\right]$, and $E\left[\boldsymbol{\Delta}_k^H\boldsymbol{N}_k\right]$ are null, and that

$$E\left[\boldsymbol{A}_k^H\boldsymbol{A}_k\right] = \boldsymbol{R}_S = 2\sigma_S^2\boldsymbol{I}_U, \tag{5.80}$$

$$E\left[\boldsymbol{N}_k^H\boldsymbol{N}_k\right] = \boldsymbol{R}_N = 2\sigma_N^2, \tag{5.81}$$

with σ_S^2 as the real and imaginary variance of the data symbols, and

$$E\left[\boldsymbol{\Delta}_k^H\boldsymbol{\Delta}_k\right] = \boldsymbol{R}_\Delta = \boldsymbol{R}_S - \boldsymbol{\rho}^H\boldsymbol{R}_S\boldsymbol{\rho} = 2\sigma_S^2\left(\boldsymbol{I}_U - \boldsymbol{\rho}^H\boldsymbol{\rho}\right), \tag{5.82}$$

we are able to obtain the feedforward and feedback coefficient matrices from (5.76). After some lengthy but straightforward calculations, we get

$$\begin{aligned} E\left[\boldsymbol{e}^H\boldsymbol{e}\right] = {} & \boldsymbol{F}_k^H\boldsymbol{H}_k^H\boldsymbol{R}_S\boldsymbol{H}_k\boldsymbol{F}_k - \boldsymbol{F}_k^H\boldsymbol{H}_k^H\boldsymbol{R}_S\boldsymbol{\rho}\boldsymbol{B}_k \\ & -\boldsymbol{F}_k^H\boldsymbol{H}_k^H\boldsymbol{R}_S + \boldsymbol{F}_k^H\boldsymbol{R}_N\boldsymbol{F}_k - \boldsymbol{B}_k^H\boldsymbol{\rho}^H\boldsymbol{R}_S\boldsymbol{H}_k\boldsymbol{F}_k \\ & +\boldsymbol{B}_k^H\boldsymbol{\rho}^H\boldsymbol{R}_S\boldsymbol{\rho}\boldsymbol{B}_k + \boldsymbol{B}_k^H\boldsymbol{\rho}^H\boldsymbol{R}_S + \boldsymbol{B}_k^H\boldsymbol{R}_\Delta\boldsymbol{B}_k \\ & -\boldsymbol{R}_S\boldsymbol{H}_k\boldsymbol{F}_k + \boldsymbol{R}_S\boldsymbol{\rho}\boldsymbol{B}_k + \boldsymbol{R}_S. \end{aligned} \tag{5.83}$$

Taking into account that

$$\frac{\partial\boldsymbol{X}_k^H}{\partial\boldsymbol{X}_k} = 0 \tag{5.84}$$

to obtain $\boldsymbol{B}_k$ we calculate

$$\boldsymbol{\nabla}_{\boldsymbol{B}_k}\left\{E\left[\boldsymbol{e}^H\boldsymbol{e}\right]\right\}=0\Leftrightarrow\boldsymbol{B}_k=\boldsymbol{\rho}^H\left(\boldsymbol{H}_k\boldsymbol{F}_k-\boldsymbol{I}_U\right). \tag{5.85}$$

Since the total system feedback is

$$\widehat{\boldsymbol{A}}_k\boldsymbol{\rho}^H\left(\boldsymbol{H}_k\boldsymbol{F}_k-\boldsymbol{I}_U\right), \tag{5.86}$$

and given that the feedback data symbols are based on soft decisions $\overline{\boldsymbol{A}}_k$, which relate to the hard decisions by $\overline{\boldsymbol{A}}_k\approx\widehat{\boldsymbol{A}}_k\boldsymbol{\rho}^H$, the feedback coefficients equation is finally obtained from

$$\boldsymbol{B}_k=\boldsymbol{H}_k\boldsymbol{F}_k-\boldsymbol{I}_U. \tag{5.87}$$

To obtain $\boldsymbol{F}_k$ we calculate

$$\boldsymbol{\nabla}_{\boldsymbol{F}_k}\left\{E\left[\boldsymbol{e}^H\boldsymbol{e}\right]\right\}=0\Leftrightarrow\boldsymbol{F}_k=\frac{\boldsymbol{H}_k^H\left(\boldsymbol{I}_U-\boldsymbol{\rho}\boldsymbol{\rho}^H\right)}{\boldsymbol{H}_k^H\left(\boldsymbol{I}_U-\boldsymbol{\rho}\boldsymbol{\rho}^H\right)\boldsymbol{H}_k+\boldsymbol{\alpha}}, \tag{5.88}$$

together with [Luz+13], the feedforward coefficients can be obtained from

$$\boldsymbol{F}_k^{(J)}=\begin{bmatrix}F_{k,1}^{(J)}\\ \vdots\\ F_{k,U}^{(J)}\end{bmatrix}^T=\frac{\breve{\boldsymbol{H}}_k^{(J)H}\left(\boldsymbol{I}_U-\boldsymbol{\rho}\boldsymbol{\rho}^H\right)}{\breve{\boldsymbol{H}}_k^{(J)H}\left(\boldsymbol{I}_U-\boldsymbol{\rho}\boldsymbol{\rho}^H\right)\breve{\boldsymbol{H}}_k^{(J)}+\boldsymbol{\alpha}}R_k^{(J)*}. \tag{5.89}$$

5.3.5 Performance Results

In this section we present a set of performance results concerning the presented iterative receiver for OQPSK signal constellations with blocks of $N=256$ data symbols and two different users ($U=2$) employing MSK support pulses. These pulses have a main lobe in the frequency domain three times the size of the minimum Nyquist band, with this system, the spectral efficiency increases by a factor of two (Figure 5.13), with relatively the same complexity as receiving two separate signals in different frequency bands, since for this system, with $U=2$, the feedforward coefficients (5.65) are reduced to

$$F_{k,u}^{(J)}=\frac{\breve{H}_{k,u}^{(J)*}\left(1-\rho_u^2\right)}{\left(1-\rho_1^2\right)\left|\breve{H}_{k,1}^{(J)}\right|^2+\left(1-\rho_2^2\right)\left|\breve{H}_{k,2}^{(J)}\right|^2+\alpha}R_k^{(J)*}. \tag{5.90}$$

As an example, we considered a severely time dispersive propagation channel, indispensable for the problem at hand, characterized by the power delay profile type C for High Performance Local Area Lan [ETS98], with uncorrelated Rayleigh fading in different taps. The duration of the useful part of the data block (N symbols) is $4\mu s$. It is also assumed perfect synchronization and channel estimation.

In Fig. 5.13 we present the frequency spectrum of the used support pulses. As we can see, both have a higher frequency occupation than the Nyquist bandwidth (N samples). The main lobe of the MSK pulse have a $B=3N$ with relevant side lobes of $B=N$. For

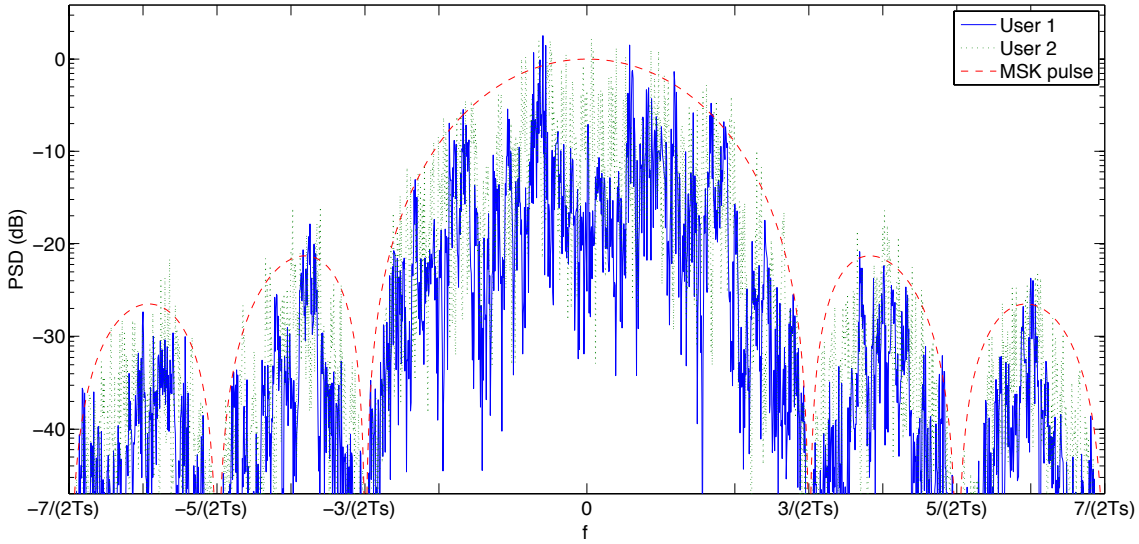

Figure 5.13: Power spectral density of a data blocks from each user and of MSK support pulses.

a system employing this support pulse, the proposed system is capable of detecting a maximum of two concurrent users in the same frequency channel, raising the spectral efficiency by a factor of two, and maintain good BER after four or five iterations (Fig. 5.14). These results show the average BER for six iterations of the two different co-channel users for an MSK support pulse. The results also show that after four or five iterations, the BER is near the MFB in spite of the strong ISI, IQI and CCI levels. To the best of our knowledge this is the first receiver capable of dealing with more than one co-channel user employing offset modulations.

5.3.6 Conclusions

In this section we considered an system employing SC-FDE schemes with OQPSK modulations with co-channel interference due to multiple users in the same frequency channel. The major obstacles of this system are the high IQI and CCI. The conventional FDE designs and even FDE designs specifically designed for IQI and ACI are unable to cope with the high CCI and IQI levels. Therefore we proposed a low complexity iterative receiver able to cope with strong co-channel interference and the interference between in-phase and quadrature components, while obtaining high power and higher spectral efficiency due to the offset modulations and the sharing of the channel by different users. Our performance results show that this receiver only requires few iterations to remove IQI and CCI, allowing a good performance vs. complexity tradeoff, for scenarios with strong CCI levels.

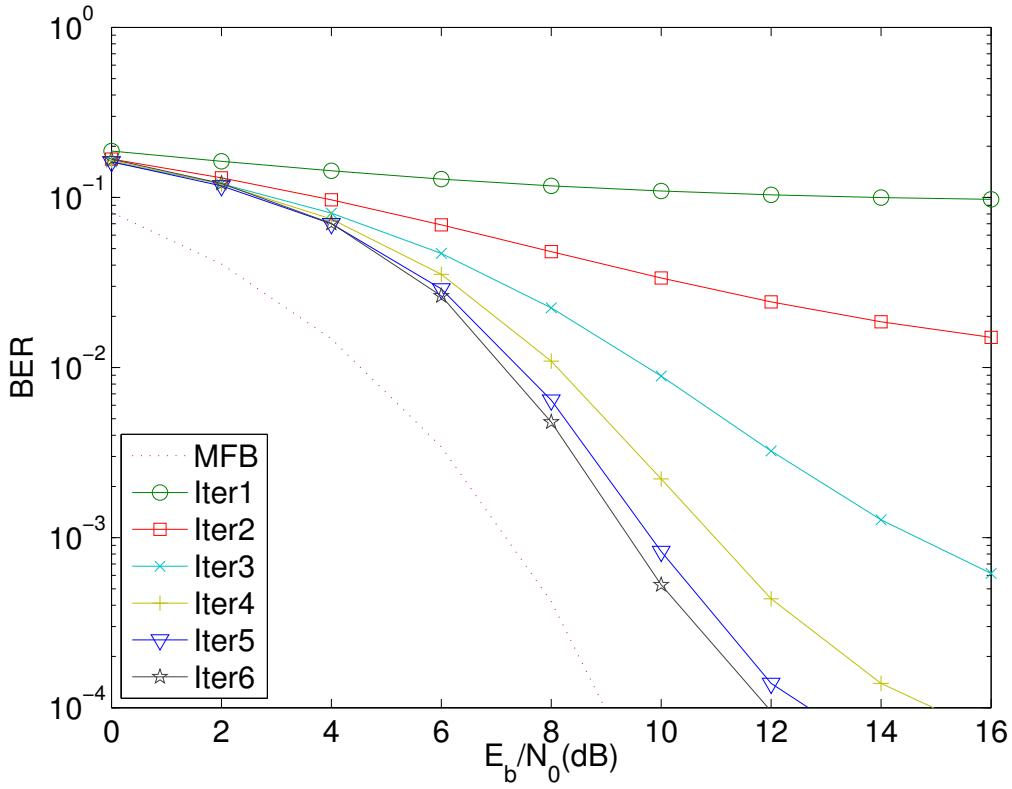

Figure 5.14: BER results for a system with MSK support pulse and two co-channel users ($U = 2$).

CHAPTER 6

CONCLUSIONS

6.1 Synthesis and Final Remarks

This PhD thesis aimed to improve the transmission rates of offset signals over FDE. The biggest challenges were to overcome the inherent IQI and increase the frequency efficiency of these signals.

The first challenge was met, since we were able to design a receiver capable of producing a BER similar to those of non-offset modulations, with a similar level of complexity, for any given constellation order.

The second challenge fell short of the desired accomplishment since the increased spectral efficiency was only achieved in OQPSK modulations at the expense of some BER performance.

Nevertheless, we developed systems capable of dealing with incredibly high levels of IQI, ACI and CCI, being able to genuinely restore the information from two users that send their transmission over the same channel, without any kind of pre-determined orthogonality between them.

6.2 Future Work

During the presented work, it was assumed perfect time synchronization and channel estimation. Therefore, a logic improvement will be to analyze the impact of time synchronization and channel estimation techniques in the overall performance of the proposed systems. As complement to the work developed here, it is possible to identify the overall improvement of the equalization of the ACI and CCI methods for decoding co-channel and adjacent channel users and the comparison between the SIC and PIC approach of the ACI method, developed respectively in [Din+05] and the previous chapter.

BIBLIOGRAPHY

[Ada+09] F. Adachi, K. Takeda, T. Obara, T. Yamamoto, and H. Matsuda. "Recent advances in single-carrier frequency-domain equalization and distributed antenna network". In: *7th IEEE International Conference on Information, Communications and Signal Processing*. 2009. ISBN: 978-1-4244-4656-8. DOI: 10.1109/ICICS.2009.5397650.

[Aul+81] T. Aulin, N. Rydbeck, and C.-E. Sundberg. "Continuous phase modulation - Part II: partial response signaling". In: *IEEE Transactions on Communications* 29.3 (1981), pp. 210–225. ISSN: 0090-6778. DOI: 10.1109/TCOM.1981.1094985.

[BT02a] N. Benvenuto and S. Tomasin. "Block iterative DFE for single carrier modulation". In: *Electronics Letters* 38.19 (2002), pp. 1144 –1145. ISSN: 0013-5194. DOI: 10.1049/el:20020767.

[BT02b] N. Benvenuto and S. Tomasin. "On the comparison between OFDM and single carrier modulation with a DFE using a frequency-domain feedforward filter". In: *IEEE Transactions on Communications* 50.6 (2002), pp. 947–955. ISSN: 0090-6778. DOI: 10.1109/TCOMM.2002.1010614.

[BT05] N. Benvenuto and S. Tomasin. "Iterative design and detection of a DFE in the frequency domain". In: *IEEE Transactions on Communications* 53.11 (2005), pp. 1867 –1875.

[Ben+10] N. Benvenuto, R. Dinis, D. Falconer, and S. Tomasin. "Single Carrier Modulation With Nonlinear Frequency Domain Equalization: An Idea Whose Time Has Come-Again". In: *Proceedings of the IEEE* 98.1 (2010), pp. 69 –96. ISSN: 0018-9219. DOI: 10.1109/JPROC.2009.2031562.

[CC09] A. Carlson and P. Crilly. *Communication Systems*. 5th edition. McGraw-Hill, 2009.

[Cim85] J. Cimini L. "Analysis and Simulation of a Digital Mobile Channel Using Orthogonal Frequency Division Multiplexing". In: *IEEE Transactions on Communications* 33.7 (1985), pp. 665 –675. ISSN: 0090-6778. DOI: 10.1109/TCOM.1985.1096357.

[CF07] D. Costello and G. Forney. "Channel Coding: The Road to Channel Capacity". In: *Proceedings of the IEEE* 95.6 (2007), pp. 1150–1177. ISSN: 0018-9219. DOI: 10.1109/JPROC.2007.895188.

[DGa95] R. Dinis and A. Gusmão. "Adaptive serial OQAM-type receivers for mobile broadband communications". In: *45th IEEE Vehicular Technology Conference*. 1995. DOI: 10.1109/VETEC.1995.504857.

[Din+03] R. Dinis, A. Gusmao, and N. Esteves. "On Broadband Block Transmission over Strongly Frequency-Selective Fading Channels". In: *15th International Conference on Wireless Communications*. 2003.

[Din+04] R. Dinis, R. Kalbasi, D. Falconer, and A. Banihashemi. "Iterative layered space-time receivers for single-carrier transmission over severe time-dispersive channels". In: *IEEE Communications Letters* 8.9 (2004), pp. 579 –581.

[Din+05] R. Dinis, D. Falconer, and B. Ng. "Iterative frequency-domain equalizers for adjacent channel interference suppression". In: *IEEE Global Telecommunications Conference*. 2005. ISBN: 0780394143. DOI: 10.1109/GLOCOM.2005.1578439.

[Din+07] R. Dinis, P. Silva, and A. Gusmão. "IB-DFE receivers with space diversity for CP-assisted DS-CDMA and MC-CDMA systems". In: *European Transactions on Telecommunications* 18.791 - 802 (2007).

[Din+08] R. Dinis, C. Lam, and D. Falconer. "Joint Frequency-Domain Equalization and Channel Estimation Using Superimposed Pilots". In: *IEEE Wireless Communications and Networking Conference*. 2008. ISBN: 978-1-4244-1997-5. DOI: 10.1109/WCNC.2008.84.

[Din+10a] R. Dinis, P. Montezuma, N. Souto, and J. Silva. "Iterative Frequency-Domain Equalization for general constellations". In: *IEEE Sarnoff Symposium*. 2010. DOI: 10.1109/SARNOF.2010.5469792.

[Din+10b] R. Dinis, M. Luzio, and P. Montezuma. "On the design of frequency-domain equalizers for OQPSK modulations". In: *IEEE Sarnoff Symposium*. 2010. DOI: 10.1109/SARNOF.2010.5469761.

[Din+10c] R. Dinis, J. Silva, N. Souto, and P. Montezuma. "On the design of turbo equalizers for SC-FDE Schemes with different error protections". In: *72nd IEEE Vehicular Technology Conference Fall*. 2010. DOI: 10.1109/VETECF.2010.5594185.

[ETS98] ETSI. *Channel Models for HIPERLAN/2 in Different Indoor Scenarios*. ETSI EP BRAN 3ERI085B. 1998.

[Fal+02] D. Falconer, S. Ariyavisitakul, A. Benyamin-Seeyar, and B. Eidson. "Frequency domain equalization for single-carrier broadband wireless systems". In: *IEEE Communications Magazine* 40.4 (2002), pp. 58 –66. ISSN: 0163-6804. DOI: 10.1109/35.995852.

[For72] G. Forney. "Maximum-likelihood sequence estimation of digital sequences in the presence of intersymbol interference". In: *IEEE Transactions on Information Theory* 18.3 (May 1972), pp. 363–378. ISSN: 0018-9448. DOI: 10.1109/TIT.1972.1054829.

[FG98] G. Foschini and M. Gans. "On limits of wireless communications in a fading environment when using multiple antennas". In: *Wireless personal communications* 6.3 (1998), pp. 311–335. ISSN: 0929-6212.

[Gar91] W. Gardner. "Exploitation of spectral redundancy in cyclostationary signals". In: *IEEE Signal Processing Magazine* 8.2 (1991), pp. 14 –36. ISSN: 1053-5888. DOI: 10.1109/79.81007.

[GM76] S. Gronemeyer and A. McBride. "MSK and offset QPSK modulation". In: *IEEE Transactions on Communications* 24.8 (1976), pp. 809 –820. ISSN: 0090-6778. DOI: 10.1109/TCOM.1976.1093392.

[Ga+97] A. Gusmão, V. Gonçalves, and N. Esteves. "A novel approach to modeling of OQPSK-type digital transmission over nonlinear radio channels". In: *IEEE Journal on Selected Areas in Communications* 15.4 (1997), pp. 647–655. ISSN: 0733-8716. DOI: 10.1109/49.585775.

[Ga+00] A. Gusmão, R. Dinis, J. Conceição, and N. Esteves. "Comparison of two modulation choices for broadband wireless communications". In: *51st IEEE Vehicular Technology Conference* (2000).

[Ga+03] A. Gusmão, R. Dinis, and N. Esteves. "On frequency-domain equalization and diversity combining for broadband wireless communications". In: *IEEE Transactions on Communications* 51.7 (2003), pp. 1029–1033. ISSN: 0090-6778. DOI: 10.1109/TCOMM.2003.814204.

[Ga+07] A. Gusmão, P. Torres, R. Dinis, and N. Esteves. "A turbo FDE technique for reduced-CP SC-based block transmission systems". In: *IEEE Transactions on Communications* 55.1 (2007), pp. 16 –20. ISSN: 0090-6778. DOI: 10.1109/TCOMM.2006.887482.

[IEE09] IEEE Standard Organization. *IEEE Standard for local and metropolitan area networks Part 16: Air Interface for Broadband Wireless Access Systems*. Tech. rep. 2009. URL: http://standards.ieee.org/getieee802/download/802.16-2009.pdf.

[IST06] D. IST-4-027756 WINNER II. *The WINNER II Air Interface: Refined Multiple Access Concepts*. Tech. rep. 2006.

[Kim+03] Y. Kim, B. Jeong, J. Chung, C. Hwang, J. Ryu, K. Kim, and Y. Kim. "Beyond 3G: vision, requirements, and enabling technologies". In: *IEEE Communications Magazine* 41.3 (2003), pp. 120–124. ISSN: 0163-6804. DOI: 10.1109/MCOM.2003.1186555.

[Lam+07] C.-T. Lam, G. Auer, F. Danilo-Lemoine, and D. Falconer. "Design of time and frequency domain pilots for generalized multicarrier systems". In: *IEEE International Conference on Communications*. 2007. ISBN: 1-4244-0353-7. DOI: 10.1109/ICC.2007.671.

[Lau86] P. Laurent. "Exact and approximate construction of digital phase modulations by superposition of amplitude modulated pulses (AMP)". In: *IEEE Transactions on Communications* 34.2 (1986), pp. 150 –160. ISSN: 0090-6778. DOI: 10.1109/TCOM.1986.1096504.

[LH09] J. Lim and D. Hong. "Inter-carrier interference estimation in OFDM systems with unknown noise distributions". In: *IEEE Signal Processing Letters* 16.6 (2009), pp. 493–496. DOI: 10.1109/LSP.2009.2017571.

[LV02] R. Lopez-Valcarce. "Channel equalization with staggered modulation formats". In: *14th International Conference on Digital Signal Processing (DSP)*. Vol. 2. 2002, pp. 769 –772. DOI: 10.1109/ICDSP.2002.1028204.

[Luz+09] M. Luzio, R. Dinis, and P. Montezuma. "Frequency-domain parallel multiuser detection for quasi-constant envelope OQPSK schemes with high spectral efficiency". In: *3rd International Conference on Signal Processing and Communication Systems*. 2009. ISBN: 978-1-4244-4473-1. DOI: 10.1109/ICSPCS.2009.5306422.

[Luz+10a] M. Luzio, R. Dinis, and P. Montezuma. "On the design of iterative FDE receivers for OQAM modulations". In: *IEEE Global Telecommunications Conference Workshops*. 2010. ISBN: 978-1-4244-8863-6. DOI: 10.1109/GLOCOMW.2010.5700153.

[Luz+10b] M. Luzio, R. Dinis, and P. Montezuma. "On the design of linear receivers for SC-FDE schemes employing OQPSK modulation". In: *72nd IEEE Vehicular Technology Conference Fall*. 2010. DOI: 10.1109/VETECF.2010.5594203.

[Luz+11] M. Luzio, R. Dinis, and P. Montezuma. "On the use of multiple grossly nonlinear amplifiers for an efficient amplification of OQAM signals with FDE receivers". In: *74th IEEE Vehicular Technology Conference*. 2011. DOI: 10.1109/VETECF.2011.6092820.

[Luz+12a] M. Luzio, R. Dinis, and P. Montezuma. "A Pragmatic Design of Frequency-Domain Equalizers for Offset Modulations". In: *76th IEEE Vehicular Technology Conference*. 2012. DOI: 10.1109/VTCFall.2012.6398933.

[Luz+12b] M. Luzio, R. Dinis, and P. Montezuma. "SC-FDE for offset modulations: an efficient transmission technique for broadband wireless systems". In: *IEEE Transactions on Communications* 60.7 (2012), pp. 1851–1861. ISSN: 0090-6778.

[Luz+13] M. Luzio, R. Dinis, and P. Montezuma. "Pragmatic Frequency Domain Equalization for Single Carrier with Offset Modulations". In: *IEEE Transactions on Wireless Communications* 12.9 (2013), pp. 4496–4505. ISSN: 1536-1276. DOI: 10.1109/TWC.2013.072513.121624.

[Mol11] A. Molisch. *Wireless Communications*. 1st ed. IEEE Wiley, 2011, p. 888. ISBN: 9781119992806.

[Mon06] P. Montezuma. "Highly efficient encoded OQPSK signals: emission and reception design aspects". In: *IEEE Military Communications Conference*. 2006. DOI: 10.1109/MILCOM.2006.302089.

[MG99] P. Montezuma and A. Gusmao. "Design of TC-OQAM schemes using a generalised nonlinear OQPSK-type format". In: *Electronics Letters* 35.11 (1999), pp. 860 –861. ISSN: 0013-5194. DOI: 10.1049/el:19990616.

[Mon+09] P. Montezuma, R. Dinis, and M. Luzio. "Analytical characterization of nonlinearly distorted TC-OQAM signals". In: *3rd IEEE International Conference on Signal Processing and Communication Systems*. 2009. ISBN: 978-1-4244-4473-1. DOI: 10.1109/ICSPCS.2009.5306370.

[Mon+11] P. Montezuma, R. Dinis, and M. Luzio. "Power efficient coded 16-OQAM schemes over nonlinear transmitters". In: *34th IEEE Sarnoff Symposium*. 2011. DOI: 10.1109/SARNOF.2011.5876451.

[MH81] K. Murota and K. Hirade. "GMSK modulation for digital mobile radio telephony". In: *IEEE Transactions on Communications* 29.7 (1981), pp. 1044 –1050. ISSN: 0090-6778. DOI: 10.1109/TCOM.1981.1095089.

[Myu+06] H. Myung, J. Lim, and D. Goodman. "Single carrier FDMA for uplink wireless transmission". In: *IEEE Vehicular Technology Magazine* 1.3 (2006), pp. 30–38. ISSN: 1556-6072. DOI: 10.1109/MVT.2006.307304.

[Nai+94] A. Naik, K. Regan, and D. Sivakumar. *Quasilinear time complexity theory*. Vol. 775. Springer Berlin / Heidelberg, 1994, pp. 97–108. ISBN: 978-3-540-57785-0.

[Nik+09] K. Nikitopoulos, S. Stefanatos, and A. Katsaggelos. "Decision-aided compensation of severe phase-impairment-induced inter-carrier interference in frequency-selective OFDM". In: *IEEE Transactions on Wireless Communications* 8.4 (2009), pp. 1614–1619. DOI: 10.1109/TWC.2009.071029.

[Oba+09] T. Obara, H. Tomeba, K. Takeda, and F. Adachi. "Oversampling Frequency-domain Equalization for Single-carrier Transmission in the Presence of Timing Offset". In: *6th IEEE VTS Asia Pacific Wireless Communications Symposium*. 2009.

[PS02] J. Pearsall and C. Soanes. *The Concise Oxford English Dictionary*. Oxford University Press, 2002.

[RC98] G. Raleigh and J. Cioffi. "Spatio-temporal coding for wireless communication". In: *IEEE Transactions on Communications* 46.3 (1998), pp. 357–366. ISSN: 0090-6778. DOI: 10.1109/26.662641.

[SF08] M. Sabbaghian and D. Falconer. "Joint Turbo Frequency Domain Equalization and Carrier Synchronization". In: *IEEE Transactions on Wireless Communications* 7.1 (2008), pp. 204–212. ISSN: 1536-1276. DOI: 10.1109/TWC.2008.060451.

[SF09] M. Sabbaghian and D. Falconer. "An Analytical Approach for Finite Block Length Performance Analysis of Turbo Frequency-Domain Equalization". In: *IEEE Transactions on Vehicular Technology* 58.3 (2009), pp. 1292 –1301. ISSN: 0018-9545. DOI: 10.1109/TVT.2008.928000.

[Sal81] A. Saleh. "Frequency-independent and frequency-dependent nonlinear models of TWT amplifiers". In: *IEEE Transactions on Communications* 29.11 (1981), pp. 1715–1720. ISSN: 0096-2244. DOI: 10.1109/TCOM.1981.1094911.

[SS00] F. Sanzi and J. Speidel. "An adaptive two-dimensional channel estimator for wireless OFDM with application to mobile DVB-T". In: *IEEE Transactions on Broadcasting* 46.2 (2000), pp. 128–133. ISSN: 0018-9316. DOI: 10.1109/11.868928.

[Sar+94a] H. Sari, G. Karam, and I. Jeanclaude. "An analysis of orthogonal frequency-division multiplexing for mobile radio applications". In: *44th IEEE Vehicular Technology Conference*. 1994. DOI: 10.1109/VETEC.1994.345373.

[Sar+94b] H. Sari, G. Karam, and I. Jeanclaud. "Frequency-domain equalization of mobile radio and terrestrial broadcast channels". In: *IEEE Global Telecommunications Conference*. 1994. ISBN: 0-7803-1820-X. DOI: 10.1109/GLOCOM.1994.513297.

[Sun95] L. Sundstrom. "Automatic adjustment of gain and phase imbalances in LINC transmitters". In: *Electronics Letters* 31.3 (1995), pp. 155–156. ISSN: 0013-5194. DOI: 10.1049/el:19950142.

[Tom05] S. Tomasin. "Overlap and save frequency domain DFE for throughput efficient single carrier transmission". In: *16th IEEE International Symposium on Personal, Indoor and Mobile Radio Communications*. 2005. ISBN: 978-3-8007-29. DOI: 10.1109/PIMRC.2005.1651631.

[TB04] S. Tomasin and N. Benvenuto. "A reduced complexity block iterative DFE for dispersive wireless applications". In: *59th IEEE Vehicular Technology Conference*. 2004. ISBN: 0-7803-8521-7. DOI: 10.1109/VETECF.2004.1400323.

[Tra+07] W. Tranter, D. Taylor, and R. Ziemer. *The best of the best: fifty years of communications and networking research*. 1st ed. Wiley-IEEE Press, 2007, p. 692. ISBN: 9780470546543.

[Tu93] J. Tu. "Optimum MMSE equalization for staggered modulation". In: *27th Asilomar Conference on Signals, Systems and Computers*. 1993. DOI: 10.1109/ACSSC.1993.342310.

[TH00] M. Tüchler and J. Hagenauer. *"Turbo equalization" using frequency domain equalizers*. 2000. DOI: 10.1.1.32.6144.

[TH01] M. Tüchler and J. Hagenauer. "Linear time and frequency domain turbo equalization". In: *53rd IEEE VTS Vehicular Technology Conference*. 2001. DOI: 10.1109/VETECS.2001.944627.

[Tüc+02] M. Tüchler, R. Koetter, and A. Singer. "Turbo equalization: principles and new results". In: *IEEE Transactions on Communications* 50.5 (2002), pp. 754 –767. ISSN: 0090-6778. DOI: 10.1109/TCOMM.2002.1006557.

[WE71] S. Weinstein and P. Ebert. "Data transmission by frequency-division multiplexing using the discrete Fourier transform". In: *IEEE Transactions on Communication Technology* 19.5 (1971), pp. 628–634. URL: http://ieeexplore.ieee.org/xpls/abs_all.jsp?arnumber=1090705.